Comparative study of the effect of silver nanoparticles on the hexokinase activity from human and *Trypanosoma brucei*

A thesis submitted in partial fulfilment of the requirements for the degree of

MASTERS OF SCIENCE IN BIOCHEMISTRY

In the

Department of Biochemistry, Microbiology and Biotechnology

Faculty of science

Rhodes University

Grahamstown

South Africa

By

MADALITSO MARTIN MLOZEN

May, 2014

Supervisor: Prof. C.G. Whiteley

Co-Supervisors: Dr. B. Wilhelmi

Dr. J. van Marwijk

Abstract

Despite efforts to reduce cases of Human African trypanosomiasis (HAT), increased cases are reported. This is because of drug resistant *Trypanosoma brucei (Tb),* the organism linked to the disease. This has renewed the call for original approaches to anti-trypanosomal drugs. The recognition of biomedical targets and their role in a disease constitutes the start of the model for target-based therapies or probes. The blood stream form (BSF) of the parasite relies solely on the glycolytic pathway for energy production while in the human host. Disruption of this pathway effectively kills the parasite. *Trypanosoma brucei* hexokinase (*Tb*HK) is the first enzyme in the pathway and any effectors or inhibitors of *Tb*HK would have potential as anti-trypanosomal agents.

*Tb*HK and human glucokinase (*h*GCK) were over-expressed containing a 6 histidine-tag in *E. coli* BL21(DE3) cells containing the pRARE2 plasmid. *Tb*HK exhibited thermal stability between 30°C and 55°C and pH stability between 7.5 and 8.5, while the *h*GCK was thermally stable between 30°C and 40°C and pH stable between pH 7.0 and 8.0. Kinetic studies revealed that *Tb*HK had a K_m of 39 µM, a of 0.066 µmol.min^{-1}.ml^{-1}, a K_{cat} of 2.05 min^{-1} and a K_{cat}/K_m of 0.0522 min^{-1}.µmol^{-1}. *h*GCK exhibited a K_m of 4.5 mM, a V_{max} of 0.032 µmol.min^{-1}.ml^{-1}, a K_{cat} of 11.25, a K_{cat}/K_m of 2.5 min^{-1}.µmol^{-1} and a hill coefficient of 1.5.

Interaction kinetic studies of 0.1 µM, chemically synthesized silver nanoparticles with an average size of 6 nm with *Tb*HK and *h*GCK were conducted. The silver nanoparticles selectively inhibited *Tb*HK over *h*GCK. *Tb*HK showed a mixed type inhibition with a 38%, 50%, 28% reduction in K_m, V_{max} and K_{cat}/K_m respectively. *h*GCK indicated an uncompetitive inhibition pattern with a 33% increase in K_m, a 9% decrease in V_{max} and a 50% increase in K_{cat}/K_m. The highly selective inhibitory effects of AgNPs observed between *Tb*HK and *h*GCK may be used in development of novel anti-trypanosomal drugs.

This thesis is dedicated to my loving family and to the memory of my late father, may his soul rest in eternal peace.

Acknowledgements

I would like to express my sincere and heartfelt gratefulness to the following persons, without them this thesis would have not been possible.

Firstly, I would like to thank God for the gift of life freely given to me,

The Beit Trust for the offer of their scholarship,

Prof. C. Whiteley for his priceless assistance during the entire project and for the assistance with the final preparation of this thesis,

Dr J. Van Marwijk and Dr B. Wilhelmi for their tireless assistance and invaluable advice during my studies and the preparation of this document,

Special thanks to all members of Prof C. Whiteley research group, the Head of Department and all members of the Department of Biochemistry, Microbiology and Biotechnology at Rhodes University for all the support both academically and socially,

Dr Buddy Ullman, for the gift of the genomic *Trypanosoma brucei* DNA,

Jason for the unselfish help with the running of western blot,

My employer, Mulanje Mission Hospital for allowing me to pursue these studies,

Last but not least, my family for their untiring support, constant love and encouragements that they offered throughout my entire study period.

Contents

List of Abbreviations

ADP	Adenosine-5-diphosphate
AFM	Atomic Force Microscopy
$AgNO_3$	Silver nitrate
AgNPs	Silver NPs
$[Ag(NH_3)_2]$	The Tollens reagent
AIDS	Acquired Immune Deficiency Syndrome
AMP	Ampicillin
ATP	Adenosine-5-triphosphate
BHK	Baby hamster kidney
BCA	Bicinchoninic acid
BSA	Bovine Serum Albumin
BSF	Blood Stream Form
CAM	Chloramphenicol
CDC	Center for Disease Control and prevention
CHO	Chinese hamster ovary
CMC	Carboxymethylchitosan
Co	Cobalt
CRP	C-reactive protein
DDT	Dichlorodiphenyltrichloroethane
DLS	Dynamic Light Scattering
DNA	Deoxyribo Nucleic acid
EDAX	Energy Dispersion and Analysis of X-rays

EDTA	Ethylenediaminetetracetic acid
EGFR	Epidermal Growth Factor Receptor
ERAT	Exploratory Research for Advanced Technology
EtOH.PVP	Ethanolic Polyvinylpyrrolidone
Fe	Iron
FeO_3O_4	Magnetite
FPLC	Fast protein liquid chromatography
FS	Fluorescence Spectroscopy
FTIS	Fourier Transform Infrared Spectroscopy
Gd	Gadolinium
GI	Gastrointestinal
G6PDH	Glucose-6-phosphate dehydrogenase
HAT	Human African Trypanosomiasis
HCl	Hydrochloric acid
HEK	Human embryonic kidney
HSV	Herpes simplex virus
Hsp 60	Heat shock protein 60
H1N1	Influenza-A virus
ICA/OES	Inductively Coupled Atomic/Optical Emission Spectroscopy
IMAC	Immobilized metal affinity chromatography
IPTG	Isopropyl β-D-1-thiogalactopyranoside
IHL	Interstitial Laser Hyperthermia
KAN	Kanamycin
kDa	Kilo Dalton
KH_2PO_4	Mono potassium phosphate

Km	Michaelis Menten constant
LB	Lauria Bertani
LED	Light Emitting Diodes
LND	Lonidamine
Mag-TE	Magnetic force-based Tissue Engineering
MES	(N-morpholino) ethanesulfonic acid
MgATP	Magnesium-Adenine triphosphate
$MgCl_2$	Magnesium chloride
$MgSO_4$	Magnesium Sulfate
mM	Milli molar
MRI	Magnetic Resonance Imaging
MWCO	Molecular weight cut off
Na_2HPO_4	Sodium phosphate dibasic
NAD	Nicotinamide Adenine Dinucleotide
NADH	Reduced Nicotinamide Adenine Dinucleotide
Ni	Nickel
$NiSO_4$	Nickel sulphate
$(NH_4)_2SO_4$	Ammonium sulfate
nm	Nano meter
NPs	Nanopartcles
PEG	Polyethyleneglycol
Pi	Inorganic Phosphate
PMMA	poly(methylmethacrylate)
PPTT	Plasmonic Photothermal Therapy
PTS 1/PTS 2	Peroxisomal Targeting Proteins 1 and 2

PVP	Polyvinylpyloridone
QCAs	Quantum Caged Atoms
QCN	Quercetin
RSA	Republic of South Africa
SDS	Sodium Dodecyl Sulphate
SDS-PAGE	Sodium Dodecyl Sulphate Polyacrylamide Gel Electrophoresis
SEC	Size Exclusion Chromatography
SEM	Scanning Electron Microscopy
SiO_2	Silica
SIT	Sterile Insect Technique
SPR	Surface plasmon resonance
SPSM	Spectinomicin
*Tb*HK1	*Trypanosoma brucei* hexokinase 1
*Tb*HK2	*Trypanosoma brucei* hexokinase 2
Tb	*Trypanosoma brucei*
TCA	Trichloroacetic acid
TCA cycle	Tricarboxylic acid cycle (Krebs cycle)
TCRV	Tacaribe virus
TEM	Transmission Electron Microscopy
TiO_2	Titanium dioxide
TNF	Tissue Necrotic Factor
USA	United States of America
UV-Vis	Ultraviolet-Visible
3’ UTR	3 prime Untranslated Region
V_{max}	Maximum enzyme velocity

VSG	Variant Surface Glycoprotein
WHO	World Health Organization
XPS	X-ray Photoelectron Spectroscopy
y-Fe_2O_3	Maghemite
µM	Micro molar
µl	Micro liter

List of figures

List of Tables

Chapter 1

Literature review

1.1. Introduction

Human African trypanosomiasis (HAT), also called African sleeping sickness is a fatal and much neglected disease that plagues parts of Africa, it is a vector-borne parasitic disease. The parasites that are involved are protozoa belonging to the Trypanosoma genus. The tsetse fly (Glossina genus) is the insect vector for *Trypanosoma* that transmit the parasite to human hosts by bites. African sleeping sickness occurs in 36 sub-Saharan African countries where the tsetse flies are found, putting 70 million people at risk (Fèvre *et al.,* 2008; Simarro *et al.,* 2012; WHO, 2014).

It is also reported that people living in rural populations in these regions where transmission occurs depend on their activities including fishing, animal husbandry and hunting. The ones that are most exposed to the tsetse fly have a greater possibility of being infected. The disease does develop in areas ranging from a single village to an entire region. Within an infected area it is said that the intensity of the disease can vary from one area to the next. There are about 20 000 – 30 000 suspected cases world wide but 10 000 cases are reported (WHO, 2014). The World Health Organization reported that the disease was nearly eliminated in the 1960s, but it made a comeback of the disease in epidemic proportions mainly due to reasons including war, population movements as well as the collapse of health systems over the past two decades.

1.2. Trypanosomiasis

1.2.1. Human African Trypanosomiasis

Depending on the parasite involved, the human African trypanosomiasis may take two forms:
(i) *Trypanosoma brucei gambiense* (*Tb gambiense*) is found in west and central Africa, also termed as West African trypanosomiasis (CDC, 2012). This form is currently known to be responsible for over 95% of reported cases of sleeping sickness and causes a chronic infection. Most of the reported cases are in central Africa (Chad, Central African Republic, Angola, Sudan, Northern Uganda and Democratic Republic of Congo).

(ii) *Trypanosoma brucei rhodesiense (Tb rhodesiense)* found in eastern and southern Africa, also referred to as East African trypanosomiasis. Currently this form represents about 5% of reported cases and causes an acute infection. More than 95% of cases are reported from Malawi, Uganda, Zambia and Tanzania. Further distribution, disease, disease profile host preference and subspecies are presented in table 1.1

Table 1.1: *Tb* subspecies characteristics.

Subspecies	**Host**	**Disease**	**Disease profile in humans**	**Distribution**
Trypanosoma brucei brucei	Wild and domestic animals	Nagana	None	Tropical Africa
Trypanosoma brucei rhodesience	Humans, wild and animals	Rhodesian sleeping sickness	Acute	East and south Africa
Trypanosoma brucei ganbiense	Humans,wild and domestic animals	Gambian sleeping sickness	Chronic	West and centra Africa

1.2.2. Animal trypanosomiasis

African animal trypanosomiasis also referred to as Nagana is caused by *Tb spp, Tb congolense and Tb vivax*. These parasites cause relatively mild infections in wild animals while in domestic animals they cause often a severe and fatal disease. Domesticated animals can be affected by Nagana. As the illness progresses, the infected animals becomes more weaken and eventually become unfit for work, hence the name of the disease "Nagana" which is a Zulu word meaning "powerless / useless / depressed" (Steverding, 2008). Infections caused by certain trypanosomes occur outside Africa. *Tb evansi*, the causative agent of "Surra" occurs not only in Africa but infections are reported in the Middle East, Asia and South and Central America. Camels, horses, cattle, dogs and buffaloes can be affected by *Tb evansi*. *T. vivax* was also reported in Latin America (Jones, T.W and Davila, A.M., 2001)

1.2.3. *Tb* epidemiology and transmission

1.2.3.1. Epidemiology

All cases of HAT are exported from Africa to other parts of the world by travelers. On an international perspective, HAT is confined to tropical Africa (table 1.1). The prevalence of HAT varies by country and region (figure 1.1). In 2005, major outbreaks were observed in the Democratic Republic of Congo, Angola and Sudan (Truc *et al*., 2012). Simarro *et al.* (2008)

reported that sleeping sickness remains an important public health problem in countries like the Malawi, Central African Republic, Congo, Chad, Côte d'Ivoire, Uganda, Guinea and Tanzania in central Africa. However, Kohagne *et al.* (2011) reported that less than 50 new cases per year are reported in Cameroon, Burkina Faso, Equatorial Guinea, Kenya, Gabon, Mozambique, Rwanda, Nigeria, Zimbabwe and Zambia. *Tb* transmission seems to have stopped and no new cases of African trypanosomiasis have been reported for several decades in countries such as Botswana, Benin, Burundi, Gambia, Ghana, Guinea, Ethiopia, Bissau, Mali, Liberia, Namibia, Sierra Leone, Niger, Senegal, Togo and Swaziland.

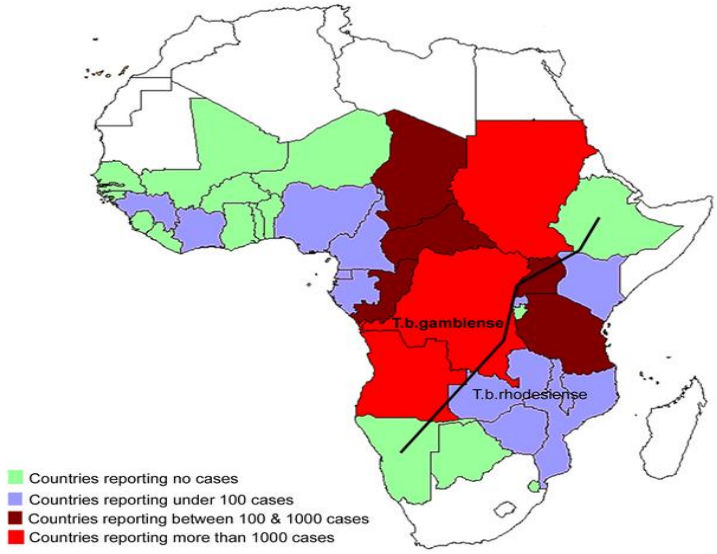

Figure 1.1: Map of sleeping sickness distribution (Adapted from Fevre *et al.*, 2008).

1.2.3.2. Transmission

Infection occurs through the bite of infected tsetse flies. The main reservoir host, are humans for *Tb gambiense*. Wild animals including antelopes and domesticated cattle are the main animal reservoir of *Tb rhodesiense* (WHO, 2012). Khonde *et al.* (1997) also reported on the rising incidences of HAT in specific communities relative to others have been linked to more intense human-fly contact.

Humans are exposed to the disease as far as it is in the vicinity of tsetse fly infested areas. Various human activities and not limited to farming, fishing, hunting, water-related activities and herding are known to be risk factors for acquiring sleeping sickness (Laveissière *et al.*, 1986;

Gouteux *et al*., 1993; Kohagne, 2011) Despommier *et al*. (2005) reported that infection can be acquired by eating raw meat from an infected animal. Mother to child infection (Oba *et al*., 2011); accidental infections in the laboratory, organ transplantation, blood transfusion and sexual activities, congenital African trypanosomiasis may also occur (Rocha *et al.*, 2004).

1.2.3.3. The vector

Tsetse, sometimes spelt as tzetze and also referred to as tik-tik flies (figure 1.2), are large biting flies. Tsetse flies are from the genus Glossina, family Muscidae and from the order Diptera (WHO, 2013). Tsetse flies are also the primary biological vectors of *Wunchereria bancrofti* that causes Elephantiasis.

Figure 1.2: **(**Left and right) *Tb* ssp. in thin blood smears stained with Giemsa. (Center) A close up of a tsetse fly, insect vector of *Tb* (taken from CDC, 2012).

1.3. *Tb* life cycle, clinical features and pathogenesis

1.3.1. Life cycle

Tb has a biphasic life cycle, which starts in the insect vector, tsetse fly, followed by human host.

1.3.1.1. Life cycle in insect vector

The tsetse fly becomes infected by ingesting a blood meal from an infected host (figure 1.3 step 5). In the insect vector's midgut (figure 1.3 step 6) the trypanosomes transforms into procyclic trypomastigotes then into epimastigotes in the salivary glands (Sharma *et al.*, 2009; Chou *et al.*, 2010), these epimastigotes continue multiplication by binary fusion (figure 1.3 step 7). These forms, in turn divide and transform further into metacyclic trypanosomes (figure 1.3 step 8), the

infective stage (Hunt, 2010). During a blood meal the tsetse fly can inject over 40 000 metacyclic trypanosomes. The minimum infective dose for most hosts is 300-500 parasites, although experimental animals have been infected with a single trypanosome (Murakami, 2003).

1.3.1.2. Life cycle in the human host

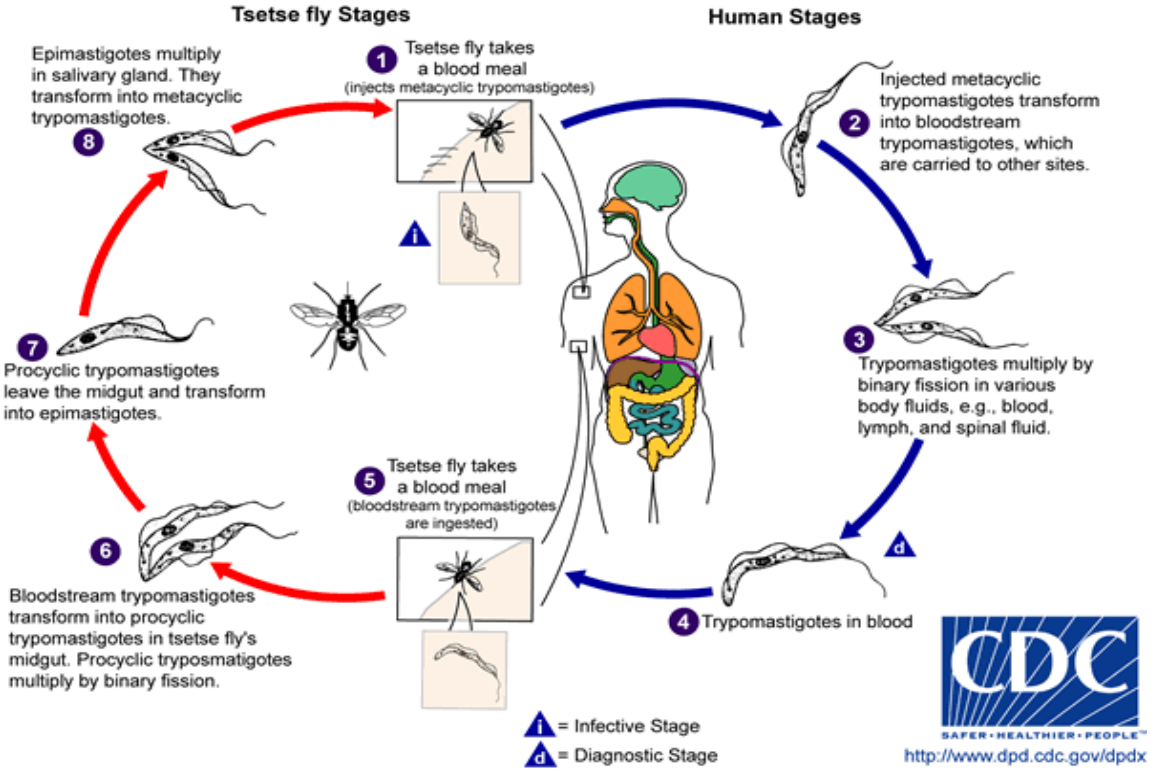

Figure 1.3: Life cycle of *Tb rhodesience* and *Tb gambience* parasites (taken from CDC, 2012).

During a blood meal of tsetse flies, the metacyclic trypomastigotes are injected into the skin of the humans (figure 1.3, step 1). The parasites enter the lymphatic system and pass into the blood stream. The metacyclic trypomastigotes undergo an asexual binary fission, transforming into long slender trypomastigotes (figure 1.3, step 2). They are transported to other sites throughout the body and they reach the lymph and spinal fluid whilst they continue the replication by binary fission (figure 1.3, step 3). Within the blood stream of the mammalian host, the long slender trypomastigotes develops into short stumpy forms (figure 1.3, step 4). The short stumpy forms are thought to be pre-adapted to tsetse flies (CDC, 2012).

1.3.2. Clinical features, pathogenesis and pathophysiology of HAT

African trypanosomiasis has an extremely variable clinical picture. Asymptomatic carriers of both *Tb gambiense* and *Tb rhodesiense* have been reported (Wurapa *et al*., 1984). Southern Africa trypanosomiasis becomes symptomatic 1 to 3 weeks after infection which develops rapidly. It is more disabling and often causes death within 3 to 6 months in untreated patients (CDC, 2012; WHO, 2013). Western Africa trypanosomiasis however, is known to cause chronic infection characterized by a more prolonged course. Clinically both Western and Southern trypanosomiasis develops in 3 clinical stages: chancre, hemolymphatic invasion and meningoencephalitis (figure 1.4). Without treatment all African trypanosomiasis patients may progress to death. The hallmark of the disease is the disturbances in sleeping cycles (Odiit *et al.*, 1997).

The injected trypomastigotes divide in the blood and lymphatic system and eventually, the parasite invades the central nervous system, causing behavioral and neurologic changes, death may also occur (Odiit, 1997). CNS manifestation include meningoencephalitis that is accompanied by edema, bleeding and granulomatous lesions. (Poltera *et al*., 1977; Poltera, 1985; Enanga *et al.*, 2002; Checchi *et al.*, 2008; Klassen *et al*., 2011).

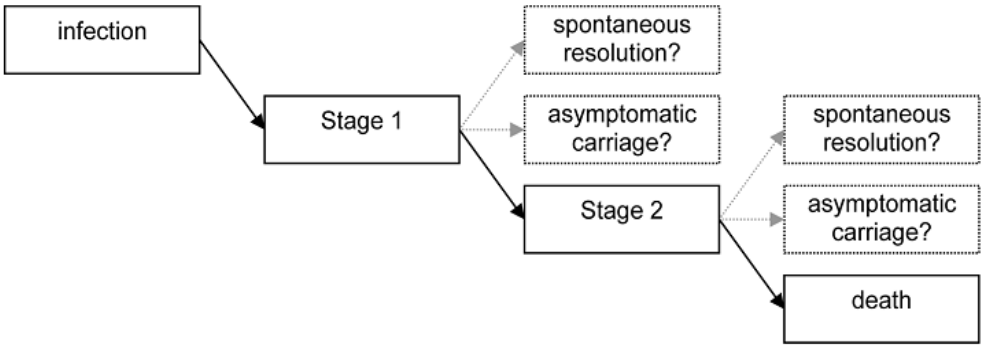

Figure 1.4: Possible outcomes of untreated HAT that progresses to stage one and two with a resultant death if remains untreated (taken from Checchi *et al*., 2008).

1.4. Prevention/control

1.4.1. Prevention

No vaccine against human African trypanosomiasis exists at present. Chemoprophylaxis is not recommended due to the toxicity of the available drugs. Prevention mainly relies on passive and active case detection, early treatment and vector control to reduce exposure to tsetse bites (CDC, 2012). Vector control activities in highly endemic and epidemic areas include fly traps, sequential aerosol spraying, spraying animals and sterile insect techniques. Early techniques involved slaughtering all the wild animals which tsetse fed on. Another early technique involved complete removal of brush and woody vegetation from an area. The inorganic metal based pesticides such as Dichlorodiphenyltrichloroethane (DDT) has been applied as aerosol (Kuzoe and Schofield, 2004).

Sterile Insect Technique (SIT) involves the separation of the males and then irradiating them with large doses of gamma rays to make them sterile and then releasing them, any mating with a sterile male prevents any reproduction. This technique has lead to possible local eradication of the flies from Zanzibar (Allosopp, 2001).

1.4.2. Treatment

The type of treatment of African sleeping sickness depends on the stage of the disease.

1.4.2.1. First stage treatment

Pentamidine was discovered in 1941, despite non-negligible undesirable effects, Pentamidine is well tolerated by patients. Side effects include hypotension in 10% of patients, skin rash, nephrotoxicity, leucopenia and liver enzyme abnormalities (Barrett *et al.,* 2003). Suramin was discovered in 1921 and used for the treatment of the first stage of *Tb rhodesiense*. Barrett *et al.* (2003) indicated that Suramin incites some undesirable effects, in the urinary tract resulting in patients taking suramin experiencing cloudy urine, crawling or tingling of the skin, diarrhea, faintness, skin rash, hypocalceia, anaemia and loss of appetite.

1.4.2.2. Second stage treatment

Melarsoprol was discovered in 1949, is used in both forms of infection. The most striking side effect of Melarsporol is reactive encephalopathy (encephalopathic syndrome) which can be fatal (3% to 10%). Eflornithine was registered in 1990 and has been reported to be less toxic than Melarsoprol (Chappuis *et al.,* 2005). It is only effective against *Tb gambiense* and the regimen is

strict and difficult to apply. Side effects of eflornithine may include sore throat, fever, unusual bleeding or bruising, and unusual fatigue or weakness (McAtee, 2010). Inorder to simplify the use of Eflornirthine in monotherapy, a combined treatment of Nifurtimox and Eflornithine has been recently introduced (Alirol *et al.,* 2013).

1.4.2.3. The phenomenon of treatment failures

Robays *et al.* (2008) reported increasing cases of treatment failure in the Democratic republic of Congo in which a suggestion was made to switch to a safer Eflornithine regimen. In 1977, Ruppol and Burke (1977), reported up to 40% Melarsoprol relapses in *Tb* patients in Zaire; this was also observed by Perez *et al.,* 1991; Brun *et al*., 2001). This present situation of increasing drug resistant cases of human African trypanosomiasis raises a number of questions as to its actual cause. Are they due to the intrinsic character of the parasite or they are associated with patient's metabolism? Is the drug resistance due to an acquired feature of the parasite when exposed to inadequate doses or is it due to the genetic trait of parasitic strains and can that strain be transmitted (WHO, 1999) all these questions inspires scientists globally to put more efforts in research.

Brun *et al.* (2001), Gehrig and Efferth (2008) reported that *Trypanosome brucei* drug resistance could be caused by different mechanisms including changes in the metabolic pathways in the parasite that prevents the drug from reaching its target, intracellular accumulation of the drug is reduced by the impacted drug intake and increased drug export by various transporters. Baker *et al.,* 2013 reported that Melarsprol and Pentamidine drug resistance can possibly be caused by the mutation of *AQP2*, a receptor associated with the accumulation of the drugs in the parasites.

1.5. Hexokinase

Tb relies entirely on the glycolytic pathway for its energy production in the mammalian host (Dodson, 2010). This shift in the metabolic pattern presents a chance to exploit and kill the parasite. A number of approaches have been reported of the exploitation of the enzymes and other associated proteins involved in the pathway for the development of therapy. Disruption of the glycolytic pathway in the bloodstream form trypanosomes has proved to kill the parasite (Verlinde, 2001). Hexokinase catalyzes the first step of the pathway; its inhibition will result in disrupting the glycolytic pathway, concomitantly killing the parasite.

Evidence supporting the targeting of hexokinase as a drug target includes; (i) genetically, ribonucleic acid interference (RNAi) of 3UTR of *Tb*HK in BSF trypanosomes results to cell death due to the resultant disruption of the glycolytic flux (Morris, 2002; Albert, 2005; Lyda, 2009); (ii) biochemically, *Tb* was validated to be a promising therapeutic target by the employment of structurally and chemically based inhibitors that have proven to kill the parasite in high concentrations (Trinquir *et al.,* 1995; Wilson *et al.,* 2002; Chembers *et al.,* 2008). Joice *et al.* (2013) reported the use of the high throughput approach in finding more compounds that successfully inhibit the activity of *Tb*HK, with the evidence above it proves that *Tb*HK is very different from the human hexokinase and this fact is also supported by the evidence that as compared to its counterpart in humans, *Tb*HK has only 30-33% sequence identity (Sharlow *et al.,* 2010).

1.5.1. Human hexokinase

Hexokinase (D-hexose 6-phospho-transferase, EC 2.7.1.1.) is a protein which is classified under the main grouping of transferase enzymes. HK structure was first determined from yeast by Tom Steitz at Yale University. It is the first enzyme in the glycolytic pathway converting glucose into glucose-6-phosphate (Wilson, 2003). It uses ATP to phosphorylate the 6-hydroxyl group of glucose. Although HK has the ability to phosphorylate different hexoses, phosphorylation of glucose is by far its most important function. Four different isozymes of HK have been identified in mammals, namely, type I, type II, type III, and type IV which vary in their tissue distribution and kinetic properties (Grifin *et al*., 1991; Wilson, 2003). As the latter isozyme has a strong specificity for D-Glucose is also known as glucokinase. It is different from the other isoenzymes by its low affinity for glucose, its lack of inhibition by glucose-6-phosphate and its molecular mass of 50 kDa as compared to the other isoforms with molecular mass of 100 kDa (Tanizawa *et al.*, 1991).

The structure of human hexokinase (figure 1.5) types I-III isozymes consists of two globular halves; the N-terminal and C-terminal regions which are held together by a connecting helix and a few hydrogen bonds. The structure of each half is similar to that of yeast HK, which consists of two regions, i.e. the large and the small lobe. The glucose binding site is located in the bottom of the cleft between the two lobes. These three types of mammalian hexokinases appear to have

evolved from an ancestral HK of 50 kDa, by means of gene duplication and fusion. They display extensive sequence repetition (Wilson, 2003) both between them and between their N-terminal and C-terminal regions.

Figure 1.5: Human hexokinase structure (Adapted from Rabeth *et al*., 2006).

A common feature of these isozymes, also present in the ancestral HK, is the regulatory role of glucose phosphorylation through inhibition by its product (glucose-6-phosphate). However, each isoenzyme displays particular properties and differs from the others in its tissue specificity and probable activity. For example, while type II isozyme possesses catalytic activity in both halves, type I and type III isozymes have lost the catalytic activity of the N-terminal region. HK type I show a very unique regulatory property which is that the physiological levels of inorganic phosphate (Pi) can reverse the inhibition of glucose phosphorylation affected by glucose-6-phosphate. This characteristic defines HK type I as an enzyme with a catabolic role, while the other hexokinase isozymes are considered to have mainly an anabolic role. This supports the fact that hexokinase type I is particularly abundant in highly energy-demanding cells (Wilson, 2003). The intracellular reactions mediated by HK can be typified by equation 1.1, where hexose-CH_2OH represents any of several hexoses (like glucose) that contain an accessible -CH_2OH moiety. The hexose in the presence of magnesium ions and ATP is phosphorylated to glucose-6-phosphate (figure 1.6) that also results in releasing ADP and hydrogen ion as by products.

Equation 1.1:

$Hexose\text{-}CH_2OH + MgATP_2 \rightarrow Hexose\text{-}CH_2O\text{-}PO_2^{-3} + MgADP^- + H$

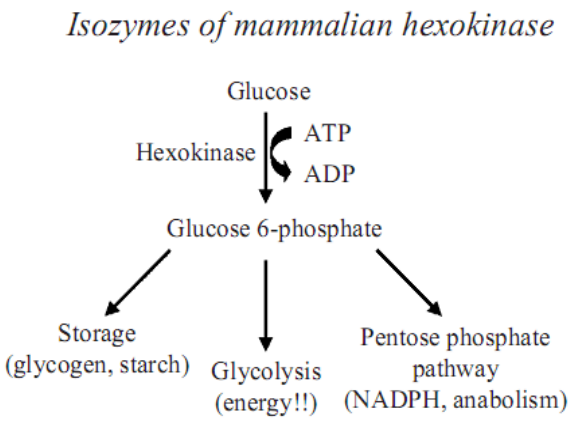

Figure 1.6: Phosphorylation, catalyzed by hexokinase, is the first step in common pathways of glucose metabolism (taken from Wilson, 2003).

In brief, glycolysis is a sequence of 10 enzyme-catalyzed reactions by which glucose is converted to pyruvate. Most of the enzymes found in this pathway are present in all living species and they are found in the cytosol of the cells. The conversion of one molecule of glucose to two molecules of pyruvate is also accompanied by the net conversion of two molecules ADP to two molecules ATP (figure 1.6). In addition to the two molecules of ATP produced (figure 1.7), two molecules of NAD^+ are reduced to NADH. In multicellular organisms, this pathway is found in all differentiated cell types. The overall reaction of glycolysis may be represented by equation 1.2 where glucose is converted into 2 molecules of pyruvate, with a resultant production of adenosine triphosphate and reduced nicotinamide adenine dinucleotide and 2 hydrogen molecules.

Equation 1.2:

$C_6H_{12}O_6 + 2\ NAD^+ + 2\ ADP + 2\ P \rightarrow 2(CH_3(C{=}O)\ COOH + 2\ ATP + 2\ NADH + 2\ H^+$

1.5.2. *Tb* hexokinase

Tb expresses two hexokinases named *Tb*HK1 and *Tb*HK2 which are expressed in blood stream form and procyclic forms of the parasite (Colasante *et al*., 2006). The genes are arranged in tandem on chromosome 10. Other medically important parasites have similarly arranged hexokinase genes. *Leishmania major* has a pair of hexokinase gene located on chromosome 21 which is 62% identical to *Tb*HK (Morris *et al*., 2006). The two polypeptides are approximately 98% identical, with 7 of 10 differences in the C-terminus region of the protein. These changes are very influential in ATP binding and hence its activity (Chambers *et al.,* 2008). *Tb*HK have previously been reported to be localized to the glycosome where *Tb* glycolysis occurs (Misset and Opperdoes, 1984; Colasante *et al*., 2006). Biochemical studies have revealed that authentic and recombinant *Tb*HK multimerize to hexamers (Misset and Opperdoes, 1984; Morris *et al.,* 2006). Notably recombinant *Tb*HK2 (r*Tb*HK2) is not active by itself but in complex with *Tb*HK1 the enzyme is active (Chambers *et al*., 2008).

1.5.2.1. *Tb* glycolytic pathway as a drug target

Glycolysis has proved to be an exploitable pathway for anti-trypanosome therapeutic development. This change in metabolic pattern is the weakness that can be exploited to kill the parasite.

The BSF of the parasite cannot survive disruption of glycolysis (Verlinde *et al.,* 2001). When the parasites differentiate to the BSF they change not only their metabolic pathway to that of glycolysis but also lose most functionality of the singular mitochondrion through the repressed expression of mitochondrial targeted proteins (Williams, 2008). Therefore, without a completely functional mitochondrion, inhibition of the glycolytic pathway is toxic. Glycolysis in the African trypanosome occurs in the specialized organelles known as glycosomes (Opperdoes and Szikora, 2006). This is distinct from most organisms in which glycolytic activities are cytosolic. Targeting of proteins to the glycosome is mediated by two peptide sequences known as peroxisomal targeting sequence 1 (PTS 1) (Gould, 1989) and peroxisomal targeting sequence 2 (PTS 2). PTS1 sequences are found on the C-terminus of proteins while PTS2 sequences are found on the N-terminus of proteins. Both PTS sequences mediate the incorporation of glycosomal proteins (Blattner *et al*., 1995; Lyda, 2009). However, all glycolytic and metabolic

enzymes are not exclusive to the glycosome. Some of these metabolic enzymes such as adenylate kinase, enolase and phosphoglycerate mutase have been shown to be found in flagellum and cytosol of *Tb* (Pullen *et al.*, 2004).

1.5.2.2. *Tb*HK as drug target

Studies on genetic evidence support the targeting of *Tb*HK1 in anti-trypanosome therapeutic development. RNA interference of *Tb*HK1 and *Tb*HK2 in the blood stream form parasites, led to cell death due to a disruption of glycolytic flux (Albert *et al*., 2005; Lyda, 2009), however gene silencing of *Tb*HK1 and *Tb*HK2 in the insect form parasite had not significant effect as the parasite can adapt to the inactivation of hexokinase and switch to the use of amino acid metabolism for its energy production (Chembers *et al*., 2008). Biochemical validation of *Tb*HK as therapeutic targets has also been carried out. Inhibitors of *Tb*HK1 can be tested easily *in vitro* by using a simple hexokinase assay to monitor the inhibition patterns. Chambers *et al.* (2008) demonstrated that *Tb*HK have showed inhibition by fatty acids.

Structurally based inhibitors of *Tb*HK have been used in the past but are trypanocidal at high concentrations (Trinquier *et al.,* 1995; Willson *et al*., 2002). Known hexokinase inhibitors were tested against *Tb*HK1 and trypanosomes, and from these inhibitors of hexokinases, two were investigated, lonidamine (1-(2, 4-dichlorobenzyl)-1H-indazole-3-carboxylic acid) and quercetin (QCN) (Sharlow *et al.,* 2010). Lonidamine has shown to inhibit hexokinases bound to the mitochondrion of mammals; hence lonidamine is described as an inhibitor of aerobic glycolysis. In the past, lonidamine mediated hexokinase inhibition has been used for cancer therapeutics and male contraception (Silvestrini *et al*., 1984 and 1991; Lyda. 2009). However, lonidamine has not yet been approved for use as a male contraceptive in humans. In recent years, lonidamine has been found to inhibit recombinant *Tb*HK1 *in vitro*, hence, a promising drug for *Tb* infection (Chambers *et al.,* 2008). Lonidamine has also been reported to have similar effects of inhibiting *Tb*HK counterparts in *Leishmania mexicana* promastigotes (Turrens and Cuzzulo, 1987) and *Tb cruzi* epimastigotes (Turrens, 1986). In both *L. Mexicana* promastigotes and *Tb cruzi* epimastigotes this inhibition of hexokinase resulted in concomitant inhibition of glycolysis (Chembers *et al*., 2008). Turrens in 1986 reported the impact of lonidamine on the respiration of the parasitic forms of *Tb* where the blood forms of the parasite were sensitive, however;

Chembers *et al.* (2008) reported the inhibition if the recombinant *Tb*HK1 and hence the activity of hexokinase from *Tb* trypomastigotes lysates.

Quercertin (3,5,7,3',4'-pentahydroxyflavone) is a bioflavonoid isolated from plants, has shown to exhibit antioxidant properties as well as play a role in the signaling between plants and microbes for nodulation.The key feature of QCN is that it inhibits enzymes such as tyrosine protein kinase, a phosphorylase kinase, a phosphatidyl 3-kinase and a DNA topoisomerase. QCN has been shown to inhibit the growth of cancer cell lines. QCN not only affects cancer cells it also appears to affect any rapidly dividing cell, even BSF parasites. QCN is toxic and induces apoptosis at a relatively low level with an LD_{50} of 10 µM QCN. While the connection between QCN and apoptosis is not resolved, apoptosis is linked in mammalian cells with mitochondrial associated hexokinase activity. In fact, an increase in hexokinase activity can prevent apoptosis induced by oxidative stress (Lyda, 2009; Dodson *et al.,* 2011). QCN has toxic effects against *Leishmania donovan* (Mittra *et al.,* 2000) and *Tb gambience (*Mamani-matsuda *et al.,* 2004).

1.6. Nanotechnology

Nanotechnology refers to the manipulation of matter on an atomic or molecular level. In recent years nanotechnology is emerging as the most interesting and promising technology that is used in various disciplines, such as, physics, chemistry, biology, material science and medicine. A nanometer is 1×10^{-9} m or one millionth of a millimeter. The prefix "*nano"* is derived from the Greek word "*nanos"* which means "dwarf".

1.6.1. Nanoparticles (NPs)

NPs are those particles that are in sizes ranging from 1-100 nm, classified as natural, incidental and engineered. NPs may be known by a number of alternative and trade-specific names, including particulate matter, aerosols, colloids, nanocomposites, nanopowders, and nanoceramics depending on the application of interest. During the 1970s when the first studies were conducted with NPs in the USA by Granqvist and Buhrman and in Japan by C.H. Hayashi within the ERATO project they were referred to as ultrafine particles. However in the 1990s the name NPs came to full use. The original concept of nanotechnology was spoken by Richard Feynman in his

lecture entitled “There’s plenty of room at the bottom” at the American Institute of Technology in 1959; the idea that was later published in his book in 1961.

1.6.2. Properties of NPs

Great scientific interest is put on NPs as they are said to be an effective bridge between bulk materials and atomic or molecular structures. At the nano-scale, size-dependent properties are often observed as compared to the bulk material that have constant physical properties regardless of its size, thus, the properties of materials change as their size approaches the nano-scale and as the percentage of atoms at the surface of a material becomes significant (Thakkar *et al.,* 2010; Ahmed *et al*., 2013).

1.6.2.1. Optical properties

NPs often possess unexpected optical properties as they are small enough to confine their electrons and produce quantum effects. For example gold NPs (AuNPs) appear deep red to black in solution. Silver NPs (AgNPs) appear yellow to deep reddish-yellow in color and they exhibit a plasmon resonance of ± 400 nm (Das *et al*., 2009), as compared to gold NPs that has a plasmon resonance band of ± 500 nm (Huang *et al*., 2009; Khlebtsov and Dykman, 2009).

1.6.2.2. Melting properties

AuNPs are reported to have much lower melting temperatures (~300°C for 2.5 nm sizes) than the gold slabs (1064°C) (Buffat and Borel, 1976). Lower melting temperatures were also observed (Chang-dong Zou *et al*., 2009) for Tin NPs with diameters of 81, 40, 36 and 34 nm which were 226.1, 221.8, 221.1 and 219.5°C, respectively. Tin/silver alloy nanoparticle of around 10 nm melted at 198°C, 13°C lower than the micrometer sized nanoparticle which was 222.6°C (Jiang *et al*., 2007). Yang *et al* (2013) as well as Li *et al.* (2013) reported on an increase in solar absorption observed in solar cells coated with silver NPs.

1.6.2.3. Magnetic properties

Oxides (ferrite), metallic and metallic with shell NPs (Fe, Co, Ni, Gd) are the current magnetic NPs. However these NPs have properties that largely depend on the synthesis and chemical structure. Ferrite NPs once they become smaller they display a phenomenon called

"superparamagnetism" which is a random flip of the direction of magnetism under the influence of temperature thermal energy (Conchero *et al.*, 2010). Other size-dependent property changes of NPs include quantum confinement in semiconductor particles and surface plasmon resonance in some metal particles.

1.6.3. Applications of NPs

1.6.3.1. NPs in medicine

Nanomedicine is a subdivision of nanotechnology that refers to the use of nanotechnology in the field of medicine (Sadanandan, 2011). Terms such as biomedical nanotechnology, nanobiotechnology and nanomedicine are used to refer to this new field.

1.6.3.1.1. NPs in diagnostics

NPs have been used in the detection of Influenza A DNA sequence (Bonanni *et al.* 2010; Driskell *et al.,* 2011), quantification of HIV-1 (Block *et al.,* 2012), direct detection of *Mycobacterium tuberculosis* in clinical samples (Baptista *et al*., 2006), identification of methicilline-resistant *Staphylococcus aureas* (Ramakrishnan *et al.,* 2004).

1.6.3.1.2. NPs in drug delivery systems

NPs are widely researched and actively developing in the targeted delivery of drugs (Dykman *et al*., 2011). Prepositions were made on the conjugation of various antitumor agents to NPs, with a reported high efficacy when conjugated to NPs. Antibodies, antibiotics and NP conjugates have also been studied. Vancomycine and gold NPs have been used against *E. coli, E. faecium* and *E. faecalis* (Mitra *et al*., 2001; Zamboni, 2005; Dykman and Khlebtsov, 2011; Samra *et al.,* 2013).

1.6.3.1.3. NPs in therapy

NPs have been reported to be used in a variety of ways for therapeutic purposes. Photothermal therapy (photothermal cell damage) is an emerging therapy for both tumor and infectious diseases (Dykman *et al*., 2011). Hirsch *et al.* (2003) as well as Zharov *et al.* (2003) described the application of gold NPs as an agent of Photothermal therapy; Pitsillides *et al.* (2003) reported a technique of selectively damaging targeted cells by the use of 20-30 nm. NPs could be delivered into the tumor cell by passive and active methods (Sinha *et al*., 2006), with active delivery

method reported to be the most efficient and reliable. Antibodies to the tumor markers like Epidermal Growth Factor Receptor (EGFR) and the Tumor Necrotic Factor (TNF) are employed (Dykman *et al*., 2011; Nguyen, 2012; Liu *et al.*, 2013).

Photodynamic therapy can be used in the treatment of cancer, dermal and infectious diseases. It is based on the use of light sensitive agents and visible light of a particular wavelength to destroy diseased cells and tissues by producing toxic oxygen after the photosensitizers have been exited (Dykman *et al*., 2011). Rodriguez *et al.* (2011) reported the use of photodynamic usage *in vitro* photodynamic inactivation of *Cryptococcus neoformans* cells.

Magnetic NPs have been employed in tissue engineering strategies called Magnetic force-based tissue engineering (Mag-TE). Cells may be manipulated and organized by the use of a magnetic force while maintaining their functionality. This has been tested with various cell lines including human umbilical vein, endothelial cells, retinal pigment epithelial cells, keratinocytes, mesenchymal stem cells and cardiomyocytes (Corchero *et al*., 2010). The same NP magnetic properties have been utilized in gene therapy procedures. NPs complexes with viral vectors and nucleic acids as a new approach in gene therapy called magnetoinfection were made available (Herranz *et al.*, 2011). The above approaches have reported results that are 40 fold higher in transfection efficiency over the standard conditions (Conchero *et al.*, 2010).

NPs have been reported to be used in water treatment studies (Doyle, 2006; Diallo, 2006 Shen *et al*., 2011), energy production storage and conservation (Li *et al.*, 2013), aircraft and vehicle manufacturing (Meyer *et al*., 2009), in civil engineering and construction (Mann, 2006), in production, processing, safety and packaging of food stuffs, with a reported 1317 known or claimed nano-products. In cosmetics, nanotechnology has been applied in production of sunscreens (Scown *et al.*, 2009). In sports such as soccer, football and baseball, nanotechnology also plays a role (Thomas *et al.*, 2006).

1.6.4. Metallic nanoparticle

It has been reported that metal NPs have shown and reported to have unusual properties that they normally will not have while in their bulk form. With their unlimited potential and benefits they

have been reported to be used in various nanotechnological studies and innovations such as in biochemistry as they are considered good catalysts, in information systems and in medicine, in heavy industry (Fauss, 2008; Sennuga, 2011).

1.6.4.1. Synthesis of metallic NPs

Metal NPs are an important tool for the advancement of nanotechnology in various areas. For the fact that they are not only abundant in nature since living organisms operate at a nano-scale (Doyle, 2006), and since NPs display unusual properties depending on their size and shape it is the imperative that NPs must be synthesized with limited variations in shapes and sizes (Sennuga, 2011). NPs are a product of various processes be it chemical, physical or biological, some of which have been available for long in conventional science and technology and some of these processes are fairly different (Aitken *et al.*, 2004; Sennuga, 2011).

Nanoparticle synthesis may occur in either top-down or bottom up processes. Top-down methods involves the production of NPs from its bulk material which involves the breakdown of the bulk materials into smaller pieces by the use of chemical and mechanical means via attrition or milling. This leads to NPs with a bread size distribution (10-1000 nm), varied particle shapes or geometry and impurities (Overney, 2010). The bottom-up approach involves the synthesis of NPs by the chemical reaction between atomic or molecular species; it allows the gradual growth of the precursor particles via Pyrolisis, Inert Gas Condensation, Solvothermal reaction, Sol-Gel Fabrication and Structured Media. Both top-down and bottom-up methods can be carried out in liquid, gas or supercritical fluids, solids or in a vacuum (Sennuga *et al*., 2012).

1.6.4.1.1. Chemical synthesis of metallic NPs

The major chemical methods for the synthesis of metal NPs in use are categorized into two main categories; sol-gel and gas phase synthesis. With these methods metal NPs of diameter ranges from 1-10 nm are realized with a very uniform crystal structure and also with a high level of monodispersity of about 20% variation in their sizes. However in order to achieve a much better quantum confinement, the monodispersity must be reduced to as low as 5% or even less (Murray *et al*., 1993). These chemical methods of synthesis of NPs greatly depend on the availability of the right metal/metal organic precursors (Theodore and Kunz, 2005). The main disadvantage

with this approach is that it needs high and harsh conditions, such as temperature, pressure, and the use of highly flammable organic solvents that are required in the production of the NPs. These processes have little control over the monodispersity (Mukherjee *et al.*, 2001).

Gas phase process employs the use of the following; a vacuum chamber with heating elements, the precursor metal, equipment to collect the powder as first reported in 1930 (Luther, 2004). The process utilizes an inert gas, at pressures high enough to enable the formation of NPs, but low enough to allow the production of spherical NPs. Metal precursor is then introduced onto a heated element and is rapidly melted. The metal is quickly taken to temperatures far above its melting point, but less than its boiling point in order to adequate vapor pressure. Gas is continuously introduced into the chamber and removed by the pumps, so the gas flow moves the evaporated metal away from the hot element. NPs start to be formed as the gas cools the metal vapor; the formed NPs are still in a liquid form due to the extreme high initial temperatures (Kruis *et al.*, 1998).

While the NPs are still in their liquid state they collide and fuse together in a fixed environment and the NPs grow to specification, remaining spherical and with smooth surfaces. As the liquid particles are further cooled under control, they become solid and grow no longer. At this point the NPs are very reactive, so they are coated with a material that prevents further interaction with other particles or with other materials. Other chemical techniques used in the chemical synthesis of NPs includes; sonochemical technique, cavitation technique, microemulsion technique and high-energy ball milling technique (Santra *et al.*, 2001).

1.6.4.1.2. Biological synthesis of metal NPs

The biological method of synthesis of NPs has a number of advantages as compared to the previously described chemical methods. Chemical methods involve the use of toxic solvents and the generation of toxic by-products. High energy consumption, these threaten the well being of the environment and humans. In addition their high cost and the production of limited shapes of the synthesized NPs negatively affect their potential properties and usability (Thakkar *et al*., 2010). Accordingly, there is an urgent need to develop other more environmentally friendly methods for the synthesis of NPs that will possibly eliminate all the above mentioned drawbacks

as well as produce the desired results. The biological approach looks to be the promising approach in achieving low-cost, energy-efficient, and non-toxic metallic NPs synthesis (Riddin *et al*., 2006; Thakkar *et al*., 2010).

The use of microorganisms in bioremediation technologies have previously been reported (Riddin *et al*., 2006) and due to their ability to detoxify an environment by reduction of metal, they have been reported to be very environmentally friendly nanofactories. Riddin *et al.* (2006) reported that many single-celled organisms are capable of producing mineral structures from inorganic materials be it intra- or extracellular. Studies have shown that these particles are not monodispersed and the rates at which they are formed are rather slow despite reports that NPs synthesized by microorganisms are stable (Sennuga, 2011). In order to overcome the above challenge, the optimization of some of the factors involved in the synthesis process needs to be done, parameters includes the cultivation methods of the microorganisms and the technique of harvesting or the use of combination approach such as photo-biological method (Vaidyanathan *et al*., 2010; Narayanan and Sakthivel, 2010).

A better understanding of the mechanisms involved in the synthesis of metallic NPs by these microorganisms at cellular, biochemical and molecular levels may provide vital information on how to improve the rate of synthesis, nanoparticle quality and their properties (Sennuga, 2011).
Plant extracts or biomass has also been reported to be another biological tool in the synthesis of metallic NPs (Thakkar et al., 2010). Gold and silver and other noble metallic NPs have been reported to have been synthesized using plant leaf and fruit extracts. However these routes do not sufficiently address the problem of particle monodispersity and uniformity which is very important in the applications of these NPs (Thakkar *et al*., 2010).

Recently biomeneralisation involving cage-like proteins as a growth limiting aspect in the NP synthesis has given more light as a potential method of obtaining NPs with a homogeneous size distribution. The protein is reported to serve as a guide to control nanoparticle growth and also prevents aggregation of the NPs since each nanoparticle is coated as it is produced (Xu, 2005).
Figure 1.7 summarizes the protein shells being used to synthesize various types of NPs especially of metal origin, with ferritin and apoferritin being the most commonly used. Ferritin

and apoferritin have exactly the same structure except that ferritins have an iron core and apoferritin have no iron core (Sennuga, 2011).

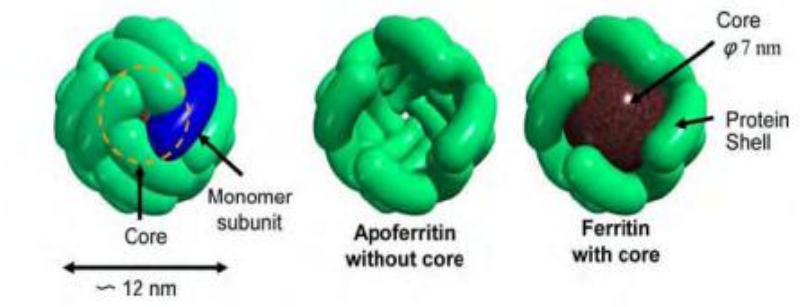

Figure 1.7: A schematic drawing of the cage of protein apoferritin without iron core and ferittin with iron core (Adapted from Iwahori and Yamashita, 2007).

NPs encapsulated in protein cages have recently been proven to be efficient in carrying food and drugs to specific targets in biological system because of their useful properties of biodegradability, non-toxicity, non-antigenicity, high stability and long shelf life (Rahimnejad *et al*., 2009; Sennuga, 2011).

1.6.5. Characterization of metal NPs

NPs can be characterized in many various ways as nanotechnology is an interdisciplinary field. Some of the more common NPs characterization techniques used is summarized in table 1.2.

There are over 700 methods for NPs characterization and about 100 of those have been documented. Nanoparticle characterization methods are mainly based on two physical processes; the first is primary (1^{o}) analytical probes such as photons, neutrons, ions and electrons. The second process is the measurable second effects obtained e.g. the release or absorption of electrons, electromagnetic radiation, volume change, mechanical distortion. During the process of characterization, the primary probe upon interaction with the analyte causes a change in its equilibrium and responds so as to gain its equilibrium state in so doing it modifies the primary probe. This primary probe modification produces secondary effects which is now the measured signal (Sennuga, 2011).

Table 1.2: Examples of techniques used to characterize NPs (adapted from Sennuga, 2011).

Characterization technique	Properties analyzed	Brief description
UV-Visible spectroscopy	Surface plasmon of metal NPs	Based on the absorbance of photons in the visible, near UV and near infrared regions of the electromagnetic spectrum.
ICP AES/OES	Identification, quantification of chemical elements in NPs	Utilizes the intensity of light emitted by exited atoms at their characteristic wavelength and quantifies it as the concentration of the elements within a sample.
TEM, SEM and EDAX	Size, shape, monodispersity and composition	TEM utilizes transmitted electrons while SEM backscattered electrons to generate sample images.
XPS	Analysis of surface/depth atoms of NPs	Very sensitive to chemical composition and environment of elements in a material, provides quantitative analysis of the surface composition.
FTIR	Functional groups of NPs	Secondary symmetrical and asymmetrical vibrations are measured and quantified by Raman and infrared spectroscopes respectively.
DLS	Size distribution in solution	Utilizes the NPs Brownian motion and relate it to an equivalent hydrodynamic diameter.
AFM	Topology/imaging/surface structure of NPs	Utilizes probe-sample interaction.

1.6.6. Safety of NPs

The novel and unique physicochemical, magnetic, optical and biological properties of NPs though very vital in science and technology compared to their bulk materials may potentially lead to serious human and environmental risks (Oberdorster *et al.,* 2005; Sennuga. 2011). However, the toxicity of the current and emerging nanomaterials is not fully understood by scientists hence its one of the growing area of investigation. In working towards dealing with toxicity associated with nanomaterials, a new field of Nanotoxicology has been developed with

the aim of investigating possible harmful effects due to exposure to nanomaterials, also encompassing proper nanomaterials characterization (Donaldson *et al*,. 2004; Oberdorster *et al*., 2005). Lam *et al*. (2003) reported pulmonary toxicity of single celled carbon nanotubes in mice 7 and 90 days following intratrachael instillation observed by induced lung lesions. Recently *in vitro* and *in vivo* studies have reported that inhalation and dermal absorption of some NPs may have very detrimental health effects (Dreher, 2004; Nowack and Bucheli, 2007; Kagan *et al*., 2005; Inoue *et al*., 2006; Linkov *et al*., 2008; Mironava *et al*., 2010). While many uptakes and translocation routes have been demonstrated (figure 1.8), many others are still hypothetical that needs investigations. Largely what are mostly unknown are translocation rates, accumulation and retention in vital sites and their underlying mechanisms (Oberdorster, 2005).

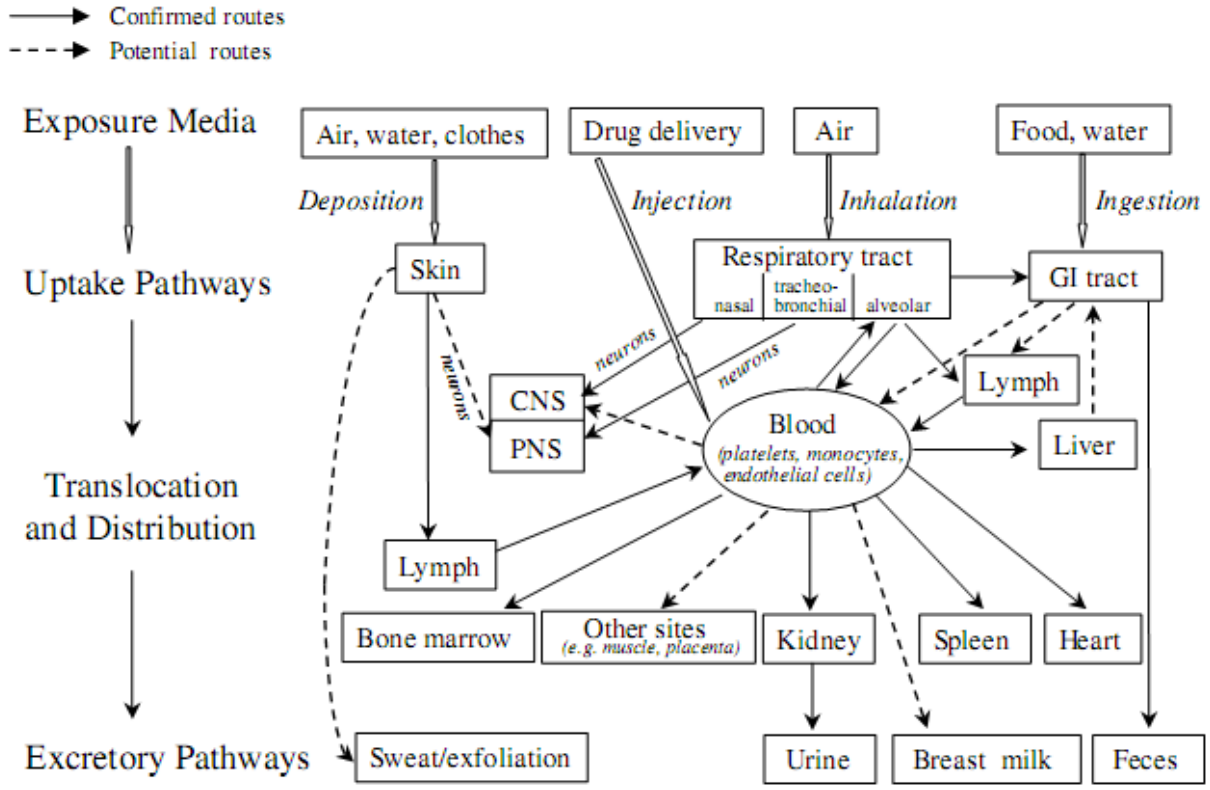

Figure 1.8: Biokinetics of NPs (taken from Oberdorster, 2005).

1.6.7 NPs – protein interaction

The study of the behavior of NPs once introduced to physiological conditions both *in vitro* and *in vivo* is receiving much interest in research circles. Its application in the medical field is also in

huge possibility. The surface of NPs, which have been introduced into a biosystem, would be covered by numerous biomolecules present; these are mainly proteins (Ashby *et al.,* 2013). These interactions govern the functions and fate of the NPs once in the biosystem. There are over 3000 proteins present in plasma, a range of equilibrium constants, each with affinities and exchange times that are different (Lynch and Dawson, 2008; Ashby *et al.*, 2013). Nanoparticle-protein corona, a concept of how NPs and proteins associate in a biosystem was introduced in 2008 by Lynch and Dawson. In this phenomenon, proteins in high concentration rate and with high affinity constants would associate first with the nanoparticle surface. This association may also dissociate rapidly and be replaced by a lower concentration, slower exchange by higher affinity protein. However, little information is available on how particle size and surface characteristics would affect the association and dissociation rates and how it would simultaneously affect the interactions between NPs and all cellular surface receptors (Ashby *et al*., 2013).

1.7. Research focus

1.7.1. Hypothesis

This research will be centered on the hypothesis as deduced below:

The inhibitory effects of silver NPs on the activity of *Trypanosoma brucei* hexokinase and human hexokinase differ.

1.7.2. Objectives

- Cloning, expression, purification and characterization of *Tb*HK and *h*GCK.
- Chemical synthesis of silver NPs.
- Evaluation of the effect of NPs on the activity of the biomedical target, human and *Tb*HK.

Chapter 2

Molecular cloning

2.1 Introduction

Molecular cloning refers to a set of experiments in the molecular biology discipline that are employed to assemble a recombinant DNA molecule and to direct its replication within a host organism. Cloning itself refers to the amplification of a single molecule of DNA to a large population of DNA molecules that are identical. Despite cloning being a set of fairly simple and straight forward procedures, it is of paramount importance because it allows the attainment of a pure sample of a specific gene (Brown, 2010). In order for the gene of interest to be successfully transferred into the host cell, the use of DNA transfer vehicles is employed. Plasmids and viral chromosomes are natural DNA molecules that are widely used as DNA transfer vehicles (Brown, 2010).

For a DNA molecule to act as a vehicle for gene transfer in molecular cloning, it should be capable of entering and replicating in a host cell (Brown, 2010). Plasmids are small circular DNA molecules that are found in almost all bacteria and other organisms including yeast and algae (Griffiths, 1995). The replication of these extra chromosomal DNA molecules depend on the encoded enzymes and proteins to enable the host bacterial cells to replicate them, they often contain genes that code for enzymes that are advantageous to the host bacteria (Brown, 2010; Sambrook and Russel, 2001). Virus chromosomes are essentially the chromosomes of bacteriophage; these are viruses that usually affect bacteria.

Further characteristics of plasmids reveal that they carry origins of replication that are derived from a single stranded bacteriophage; such vectors are also termed phagemids. Plasmid vectors have promoters from bacteriophage; these promoters may be T3, T7 and/or SP6 that are placed next to the multiple cloning sites of the plasmids. Characteristically, several plasmid vectors also contain gene sequences that encode for a lethal gene that only gets suppressed when a foreign DNA segment is inserted into the plasmid vectors on the multiple cloning sites of the plasmid

vectors. This property helps in the positive selection of the transformed host cells (Sambrook and Russel, 2001).

2.1.1. Steps in molecular cloning

A set of molecular cloning experiments usually revolves around seven main steps: (i) Selection of plasmid vector and host organism required for a specific activity: specialized applications need specialized host-vector systems, (ii) Preparation of vector DNA, (iii) Preparation of DNA to be inserted, (iv) Creation of recombinant DNA, (v) Propagation of plasmid vectors carrying foreign DNA of interest, (vi) Transfection and (vii) Identification of clones with a DNA insert (Neumann *et al*., 1982; Wirth *et al*., 1989; Russel and Sambrook, 2001; Brown, 2010).

Transformation is one of the major aspects in molecular cloning because it allows the introduction of modified DNA molecules into the host cells. Some bacteria such as *Bacillus subtilis*, *Haemophillus influenza*, *Streptococcus pneumonia* and Cyanobacteria are naturally transformable, while others such as *Salmonella* species, some *Pseudomonas* strains and *E. coli* can be made transformable by treatment with chemicals such as calcium. *E. coli* is the most widely used bacterial host in molecular cloning procedures and it effectively interacts with DNA molecules in the presence of calcium ions, lower temperatures and heat pulses (Mandel and Higa, 1970; Hanahan and Harbor, 1983).

Plasmid vectors are important because they can be used in the generation of multiple proteins, they are very small in size making them simple to manipulate and purify, they have their own origin of replication and with this property they can duplicate independently, selectable agents such as antibiotics can be incorporated for screening and separation, and commercial plasmids have restriction endonuclease sites incorporated, this facilitates easy cutting and ligation of genes (Casadaban *et al.,* 1980; Madigan and Martinko, 2006).

2.1.2. Application of molecular cloning

Molecular cloning provides an unlimited use in various disciplines including basic applied biological sciences. Molecular cloning provides a platform for the production of various recombinant proteins that may be applied in medicine. Clinically, recombinant proteins have

been approved for the treatment of patients with cystic fibrosis (Phung *et al*., 2010); various leukemias (Quesada *et al*., 1986), chronic hepatitis C infections (Yang *et al.,* 1989), genital warts (Yang *et al.,* 2009), multiple sclerosis (Sellebjerg *et al*., 2012), thrombosis (Eriksson *et al.,* 1996), anemia (Schreiber *et al*., 1996), correction of hemophilia (Oldenburg *et al*., 2009).

Anti-trypanosome therapeutic development has taken advantage of the various ways by which *Tb* glycolytic pathway can be exploited. Studies conducted by Colosante *et al.* (2006) showed that *Tb* survival was affected when the glycolytic pathway was disrupted. When the parasite differentiates into the blood stream form it almost solely depends on glycolysis for its energy production, hence disruption of the pathway is toxic to the parasite. Hexokinase is the first enzyme in the pathway; its inhibition is of importance in the disruption of the pathway. The use of structural inhibitors (Trinquier *et al.,* 1995), as well as gene silencing and RNA interference studies (Lyda, 2009; Albert *et al*., 2005) have shown that inhibition of *Tb*HK activity disrupts the glycolytic pathway, leading to cell death.

The aims of this chapter are:

1. PCR amplification of the *Tb* (TREU 927) hexokinase and human glucokinase genes.
2. Cloning of the PCR amplified genes into cloning vectors and confirming nucleotide sequences by Sanger sequencing.
3. Sub-cloning of the sequence confirmed genes into the relative expression vectors.
4. Transformation of chemically competent host cells with the recombinant DNA constructs.

2.2. Materials and Methods

In order to obtain *Tb*HK and *h*GCK genes, both genes were PCR amplified (Saiki *et al.,* 1988) using genomic DNA (gDNA) for *Tb*HK and complemetary DNA (cDNA) for *h*GCK as templates

Initial denaturation of the double strand deoxyribonucleic acid (dsDNA) with the subsequent formation of a single stranded deoxyribonucleic acid (ssDNA) is achieved by heating the dsDNA at temperatures of 95°C or 98°C. The sample is then cooled to facilitate the annealing of the

primers to their specific target sites. This also initiates the replication of the DNA by polymerase downstream of the primer binding site over a period termed elongation time. After DNA amplification, the DNA was cloned into cloning plasmid vectors, i.e. Clonejet® plasmid for *Tb*HK utilizing blunt end cloning and pGEM-T® easy plasmid for *h*GCK utilizing sticky end cloning. For further amplification, plasmids were transformed into *E. coli* JM109 cell lines for *Tb*HK and *E. coli* TOP10 cell lines for *h*GCK. DNA plasmid extractions were performed accordingly. Screening for positive insertion of the genes was performed by double restriction digestion with subsequent DNA agarose gel electrophoresis for visualization.

Sequencing of the cloning plasmid vectors harboring respective target genes was performed. Two main methods of DNA sequencing are available; the Maxan-Gilbert method, this method is based on the use of chemical modification of the DNA followed by cleavage at specific bases. This method allowed possible sequencing of purified dsDNA without further cloning. However this method was discouraged due to its extensive employment of radioactive labeles. The Sanger method also known as the chain-termination method is an automated method which takes advantage of the DNA polymerase from *E. coli* that is capable of synthesizing a compliment DNA strand from a ssDNA without employing primers. This technique utilizes 2',3'-deoxynucleotide triphosphates (ddNTPs). ddNTPs are different from the normal deoxynucleotides because they lack a hydroxyl group that is replaced with a hydrogen atom at the 3' carbon. These modified molecules are responsible for causing the termination of DNA chain extension because they are incapable of forming a phosphodiester bond with the subsequent deoxynucleotide (Sanger and Coulson, 1975). Sequencing results were analyzed using FinchTV version 1.4.0 and BioEdit Version 7.2.3 and DNAssist version 3.0 softwares.

2.2.1. Bacterial strains, plasmids and culture conditions

Chemically competent *E. coli* strains JM109 (Promega), TOP10 (Invintrogen) and BL21(DE3) containing pRARE2 (Lucigen) were used as hosts for genetic manipulation and expression of proteins. Transformed *E. coli* cells were cultured in Luria-Bertani **(**LB) medium (agar and broth) (10 $g.l^{-1}$ tryptone, 5 $g.l^{-1}$, yeast extract, 5 $g.l^{-1}$, sodium chloride, pH 7) at 37°C, aerobically (200 rpm). Selective pressure was achieved by using the required antibiotic/s, either 100 $\mu g.ml^{-1}$

ampicillin (AMP) and 100 µg.ml^{-1} spectinomycin (SPSM), 34 µg.ml^{-1} chloramphenicol (CAM) or 30 µg.ml^{-1} kanamycine (KAN).

The *Tb*HK PCR product (obtained as described in section 2.3) was sub-cloned into the CloneJet® (Thermo Scientific) vector system (figure 2.1A). CloneJet® can be used for either blunt-end or sticky end cloning. It contains a β-lactamase gene which confers resistance to AMP. It also contains a lethal gene (*eco471R)* which is disrupted by the ligation of the target gene into the vector. This facilitates screening as only cells with recombinant plasmids are able to grow on the ampicillin containing LB agar plates.

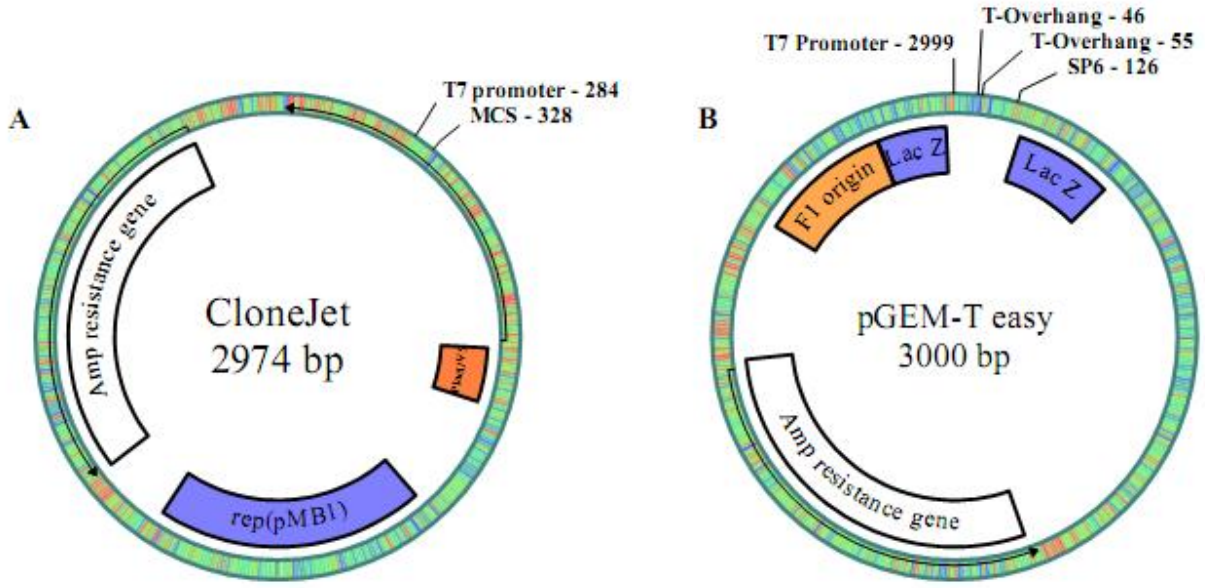

Figure 2.1: (A) Vector map of CloneJet® indicating ampicillin resistance gene, T7 promoter, and the multiple cloning site. (B) Vector map of pGEM-T® easy vector indicating ampicillin resistance gene, F1 origin of plasmid replication, T-overhangs, T7 promoter and LacZ coding Sequence.

The *h*GCK PCR product (obtained as described in section 2.3) was sub-cloned into the pGEM-T® Easy vector system (figure 2.1B). The vector contains T7 and SP6 polymerase promoters within the α-peptide coding region of the enzyme β-galactosidase. Ligation of a DNA insert into the cloning site inactivates the α-peptide and allows for the selection of recombinant DNA constructs based on blue/white screening (Chaffin, 1998). The vector has T-overhangs in the cloning site that allows for TA-cloning and it also prevents the vector from re-circularising.

The pET28b(+) plasmid vector are designed for generation of proteins fused with an N-terminal Histidine-tag / T7-tag. Proteins having their native N-terminus can be expressed by the use of the *NdeI* insertion site (figure 2.2A). The vector encodes for a protease recognition site that facilitates the removal of the N-terminal His-tag. The pET22b(+) plasmid vector (figure 2.2B) was designed for fusion of proteins to signal sequences that facilitate export into the periplasmic space. Unfused proteins can also be expressed by cloning into the *NdeI* site of the vector. pET22b(+) can be used for production of proteins fused with a C-terminal His-tag. The sequence verified *Tb*HK gene (section 2.9) was sub-cloned in pET28b(+) , while the sequence verified *h*GCK (section 2.9) was sub-cloned into pET22b(+).

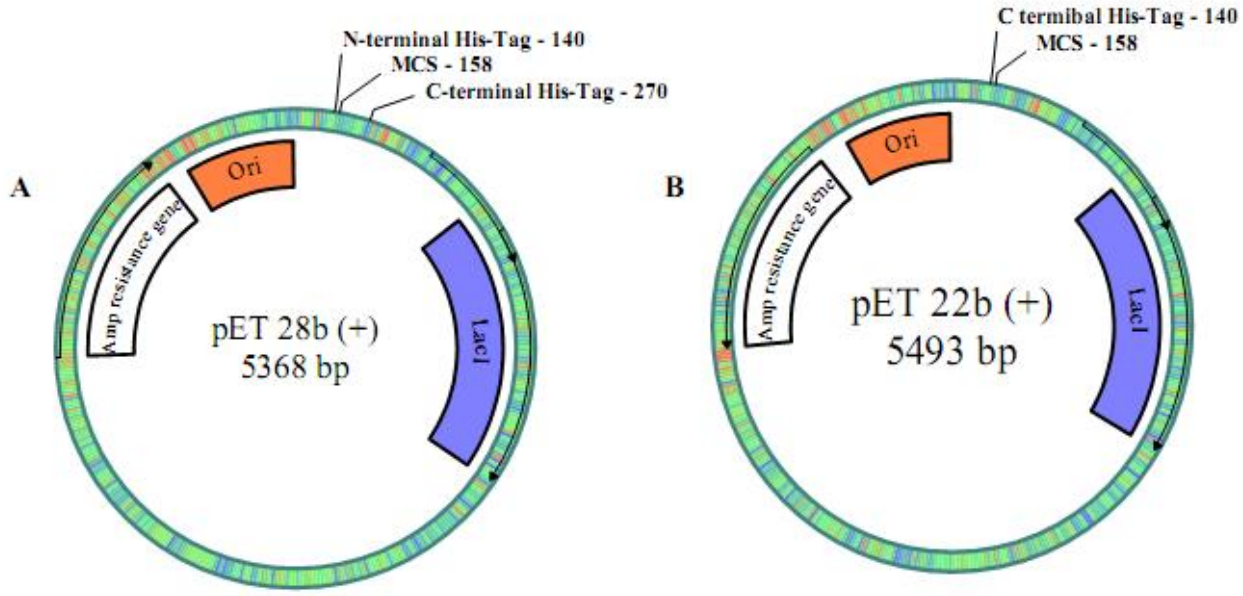

Figure 2.2: (A) Vector map of pET22b(+) expression vector system indicating Lac1, ampicillin resistance gene, replication origin, C-terminal His-tag and the multiple cloning site. (B) Vector map of pET28b(+) expression vector system showing Lac1, ampicillin resistance gene, replication origin N- and C-terminal His-tag and the multiple cloning site.

2.2.2. Primer design and virtual cloning

The *Tb*HK nucleotide sequence was obtained from the National Center for Biotechnology Information (NCBI) database, accession number XM_817363.1. *h*GCK nucleotide sequence was

obtained from Addgene Inc. using Addgene plasmid number 23750 (Jonannessen *et al.*, 2010). Reverse and forward primers (table 2.1) were designed using the ORFs and restriction sites were incorporated to facilitate cloning of the genes into the desired plasmids (section 2.4). The designed forward and reverse primers were evaluated for their theoretical parameters using freely available oligoanalyzer tool on the IDT DNA website. The primer sequences were blasted against the NCBI database. Primer properties were obtained using the oligoanalyzer tool available on the IDTDNA website. PCR fragments were virtually generated using the corresponding primers sets. These PCR fragments were used for *in silico* cloning, to assess the validity of the cloning procedures and to identify possible experimental problems that may be encountered. *In silico* cloning was achieved using pDRAW32 (AcaClone software, 2012). The generated *Tb*HK PCR fragment was cloned into the CloneJet® vector (figure 2.1A) and the generated *h*GCK PCR fragment was cloned into the pGEM-T® easy vector (figure 2.1B). The generated constructs were virtually digested using the restriction enzymes incorporated into the primer sequences to evaluate the digestion products. Evaluation of the recombinant proteins was also done using the pDRAW32 software. The generated *Tb*HK PCR fragment was cloned into the pET28b(+) vector (figure 2.2A) and the generated ORF proteins blasted against the NCBI database using the NCBI BLAST search tool. This verified whether the recombinantly expressed protein would have a fused N-terminal His-tag. The generated *h*GCK PCR fragment was cloned into the pET22b(+) vector (figure 2.2B) and the generated ORF proteins blasted against the NCBI database. This verified whether the recombinantly expressed protein would have a fused C-terminal His-tag.

Table 2.1: Oliginucleotide primers used for PCR amplification and sequence PCRs (underlined sequences indicated the introduced restriction sites for *NdeI* and *XhoI*).

Primer	**Sequence**	**Tm (°C)**
*Tb*Hex- *NdeI*	5'- CAT ATG TCT AGA CGC CTA AAC AAT ATC CTC G -3'	58.0
*Tb*Hex-*XhoI*	5'-CTC GAG TTA CTT GTC GTT CAC CAC C -3'	59.2
*h*GCK- *NdeI*	5'- ~~CAT ATG~~ CTG GAC GAC AGA GCC AGG -3'	61.3
*h*GCK-*Xho*I No stop codon (TGA)	5'- CTC GAG TCA CTG GCC CAG CAT ACA GG -3'	61.5

2.3. Gene amplification

2.3.1. Gradient PCRs

Genomic *Tb* DNA, a gift from Professor Buddy Ullman (Oregon Health Sciences University, USA) was used as template for the PCR amplification of the hexokinase gene. PCR reactions were carried out using a T100 Thermal Cycler (BIO RAD). A 100 µl master mixture was prepared and contained 20 µl 5x HF buffer, 2 µl of 10 mM dNTP's, 50 ng DNA template, 1 µl (0.02 U) Phusion Hot start polymerase, 1 µl of 10 µM of forward (*Tb*HK-*NdeI*) and reverse (*Tb*HK-*XhoI*) primers (table 2.1), filled to reaction volume with sterile distilled water. The master mixture was aliquoted (10 µl) into 8 separate PCR tubes, one for each of the selected annealing temperatures. Reaction conditions consisted of steps, durations and cycles as presented in table 2.2.

Table 2.2: Phusion hot start PCR reaction protocol.

	Temperature (°C)	**Duration (min)**	**Cycles**
Initial denaturation	98	3	
Denaturation	98	0.5	
Annealing	50 to 65	30	
Elongation	72	2.5	35x
Final elongation	72	10	
Hold	4	infinity	

PCR amplification of *h*GCK gene, a 100 µl master mixture was also prepared containing 10 µl of 10x buffer, 2 µl of 10 mM dNTP's, 50 ng NDA template (pDORN223-GCK plasmid), 1 µl of 10 µM forward and reverse primers (table 2.1), Expand high fidelity enzyme (2.6 U/reaction volume), filled to reaction volume with sterile distilled water. The master mixture was aliquoted (10 µl) into 8 separate PCR tubes, one for each of the selected annealing temperatures. A two step PCR protocol as stated in table 2.3, reactions were carried out using T100 Thermal Cycler (BIO RAD). The PCR products were analyzed by the use of agarose gel electrophoresis as described in section 2.3.3.

Table 2.3: Two step Expand polymerase PCR reaction protocol.

			Temperature (°C)	Duration (min)	Cycles
Step 1	A	Initial denaturation	94	2	
	B	Denaturation	94	0.5	
	C	Annealing (gradients)	45-65	0.5	
	D	Elongation	72	1.5	10x
Step 2	E	Initial denaturation	94	0.5	
	F	Annealing (gradients)	48-68	0.5	
	G	Elongation	72	2.5	20x
	H	Final elongation	72	10	
	I	Hold	4	infinity	

2.3.2. Optimized PCR reactions

The optimized PCR conditions ascertained from the PCR reactions described in section 2.3.1 were used to performed up-scaled PCR reactions (total reaction volume of 50 µl). The reaction mixture contained 10 µl 5X HF buffer, 1 µl 10 mM dNTP's, *Tb* gDNA (50 ng), 0.5 µl (0.02 U) Phusion hot start polymerase, 0.2 µl of 10 µmol forward (*Tb*HK-*NdeI*) and reverse (*Tb*HK-*XhoI*) primers (table 2.1), filled to the reaction volume with sterile redistilled water. A negative control reaction mixture containing everything as in the optimized mixture, except with the DNA template excluded, the negative control was run simultaneously with the optimized PCR reaction. PCR reaction conditions were as presented in table 2.2.

Up scale PCR amplification of the *h*GCK gene was done as follows: A 50 µl reaction mixture was prepared and consisted of 5 µl 10X buffer with $MgCl_2$, 1 µl 10 mM dNTP's, 50 ng DNA template, 1 µl (10 µM) forward (*h*GCK-*NdeI*) and 1 µl (10 µmol) reverse (*h*GCK-*XhoI* No stop codon) primers (table 2.1), Expand high fidelity enzyme (2.6 U / reaction volume) filled to the reaction volume with sterile redistilled water. The reaction conditions were as described in table 2.3. The PCR products and the negative control were prepared and run on 0.8% agarose gel as described in 2.3.3.

2.3.3. Agarose gel electrophoresis

All agarose gels consisted of 0.8% agarose in TAE buffer (0.04 M Tris-HCl, 1 mM EDTA pH 8.0 and 0.021 mM glacial acetic acid) with 0.6 $\mu g.ml^{-1}$ ethidium bromide. Separation of the DNA within the gel was achieved by running the gel at 100 V for 60-90 min. DNA was visualized

under a high radiation UV source (ChemiDoc XRS Gel Documentation system; Bio-Rad, USA) and a low radiation UV source (Darkreader, BioLabo, Switzerland), DNA fragment sizes were estimated based on electrophoretic mobility relative to that of the MassRuler™ DNA Ladder standards (Thermo Scientific) during the same electrophoretic run.

2.3.4. DNA gel extraction

After the PCR reaction was completed and after digestion of DNA, the products were run on agarose gel that was prepared as described in section 2.3.3, the DNA product to be extracted was visualizes using low radiation UV source at 365 nm (Darkreader, BioLabo, Switzerland) to limit DNA damage. The applicable band was excised from the gel using the BioFlux BioSpin gel extraction kit (Bioer Technology Co., Ltd), according to the manufacturer's recommendations. Briefly, the excised gel slice was added to extraction buffer and the samples incubated for 10 min at 50°C with periodic vortexing until the gel had completely liquefied.

The sample was transferred to a spin column and centrifuged at 6 000 *x*g for 1 min. The flow-through discarded. This was repeated until the entire sample had been loaded onto the column and the flow through discarded after each repeat. This was followed by washing the column with 500 µl of extraction buffer at 12 000 *x*g; 30 sec and the flow through again discarded. Seven hundred and fifty microliters of wash buffer was added and the column allowed standing for 5 min at room temperature. This was followed by centrifugation (12 000 *x*g; 60 sec) and the column transferred to a clean 1.5 ml Eppendorf tube. Fifty microliters of elution buffer was added onto the column and incubated for 15 min at 37°C. The DNA was eluted by centrifugation (12 000 *x*g; 60 sec). Concentration, purity and integrity of the nucleic acids were determined using a NanoDrop-2000 spectrophotometer at 260 nm (Thermal scientific, USA).

2.4. Ligations

The purified 1.4 kb *Tb*HK and *h*GCK PCR products were ligated into CloneJet® (Thermal Scientific) and pGEM-T® cloning vector system (Promega). Ligation reactions were set up using equations 2.1 and 2.2 to come up with the final concentrations and volumes of vector and insert DNA.

Equation 2.1:

$$\text{ng of insert} = \frac{\text{ng of vector} \times \text{kb size of insert}}{\text{kb size of vector}} \times \text{Insert : vector molar ratio}$$

Equation 2.2:

$$\mu\text{l of vector} = \frac{50 \text{ ng of vector}}{\text{ng of linearized vector}}$$

The ligation protocols were performed as per the manufacturer's instructions. For *Tb*HK ligation reaction was performed in a 20 µl reaction volume which consisted of 2 x ligation buffer, (10 µl), CloneJet® vector (50 ng), PCR product (8 µl) and T4 DNA ligase (0.3 Weiss units) with a 3:1 insert: vector DNA molar ratio. The ligation mixture was incubated for overnight at 4^{o}C. The purified 1.4 kb *h*GCK PCR product, it was ligated into pGEM-T® cloning system (Promega).

The ligation reaction was performed in a 20 µl total reaction volume consisting of 10x ligation buffer, (2 µl) pGEM-T® vector (50 ng), 6 µl PCR product (equation 2.1) and T4 DNA ligase (0.3 Weiss units) with a 1:1 insert : vector DNA molar ratio. The ligation mixture was incubated at 4°C, overnight. The 1.4 kb extracted *Tb*HK gene was ligated into pET28b(+) expression vector system (Thermal Scientific). A 10 µl reaction mixture consisted of 10x ligation buffer (1 µl), with a 1:1 insert: vector DNA molar ratio, pET28b(+) vector (50 ng), *Tb*HK gene insert (0.5 µl) and T4 DNA ligase (0.75 Weiss units) filled up to reaction volume with milliQ water. For the cleaned 1.4 kb *h*GCK gene, ligation into the linear pET22b(+) expression vector system (Thermal Scientific) was performed using the protocol as per the manufacturer's instructions. The ligation reaction was performed in a 10 µl final reaction volume which consisted of 10x ligation buffer (1 µl), with a 1:1 insert: vector DNA molar ratio, pET22b(+) vector (50 ng), *h*GCK gene insert (2.5 µl) and T4 DNA ligase (0.75 Weiss units) filled up to reaction volume with milliQ water. The ligation mixtures were then incubated at 4°C, overnight.

2.5. Preparation of competent cells

E. coli TOP10 (Invitrogen), JM109 (Promega) and BL21(DE3) containing the pRARE2 (Lucigen) plasmid, were made chemically competent using the protocol described by Hanahan (1983) with slight modifications. Briefly, flasks containing 100 ml Psi broth (5 $g.l^{-1}$ yeast extract, 20 $g.l^{-1}$ trypton, 5 $g.l^{-1}$ magnesium sulphate, pH 7.6 [adjusted with potassium hydroxide]) were inoculated with 1 ml of an overnight culture and incubated at 37°C until an optical density of 0.48 at 550 nm was achieved. Cells were placed on ice for 15 minutes, followed by centrifugation (3 000 *xg;* 5 min; 4°C). The supernatant was discarded and the pellets re-suspended in 40 ml TfbI buffer (30 mM potassium acetate, 100 mM rubidium chloride, 10 mM calcium chloride, 50 mM manganese chloride, 15% glycerol, pH 5.8 adjusted with acetic acid) and kept on ice for 15 minutes. This was followed by collection of the cells by centrifugation (3 000 *x*g*;* 5 minutes; 4^{o}C). The supernatant was discarded and pellets re-suspended in 4 ml TfbII buffer (10 mM 3- (N-morpholino) propanesulfonic acid (MOPS), 75 mM calcium chloride, 10 mM rubidium chloride, 15% glycerol, pH 6.5 adjusted with diluted sodium hydroxide). Cells were kept on ice for 15 min. The cooled cell suspension was aliquoted (50 µl) and snaps frozen in liquid nitrogen prior to storage at -80°C.

2.6. Transformations

A stock (50 µl / 100 µl) of the chemically competent *E. coli* strain (section 2.5) was retrieved from the -80°C freezer and placed on ice to thaw (~5 min). The ligation mixture / plasmids was transferred to the competent cells and the transformation mixture kept on ice for 30 min after which it was heat shocked at 42°C for 40 seconds and placed back on ice for 2 min. Two hundred and fifty microliters pre-heated (37°C) SOC media (20 $g.l^{-1}$ tryptone, 5 $g.l^{-1}$ yeast extract, 0.01 M NaCl, 2.5 mM KCl, 0.01 M $MgCl_2$, 0.01 M $MgSO_4$ and 0.02 M glucose) was added to the transformation mixture and incubated at 37°C for 1 h with intermittent gentle shaking. After the 1 h incubation, various aliquots (200 µl and 100 µl) of the transformed cultures were spread plated onto LB agar plates containing the appropriate antibiotic/s to maintain selective pressure and incubated at 37°C for 14-16 h. Positive transformants were inoculated into 5 ml LB media containing the appropriate antibiotic and grown for 16 h at 37°C. DNA mini-preparations followed the 16 h growth of the positive transformants as described in section 2.7. *E. coli* cells transformed with pET22b(+) and CloneJet® were spread plated onto

AMP/CAM plates (100 µg.ml^{-1}). *E. coli* cells that were transformed with pET28b(+) pRARE2 was spread plated onto KAN/CAM plate (30 µg.ml^{-1} and 34 µg.ml^{-1}).

When the pGEM®-T easy vector system was used, various aliquots of the transformed culture was plated onto LB plates containing ampicillin (100 µg.ml^{-1}), isopropyl β-D-thiogalactoside (IPTG, 0.12 mg.ml^{-1}) and 5-bromo-4-chloro-3-indolyl β-D-galactoside (X-Gal, 0.08 mg.ml^{-1}) and incubated overnight at 37°C to verify DNA ligation using blue / white selection. Positive transformants were inoculated into 5 ml LB media containing 100 µg.ml^{-1} ampicillin to maintain selective pressure and grown for 16 h at 37°C. DNA mini-preparations followed the 16 h growth of the positive transformants as described in section 2.7.

2.7. DNA plasmids extraction

DNA mini-preparations followed the 16 h growth of the positive transformants (section 2.6). This was performed using the BioFlux BioSpin Plasmid Extraction Kit as per the manufacturer's recommendations (Bioer Technologies Co, Ltd). Briefly; the cultured bacterial cells were centrifuged down at 10 000 *x*g for 30 sec and the supernatant discarded. Resuspension buffer (250 µl) was added followed by lysis buffer (250 µl), gently inverted (4-6 times). Neutralization buffer (350 µl) was added and gently inverted (4-6 times). Tubes were centrifuged at 13 000 *x*g (10 min), supernatants were transferred into spin columns, centrifuged at 6 000 *x*g (1 min), the flow through were discarded and wash buffer (650 µl) was added and centrifuged at 6 000 *x*g (1 min), this was done twice followed by a third dry spin. The columns were transferred into 1.5 ml Epperndorf tubes, elution buffer (50 µl) was added and tubes were incubated at 37°C for 15 minutes. This was followed by a final spin (12 000 *x*g) for 1.5 min. DNA concentrations were determined using a NanoDrop ND 2 000 spectrophotometer as described in section 2.3.4.

2.8. Screening for inserts

Plasmids obtained as described in section 2.7 were screened to confirm insertion of *Thr*HK and *h*GCK genes. The plasmids were subjected to a double digestion using *NdeI* and *XhoI* restriction enzymes. Reaction conditions for the selected restriction enzymes were obtained using the double digestion tool available on the Fermentas website. Table 2.4 lists the relationship between the selected restriction enzymes.

Table 2.4: Showing features of selected restriction enzymes.

Enzyme	Temperature (°C)	Amount	Buffer	Percentage (%)
NdeI	37	1x	*O*	100
XhoI	37	2x	*O*	100

Double digestion reaction mixtures (20 µl) were prepared and contained *NdeI* (1 µl), *XhoI* (2 µl), 10x buffer O (2 µl), 50 ng of plasmid (using equation 2.1 and 2.2), filled to reaction volume with sterile redistilled water. The double digestion mixtures were incubated at 37°C, overnight and run on an agarose gel as described in section 2.3.3.

2.9. Sequence verification

Plasmids with a positive restriction enzyme digestion profile (sections 2.8) were sent to Inqaba Biotech, (Hatfield, Pretoria, Gauteng, South Africa) for sequencing. Sequencing PCR reactions were done using the BigDye terminator kit (ABI, Life Technologies, Carlsbad, USA) according to manufacturer's instructions. The PCR reactions were cleaned using the Zymo research sequencing clean-up kit (Zymo Research). The clean products were subsequently analyzed using a 3500 XL Genetic Analyzer (ABI, Life Technologies, Carlsbad, California, USA). Electropherograms were analyzed and edited using Geospiza's FinchTV (version 1.4.0). Reverse complementation was performed using BioEdit (Hall, 1999). Sequence alignments were performed using DNAssist version 3.0.

2.10. Results and discussions

The following sub-sections of the current chapter presents the outcomes of the experimental work done to obtain *Tb*HK and *h*GCK expression ready constructs.

2.10.1. *Tb*HK and *h*GCK gene amplifications

Virtual cloning processes (section 2.2.2) conducted on the expression vectors indicated that both proteins (*Tb*HK and *h*GCK) would be expressed in frame with the N-terminal His-tag for *Tb*HK and C-terminal His-tag for *h*GCK. C-terminal His-tagged proteins can be purified using the same purification techniques as the N-terminal His-tag without significant protein activity differences.

Studies have shown that in some cases the N-terminal His-tag may not be accessible for metal affinity purification strategy; therefore the use of the C-terminal His-tag may circumvent the problem (Eschenfeldt *et al*., 2011). His-tags have shown to provide good yields of recombinant proteins as compared to other tags in use i.e. Maltose-binding protein tag (MBP tag), Glutathione S-transferase-tag (GST-tag) (Lichty *et al*., 2005), however no sole affinity tag is most advantageous in regards of all the required properties of a tag (Arnau *et al*., 2005; Waugh, 2005). Gradient PCRs (section 2.3.1) performed using *h*GCK as template indicated an optimum Tm of 59°C and this parameter was used during the upscale PCR reaction, evidenced by the 1.4 kb band that was obtained (figure 2.3.B) (Lynch *et al.,* 2000; Desai *et al.,* 2001; Willson *et al.,* 2002).

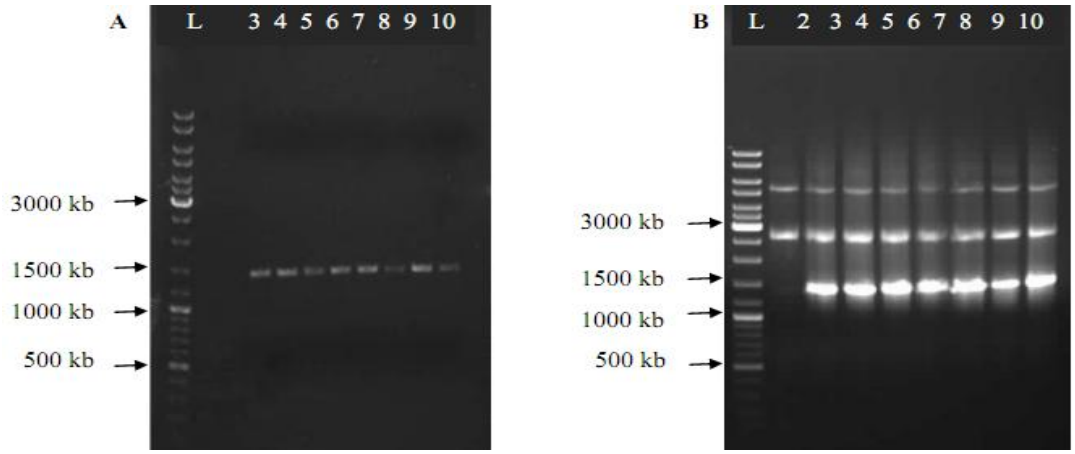

Figure 2.3: (A) Agarose gel image of the gradient PCR amplified *TbHK* gene. B: Agarose gel image showing the amplified *h*GCK gene by gradient PCR.

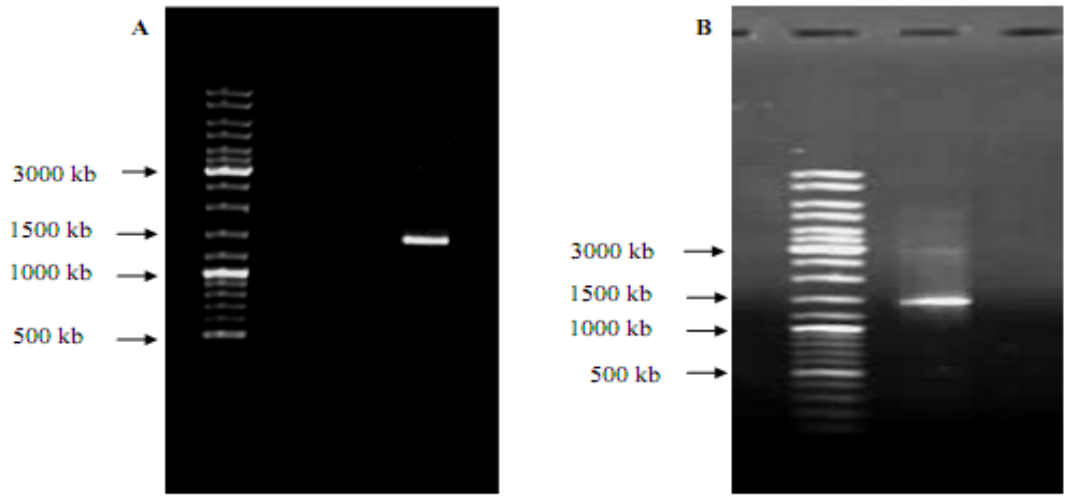

Figure 2.4 (A) Agarose gel image of the amplified *Tb*HK gene. (B) Agarose gel image showing the amplified *h*GCK gene.

The *Tb*HK (TREU 927) and human glucokinase genes were amplified by the optimized PCR reaction as described in section 2.3.2. The 1.4 kb bands were obtained (figure 2.4A for *Tb*HK and figure 2.4B for *h*GCK), confirming amplification of the target genes. The bands corresponding to the 1.4 kb products were purified from the gels using the BioFlux, BioSpin Gel Extraction kit as described in section 2.3.4. The extracts were stored at -20°C for further downstream experiments.

2.10.2. Cloning and sequencing

2.10.2.1. Cloning of *Tb*HK and *h*GCK

The PCR amplified and gel purified *Tb*HK and *h*GCK genes (sections 2.3.2 and 2.3.4) were ligated into CloneJet® and pGEM®-T easy cloning vector systems respectively as described in section 2.4. The virtual cloning of the 2 genes into the respective cloning vectors confirmed the viability of the cloning procedures (figures 2.5A and B). The cloning experiments commenced with the ligation of gel extracted PCR products into the CloneJet® cloning vector for *Tb*HK and pGEM-T® easy cloning vector for *h*GCK (Section 2.4). The *Tb*HK ligation mixture was transformed into competent *E. coli* JM109 cells, while the *h*GCK ligation mixture was transformed into competent *E. coli* TOP10 cells as described in sections 2.6.

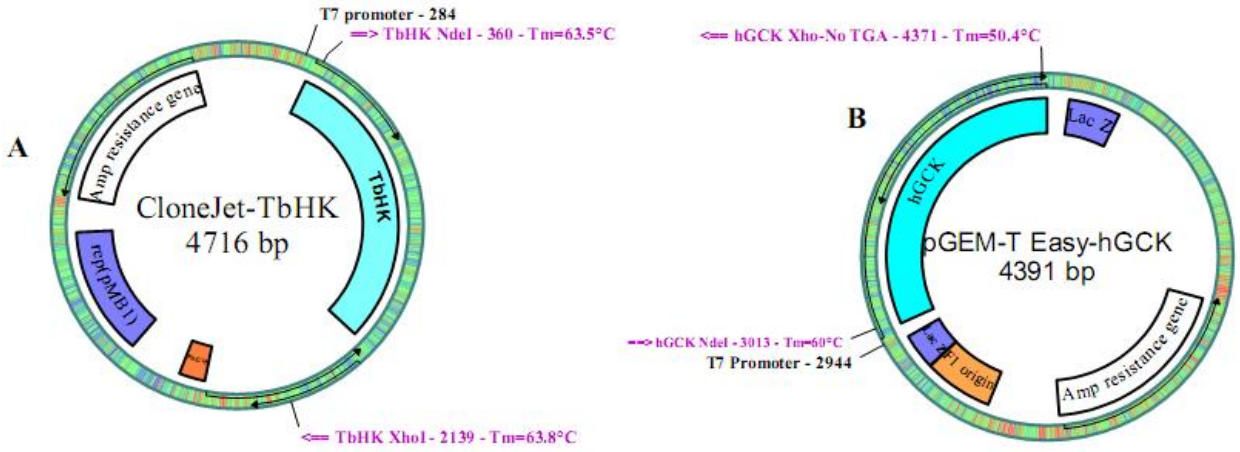

Figure 2.5: (A) Vector map of CloneJet® indicating ampicillin resistance gene, T7 promoter and *Tb*HK gene insert. (B) Vector map of pGEM-T® easy vector indicating ampicillin resistance gene, F1 origin of plasmid replication, T7 promoter and LacZ coding sequence and *h*GCK gene insert.

For *Tb*HK, 5 single colonies were picked and aseptically sub-cultured in LB broth supplemented with 100 µg.ml^{-1} ampicillin. Plasmids were extracted using the BioFlux Biospin plasmid extraction kit (Section 2.7). Plasmids were subjected to double digestion reactions using *NdeI* and *XhoI* restriction enzymes as described in section 2.8. Double digestion reactions were separated on an agarose gel (section 2.3.3). Figure 2.6A shows that plasmids 1 (lane 4), plasmid 2 (lane 5) and plasmid 4 (lane 7) had positive gene inserts (a 1.4 kb band corresponding to the *Tb*HK gene insert and a 2.9 kb band corresponding the cloneJet® backbone). Plasmid extract 1 was sequenced by Inqaba Biotech (Hatfield, Pretoria, Gauteng, South Africa) for sequencing as described in section 2.9.

For *h*GCK five single colonies were picked and aseptically sub-cultured in LB broth supplemented with 100 µg.ml^{-1} ampicillin. Plasmids were extracted using the BioFlux Biospin plasmid extraction kit (Section 2.7). Plasmids were subjected to double digestion reactions using *NdeI* and *XhoI* restriction enzymes as described in section 2.8. Double digestion reactions were separated on an agarose gel (section 2.3.3.).

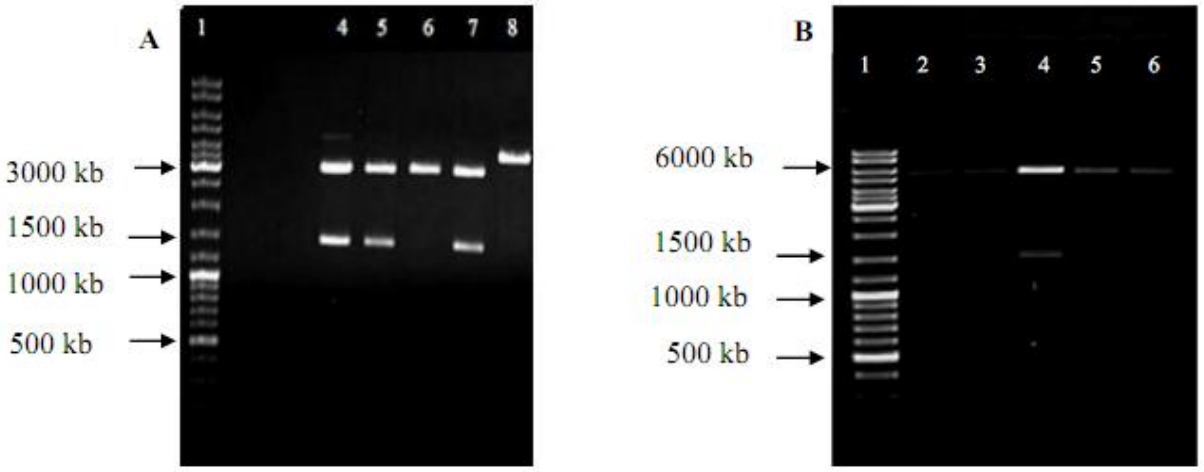

Figure 2.6: (A) CloneJet® plasmid containing *Tb*HK gene digested with *Nde*I and *Xho*I. Lane 1 represents MassRuler™ DNA Ladder standards (Thermo Scientific) and lanes 4 to 8 represents cloned plasmids screened for gene inserts. (B) pGEM-T® easy plasmid containing *h*GCK gene digested with *NdeI* and *XhoI.* Lane 1 represents the marker and lanes 2 to 6 represents cloned plasmids screened for gene inserts.

Figure 2.6B shows that plasmid number 3 (lane 4) had a positive gene insert (1.4 kb band corresponding to the *h*GCK gene insert and a 5.4 kb band corresponding the pGEM-T® easy backbone). Plasmid number 3 was sequenced by Inqaba Biotech (Hatfield, Pretoria, Gauteng, South Africa) for sequencing as described in section 2.9.

2.10.2.2 Sequence analysis

Sequencing results for both *Tb*HK and *h*GCK were analyzed using Finch TV version 1.4.0, BioEdit version 7.2.3 and DNAssist version 3.0 software as described in section 2.9. After aligning *Tb*HK sequencing results with the reference *Tb*HK gene using DNAssist (figure 2.7), it showed a 99% identity to the reference gene (NCBI accession number XM_817363.1) and the translated protein sequence of the cloned *Tb*HK gene with the protein sequence from NCBI accession number XM_817363.1 100% identical (figure 2.8).

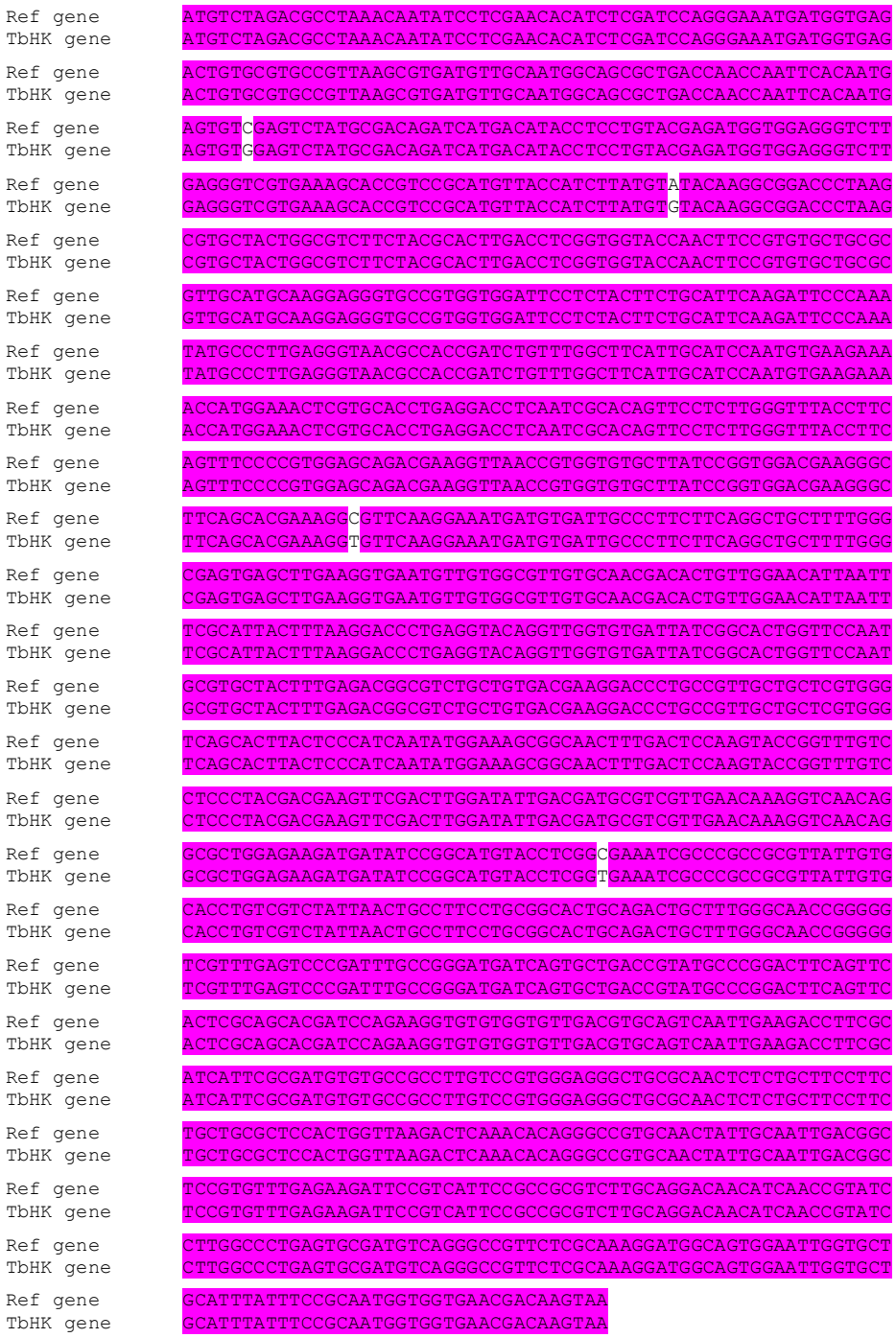

Figure 2.7: Alignments of the reference hexokinase gene sequence of *Tb* TREU 927and the cloned *Tb*HK gene.

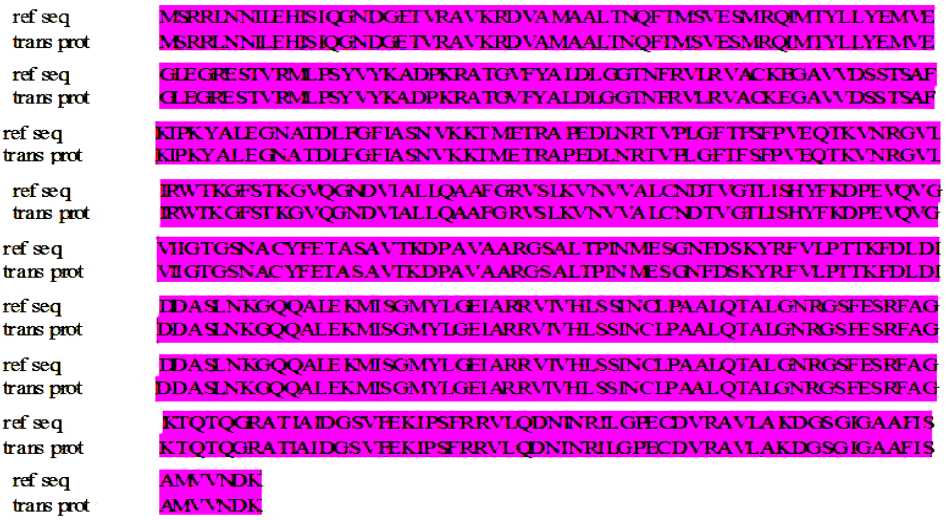

Figure 2.8: Alignments of reference protein sequence of *Tb*HK TREU 927 and the translated protein sequence of the sequenced *Tb*HK gene.

Alignments of the sequencing results for the *h*GCK gene (figure 2.9) showed a 100% identity to the Addgene author sequence, and the translated protein sequence of the cloned *h*GCK gene with the translated protein sequence were 100% identical (figure 2.10).

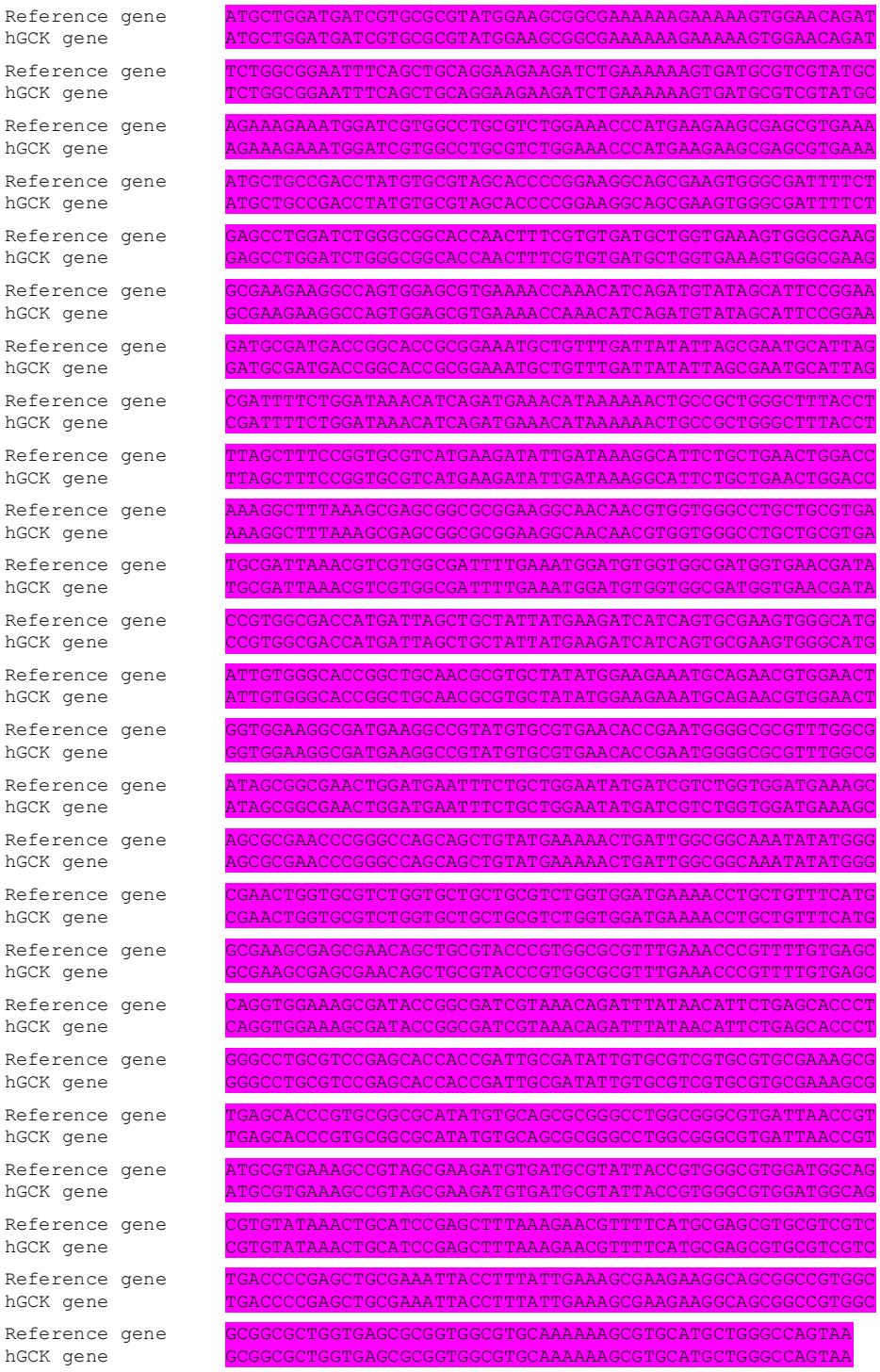

Figure 2.9: Alignments of the reference gene sequence of *h*GCK cDNA and the cloned *h*GCK gene.

trans prot	MLDDRARMEAAKKEKVEQILAEFQLQEEDLKKVMRRMQKEMDRGLRLETHEEASVKMLPTYV
ref seq	MLDDRARMEAAKKEKVEQILAEFQLQEEDLKKVMRRMQKEMDRGLRLETHEEASVKMLPTYV
trans prot	RSTPEGSEVGDFLSLDLGGTNFRVMLVKVGEGEEGQWSVKTKHQMYSIPEDAMTGTAEMLFD
ref seq	RSTPEGSEVGDFLSLDLGGTNFRVMLVKVGEGEEGQWSVKTKHQMYSIPEDAMTGTAEMLFD
trans prot	YISECISDFLDKHQMKHKKLPLGFTFSFPVRHEDIDKGILLNWTKGFKASGAEGNNVVGLLR
ref seq	YISECISDFLDKHQMKHKKLPLGFTFSFPVRHEDIDKGILLNWTKGFKASGAEGNNVVGLLR
trans prot	DAIKRRGDFEMDVVAMVNDTVATMISCYYEDHQCEVGMIVGTGCNACYMEEMQNVELVEGDE
ref seq	DAIKRRGDFEMDVVAMVNDTVATMISCYYEDHQCEVGMIVGTGCNACYMEEMQNVELVEGDE
trans prot	GRMCVNTEWGAFGDSGELDEFLLEYDRLVDESSANPGQQLYEKLIGGKYMGELVRLVLLRLV
ref seq	GRMCVNTEWGAFGDSGELDEFLLEYDRLVDESSANPGQQLYEKLIGGKYMGELVRLVLLRLV
trans prot	DENLLFHGEASEQLRTRGAFETRFVSQVESDTGDRKQIYNILSTLGLRPSTTDCDIVRRACE
ref seq	DENLLFHGEASEQLRTRGAFETRFVSQVESDTGDRKQIYNILSTLGLRPSTTDCDIVRRACE
trans prot	SVSTRAAHMCSAGLAGVINRMRESRSEDVMRITVGVDGSVYKLHPSFKERFHASVRRLTPSC
ref seq	SVSTRAAHMCSAGLAGVINRMRESRSEDVMRITVGVDGSVYKLHPSFKERFHASVRRLTPSC
trans prot	EITFIESEEGSGRGAALVSAVACKKACMLGQ
ref seq	EITFIESEEGSGRGAALVSAVACKKACMLGQ

Figure 2.10: Alignments of reference protein sequence of *h*GCK and the translated protein sequence of the sequenced *h*GCK gene.

2.11. Construction of expression vectors

Figure 2.11A and B show the results obtained for the virtual cloning of both the sequence verified.

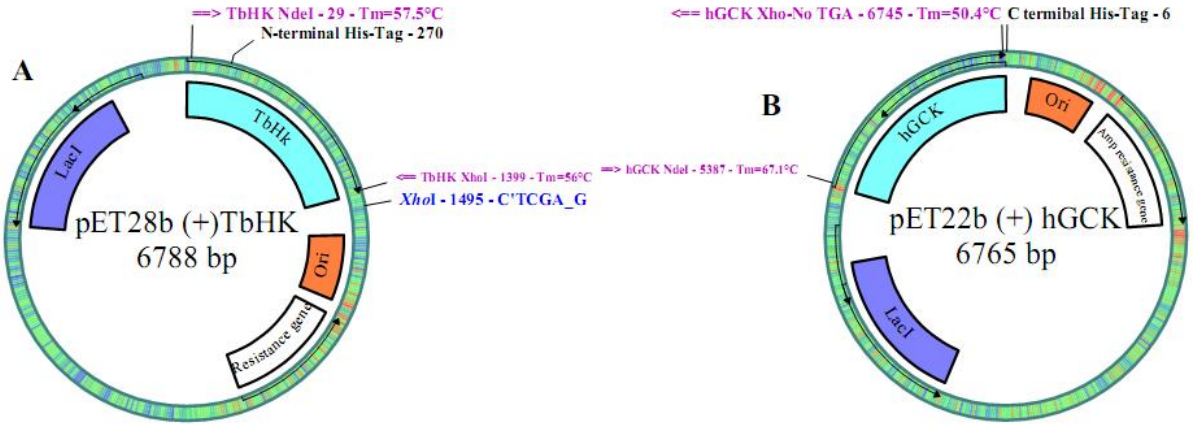

Figure 2.11 A: Vector map of pET28b(+) expression vector indicating ampicillin resistance gene, N-terminal His-tag, ori, *LacI* and *Tb*HK gene insert. B**:** Vector map of pET22b(+) expression vector indicating ampicillin resistance gene, origin of plasmid replication, C-terminal His-tag, *Lac*I and *h*GCK gene insert.

*Tb*HK and *h*GCK genes were ligated into the respective expression vectors as described in section 2.4. Analysis of the open reading frames indicated that both the proteins will be expressed in frame with the desired 6 Histidine tag. An N-terminal tag for *Tb*HK (figure 2.12) and a C-terminal tag for *h*GCK (figure 2.13).

MGSS**HHHHHH**SSGLVPRGSHMSRRLNNILEHISIQGNDGETVRAVKRDVAMAALTNQF
TMSVESMRQIMTYLLYEMVEGLEGRESTVRMLPSYVYKADPKRATGVFYALDLGGTN
FRVLRVACKEGAVVDSSTSAFKIPKYALEGNATDLFGFIASNVKKTMETRAPEDLNRTV
PLGFTFSFPVEQTKVNRGVLIRWTKGFSTKGVQGNDVIALLQAAFGRVSLKVNVVALCN
DTVGTLISHYFKDPEVQVGVIIGTGSNACYFETASAVTKDPAVAARGSALTPINMESGNF
DSKYRFVLPTTKFDLDIDDASLNKGQQALEKMISGMYLGEIARRVIVHLSSINCLPAALQ
TALGNRGSFESRFAGMISADRMPGLQFTRSTIQKVCGVDVQSIEDLRIIRDVCRLVRGRA
AQLSASFCCAPLVKTQTQGRATIAIDGSVFEKIPSFRRVLQDNINRILGPECDVRAVLAKD
GSGIGAAFISAMVVNDK

Figure 2.12: Sequence analysis of the ORF for the inserted *Tb* gene showing in frame expression with the N-terminal His-tag (bold and underlined).

MLDDRARMEAAKKEKVEQILAEFQLQEEDLKKVMRRMQKEMDRGLRLETHEEASVM
LPTYVRSTPEGSEVGDFLSLDLGGTNFRVMLVKVGEGEEGQWSVKTKHQMYSIPEDAM
TGTAEMLFDYISECISDFLDKHQMKHKKLPLGFTFSFPVRHEDIDKGILLNWTKGFKASG
AEGNNVVGLLRDAIKRRGDFEMDVVAMVNDTVATMISCYYEDHQCEVGMIVGTGCNA
CYMEEMQNVELVEGDEGRMCVNTEWGAFGDSGELDEFLLEYDRLVDESSANPGQQLY
EKLIGGKYMGELVRLVLLRLVDENLLFHGEASEQLRTRGAFETRFVSQVESDTGDRKQI
YNILSTLGLRPSTTDCDIVRRACESVSTRAAHMCSAGLAGVINRMRESRSEDVMRITVG
VDGSVYKLHPSFKERFHASVRRLTPSCEITFIESEEGSGRGAALVSAVACKKACMLGQLE
HHHHHH

Figure 2.13: Sequence analysis of the ORF for the inserted human glucokinase gene showing in frame expression with the C-terminal His-tag (bold and underlined)

Experimental assembly of the individual expression constructs started with the removal of the inserts from the CloneJet® and pGEM-T® easy constructs through double digestion reactions using *NdeI* and *XhoI* as described in section 2.8. The inserts were separated from the backbone fragments on a 0.8% agarose gel (section 2.3.3) and purified from the gel (section 2.3.4). The purified inserts were ligated into *NdeI* and *XhoI* linearised and gel purified pET vectors. *Tb*HK was sub-cloned into pET28b(+) and *h*GCK into pET22b(+) as described in section 2.4. For the *Tb*HK pET28b(+) constructs, 4 single colonies were picked and aseptically sub-cultured in LB

broth supplemented with 30 µg.ml^{-1} kanamycin. Plasmids were extracted using the BioFlux Biospin plasmid extraction kit (Section 2.7). Plasmids were subjected to double digestion reactions using *NdeI* and *XhoI* restriction enzymes as described in section 2.8. Double digestion reactions were separated on an agarose gel (section 2.3.3). Figure 2.14 showed four clones were positive for gene insertion. Clone 1 (lane 3) was selected for expression experiments and stored at -20°C.

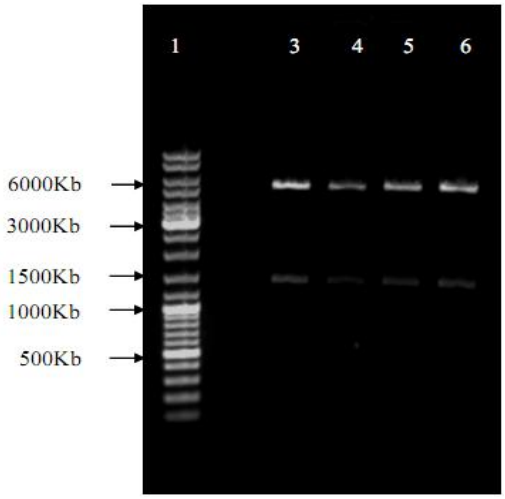

Figure 2.14: pET28b(+) plasmid containing *Tb*HK gene, double digested with *Xho*I and *Nde*I restriction enzymes. Lane 1 represents the DNA ladder, lanes 3 to 6 represents the clones screened for positive gene inserts.

For the *h*GCK pET22b(+) construct 6 single colonies were picked and aseptically sub-cultured in LB broth supplemented with 100 µg.ml^{-1} ampicillin. Plasmids were extracted using the BioFlux Biospin plasmid extraction kit (Section 2.7).

Plasmids were subjected to double digestion reactions using *NdeI* and *XhoI* restriction enzymes as described in section 2.8. Double digestion reactions were separated on an agarose gel (section 2.3.3). Figure 2.15 shows that 4 clones had insertion of the desired gene and clone 2 (lane 3) was selected for expression experiments and stored at -20°C.

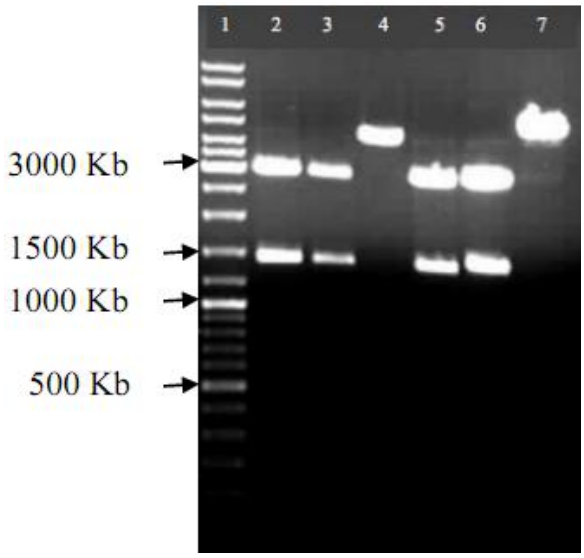

Figure 2.15: pET22b(+) plasmid containing human glucokinase gene, double digested with *Xho*I and *Nde*I restriction enzymes. Lane 1 represents the DNA ladder, lanes 2 to 7 represents the clones screened for positive gene inserts.

2.12 Conclusions

Both the *h*GCK and *Tb*HK genes were successfully PCR amplified and cloned into the respective cloning vectors (CloneJet® and pGEM-T® easy). Sequencing results showed that no mutations were incorporated during the amplification. The translated *Tb*HK and *h*GCK protein sequences with their translated reference sequences, revealed a 100% sequence identity. The sequence verified genes were sub-cloned into their respective expression vectors. pET28b(+) for *Tb*HK and pET22b(+) for *h*GCK that will facilitate N-terminal and C-terminal His-tagged *Tb*HK and *h*GCK expressions respectively (Chapter 3). Screening of the ligated pET28b(+) harboring *Tb*HK gene and pET22b(+) harboring *h*GCK gene showed positive insertion of the genes of interest.

The results obtained in this chapter allow the continuation of the research project. Since both *Tb*HK and *h*GCK genes were PCR amplified without mutations and successfully cloned into the expression vectors. This will be followed by transforming the gene constructs into the expression cell lines and continue with expression, purification and characterization of the respective recombinant proteins.

Chapter 3

Recombinant hexokinase expression and purification

3.1. Introduction

Recombinant proteins can be expressed and purified in high quantities in vector systems which can easily be handled in the laboratory. Bacteria, yeast, insect and mammalian cell systems have been reported and employed in the production of recombinant proteins (Rai and Padh, 2001). The expression and purification of the two enzymes (*Tb*HK and *h*GCK) will allow the comparison of the effects of silver NPs on their activities (chapter 4).

3.1.1. Recombinant protein expression systems

The choice of an expression system depends on several factors including; levels of expression, cell growth characteristics, intracellular and extracellular expression capabilities, post-translational modifications and biological activity of the protein of interest (Makrides, 1996).

3.1.1.1. Bacterial system

E. coli is one of the most widely used host organism for recombinant protein expression (Baneyx and Mujacic, 2004; Berrow *et al*., 2006). *E. coli* have various advantages as an expression host, these include; easy and rapid growth in large numbers on cheap media and the strain used for this purpose is non-invasive to humans and the environment (Rai and Pagh, 1996; Baneyx, 1999; Chart *et al*., 2000; Sørensen and Mortensen, 2004). For the optimization of recombinant protein expression in these prokaryotic expression systems, strategies have been developed to maximize the yields of the expressed proteins. These strategies include the configuration of the genetic elements that affect the transcriptional and translational stages of the proteins (Hannig and Makrides, 1998).

Expression of recombinant proteins in *E.coli* can be induced either by isopropyl β-D-1-thiogalactopyranoside (IPTG) or auto-induction methods. Of these, IPTG is more often used as the recombinant protein expression inducer. Protein expression induced by IPTG is based on the *lac*-type promoter; the *lac*-promoter is situated next to the *lacI* gene that suppresses the

transcription of the promoter. The removal of this repression by IPTG initiates transcription of the *lac*-promoter, thus protein expression. A small amount of IPTG is enough to induce recombinant protein expression. However, high concentrations of IPTG may negatively affect cell growth (Hansen *et al.*, 1998).

Several papers have been published on the use of the auto-induction method for the expression of recombinant proteins (Sreenath *et al*., 2005; Studier *et al*., 2005; Tyler *et al*., 2005). In this method, the production of recombinant protein is based on the function of lac-operon regulatory elements in a mixture of glucose, glycerol and lactose (Jacob and Monod, 1961). During the initial phase of growth, glucose is the first metabolite used as a carbon source and protein expression is low due to catabolite repression of alternative carbon utilization pathways and binding interactions between *lacI* and lac-operators (lacO). As glucose levels decrease, the catabolite repression is relieved; leading to a shift in cellular metabolism toward consumption of lactose and glycerol. The use of lactose results in the production of allolactose. Allolactose then acts as the physiological inducer of the lac-operon (Holms, 1996; Wong *et al*., 1997).

Auto-induction is advantageous over conventional recombinant protein expression protocols because it requires no monitoring of cell growth, it minimizes the required handling of cultures from inoculation until harvesting, produces high cell mass for harvesting, it is useful for the simultaneously induction of numerous expression clones and it can easily be performed for both small-scale screening and large-scale production (Studier *et al*., 2005; Sreenath *et al*., 2005; Tyler *et al*., 2005).

3.1.1.2. Yeast systems

Yeast systems are alternative expression systems to bacterial systems; they are mostly used in the production of pharmaceutical recombinant proteins. *S. cerevisiae*, *H. polymorphia* (Gellisen and Hollenberg, 1996), *P. pastoris* (Cereghino and Cregg, 2000) have been used in the production of recombinant proteins.

3.1.1.3. Insect cell systems

Bacculovirus vectors have been used in the production of recombinant proteins in insect cells. Insect cells have presented several advantages over other systems including; their easiness to culture, their higher tolerance to osmotic pressure and higher levels of expression (Rai and Padh, 2001; Ikonomou *et al*., 2003).

3.1.1.4. Mammalian cell systems

Some proteins that need post translational modification are expressed in mammalian cell line (Rai and Padh, 2001). Host cell types include; human embryonic kidney (HEK), baby hamster kidney (BHK) and Chinese hamster ovary (CHO) have been used to synthesize various recombinant proteins (Wurm and Benard, 1999; Matasci *et al*., 2003; Rosser *et al*., 2005; Hasebe *et al*., 2012).

The current chapter describes the expression and purification of 50 kDa proteins encoded by a 1 417 bp and 1 398 bp region of the genes that code for *Tb*HK and *h*GCK proteins, respectively. Previously, *Tb*HK and *h*GCK genes have been sub-cloned into *E. coli* pGE30 expression vectors for their expression in M15 (pREP) and *E. coli* M15 bacterial expression systems (Tiedge *et al*., 1997 and 2000; Morris *et al*., 2006). In the current study, *Tb*HK and *h*GCK genes were sub-cloned into pET28b(+) and pET22b(+) , respectively for over-expression in an *E. coli* BL21(DE3) bacterial expression system harbouring the pRARE2 plasmid. The expressed proteins will be purified using experimental procedures such as; (i) ultra-centrifugation. The rate at which these molecules sediment is dependent on the centrifugal force, shape, size and as well as the density of the particles, the density and viscosity of the suspended medium; (ii) immobilized metal ion affinity chromatography (IMAC) using a fast protein liquid chromatography system (FPLC); (iii) size exclusion chromatography, that employs the separation of proteins, polysaccharides, nucleic acids, and other biological macromolecules according to their differences in size and (iv) dialysis, which is based on the diffusion phenomenon of the smaller sized molecules through a semi permeable membrane (snake skin) until equilibrium is reached. This process allows for exchange of buffers and removal of low molecular weight contaminants without significant loss of the molecules of interest. Purified proteins will be characterized in terms of pH and temperature stability and kinetic properties.

The aims of this chapter are:

1. Expression of recombinant *Tb*HK and *h*GCK proteins.
2. Purification of the recombinant proteins (*Tb*HK and *h*GCK proteins).
3. Characterization of the purified *Tb*HK and *h*GCK proteins to obtain optimum conditions and thermal stability.
4. Determination of kinetic parameters of the purified proteins.

3.2. Methods and materials

The current section will outline procedures, equipment and consumables that were utilized in the expression, enzyme purification, optimization and characterization experiments.

3.2.1. Recombinant protein expression by auto-induction

An adaptation of the protocol that was first described by Studier *et al.* (1995) was employed in the current study for the expression of the *Tb*HK and *h*GCK proteins.

3.2.1.1. Preparation of glycerol stocks

After confirmation of the positive insertion of the *Tb*HK and *h*GCK genes into pET28b(+) or pET22b(+) expression vectors respectively, (Chapter 2, section 2.11), 2 µl of each construct was transformed into competent *E. coli* BL21(DE3) cells containing the pRARE2 plasmid using the transformation protocol described in section 2.6. Cells transformed with the pET28b(+) constructs were plated on LB plates containing 30 $\mu g.ml^{-1}$ Kan and Cam 34 $\mu g.ml^{-1}$ concentrations of antibiotics to maintain selective pressure and incubated at 37°C for 12-16 h. After growth, a swipe of the transformed colonies was sub-cultured in 50 ml LB broth containing the appropriate antibiotics. Sub-cultures were grown for 12-16 h at 30°C, revolving at 150 rpm on a PSU20 multishaker (BOECO, Germany). After growth, 1 ml aliquots of the cell cultures were added to 0.5 ml pre-sterilized 50% glycerol and mixed thoroughly followed by stored at -80°C for further downstream experiments. Glycerol stocks of cells carrying empty constructs pET22b(+) and pET28b(+) were also prepared in the same manner.

3.2.1.2. Pre-cultures for auto-inductions

The glycerol stock prepared in section 3.2.1.1 was revived prior to inoculation of the auto-induction media. For pET28b(+) constructs, 1 ml of the glycerol stock was aseptically inoculated into 50 ml LB broth containing the appropriate antibiotics (30 $\mu g.ml^{-1}$ kanamycin and 34 $\mu g.ml^{-1}$ chloramphenicol) in a 250 ml Erlenmeyer flask. For pET22b(+) plasmid containing *h*GCK, 1 ml of its glycerol stock was inoculated into 50 ml of LB broth with the appropriate antibiotics (100 $\mu g.ml^{-1}$ ampicillin and 34 $\mu g.ml^{-1}$ chloramphenicol) in a 250 ml Erlenmeyer flask. Pre-cultures were incubated at 30°C for 12-16 h, aerobically, revolving at 150 rpm on a PSU20 multishaker (BOECO, Germany). Pre-cultures for the auto induction negative controls empty pET28b(+) and pET22b(+) were also prepared similarly.

3.2.1.3. Inoculation for auto induction

After the 16 h incubation (section 3.2.1.2), 10 ml of the *Tb*HK pre-culture was aseptically inoculated into 1 liter of ZYP/5052 auto induction media composed of pre-sterilized 928 ml of ZY media (10 $mg.l^{-1}$ tryptone, 5 $mg.l^{-1}$ yeast extract), 50 ml of 20x NPS [0.5 M ammonium sulfate $(NH_4)_2SO_4$), 1 M mono-potassium phosphate (KH_2PO_4), 1 M sodium phosphate dibasic ($Na_2 HPO_4$)], 20 ml of 50x 5,052 (250 $g.l^{-1}$ glycerol, 25 $g.l^{-1}$ glucose, 100 $g.l^{-1}$ α-lactose), 2 ml of filter sterilized 1 M magnesiumsulfate ($MgSO_4$). The media was supplemented with 30 $\mu g.ml^{-1}$ kanamycin and 34 $\mu g.ml^{-1}$ chloramphenicol to maintain selective pressure. A hundred milliliters of the auto induction mixture was aliquoted into 10x 500 ml Erlenmeyer flask aseptically (with intermittent flaming).

For the human glucokinase, 10 ml of the pre-culture was inoculated into 1 liter of ZYP/5052 auto induction media with added 100 $\mu g.ml^{-1}$ ampicillin and 34 $\mu g.ml^{-1}$ chloramphenicol to maintain selective pressure. Similarly 100 ml aliquots were prepared. For the negative control of *Tb*HK protein empty pET28b(+) plasmid, 1 ml of the pre-culture was also aseptically inoculated into 100 ml of ZYP/5052 auto induction media. For the negative control of the human glucokinase protein, 1 ml of the negative control pre-culture empty pET22b(+) plasmid was also aseptically inoculated into 100 ml of ZYP/5052 auto induction media with appropriate antibiotics. Erlenmeyer flasks containing the auto induction mixture and the negative controls were then incubated aerobically at 20°C for 36 h, revolving at 150 rpm (Labotec, RSA).

3.2.1.4. Auto-induction studies

The levels of protein expression were assessed over time by collecting 500 µl of the cultures at specific times. Samples were collected at 0, 6, 12, 18, 24, 30 and 36 h intervals. Collected samples were immediately centrifuged down at 12 000 *x*g for 10 minutes, the supernatant was discarded and the pellet stored at -20°C for further experiments. The frozen cell pellets of the auto induction study samples were thawed, re-suspended in 1 ml 50 mM Tris HCl buffer, pH 8.0 and sonicated thrice at 100 mA for 30 sec (Sonics and materials Inc. USA). Samples were stored at 4°C pending further analysis. The protein concentration of the collected fractions will be determined (section 3.2.4) and subjected to SDS-PAGE analysis as described in section 3.2.3.1.

3.2.2. Protein purification

3.2.2.1. Biomass harvesting, washing

After the 36 h of incubation (section 3.2.1.3) at 20°C, biomass was harvested and washed thrice, (6 000 *x*g; 4°C; 15 minutes), using an Avanti J.E centrifuge (Beckman Coulter, CA, United states of America). Pelleted cells were re-suspended in 50 mM Tris. HCl, pH 8.0, between each centrifugation step. After the final wash, the pellet was re-suspended in 50 mM Tris.HCl buffer in a 1: 20 weight: buffer volume ratio. The cell suspension was lyzed by the addition of 1 $mg.ml^{-1}$ lysozyme (Sigma) and 1 tablet of complete EDTA free protease inhibitor cocktail (Roche) was performed to inhibit the degradation of the expressed protein by the bacterial proteases. Cell disruption was aided by freezing the lyzed mixture at -80°C for a minimum of 2 h and then allowed to thaw at 4°C.

3.2.2.2 Centrifugation

The thawed samples were centrifuged (2 900 *x*g, for 30 minutes at 4°C) using Avanti J.E (Coulter Beckman, USA) to remove cellular debris and the supernatant collected for used in downstream purification steps. The soluble (cytoplasm) fraction was separated from the insoluble fraction (membrane) by ultra-centrifugation. Ultra-centrifugation was conducted using an Optima L-90K (Coulter Beckman, USA) ultracentrifuge at 100 000 *x*g for 90 minutes at 4°C in SW 28 rotor (Coulter Beckman, USA). The resulting supernatant was pooled, measured and stored at 4°C for further experiments.

3.2.2.3. Immobilized metal affinity chromatography (IMAC)

The recombinant proteins were purified through IMAC using a 5 ml His-trap FF column (GE Lifesciences, UK). The column was equilibrated according to the manufacturer's instructions. Briefly, the column was cleaned with 50 ml distilled water, followed by the removal of the nickel sulphate using a stripping buffer (20 mM phosphate buffer, pH 8.0; 0.5 M sodium chloride; 50 mM EDTA, pH 7.4). His-trap column was then charged using a 0.1 M nickel sulphate solution followed by washing with 50 ml distilled water. The column was placed into 1x binding buffer (20 mM imidazole, 20 mM Tris-HCl pH 7.4, 0.5 M sodium chloride). The protein mixture was loaded onto the HisTrap FF and unbound proteins eluted ($5ml.min^{-1}$) using 20 mM sodium phosphate buffers, pH 7.4 containing 20 mM imidazole and 0.5M NaCl. The bound proteins were then eluted in the same buffer using a linear gradient (100 ml) of imidazole up to 0.5 M into 5 ml fractions using the AKTA FPLC system (GE Healthcare, UK). Fractions of interest were carefully selected according to the peaks on the UV absorbance. The collected fractions were subjected to SDS-PAGE analysis as described in section 3.2.3.1 and were also assayed for hexokinase activity (section 3.2.5.1).

3.2.2.4. Size exclusion chromatography

Selected His-trap samples were pooled, measured and concentrated down to 2 ml using a 6 ml Vivaspin spin column (GE Healthcare) according to manufacturer's instructions. The concentrated protein sample was mixed with a drop of glycerol and mixed by inverting and loaded onto a Sephacryl S100HR column (1.6 x 100 cm, Sigma) equilibrated with 50 mM Tris-HCl, pH 7.4, containing 50 mM NaCl. Proteins were eluted using the same buffer at a flow speed of $1ml.min^{-1}$. Fractions were subjected to SDS-PAGE analysis as described in section 3.2.3.1 and hexokinase assay for enzymatic activity (section 3.2.5.1).

3.2.2.5. Dialysis

Dialysis was conducted using 10 kDa molecular weight cut off, snake skin dialysis tubing (Thermal Scientific, USA). The dialysis protocol was performed according to the manufacturer's instructions. Sample was carefully added into the dialysis tubing and secured at both ends. The dialysis sample was suspended in 2 liters of 50 mM, pH 8.0 Tris-HCl dialysis buffer. To attain

equilibrium, the dialysis setup was kept for 4 h at 4°C while slowly stirring. Two additional buffer changes were performed, with an overnight and 12 h intervals, after which the dialyzed protein sample was carefully removed from the dialysis tubing, measured and stored at 4°C for further experiments. The dialyzed protein was subjected to SDS-PAGE analysis as described in section 3.2.3.1. The dialyzed sample was also assayed for hexokinase activity as described in section 3.2.5.1.

3.2.2.6. Protein purification studies

After each step of purification, 2x 500 µl samples were collected and stored at -20°C until needed. The sample aliquots were thawed on ice for a minimum of 5 minutes, one vial of each was used to determine protein concentration (section 3.2.4) followed by SDS-PAGE analysis (section 3.2.3.1). The second sample vial was assayed for hexokinase activity (section 3.2.5.1). This was performed in order to assess the effectiveness of the purification strategies in removing contaminating proteins and to assess if the purification had not negatively affected the proteins' enzymatic activities. Hexokinase assay protocol is described in section 3.2.5.1 and activity calculations are described in section 3.2.5.2. The obtained data from the protein determinations and enzyme assay calculations were used to construct purification tables for both the expressed *Tb*HK and *h*GCK.

3.2.3. Polyacrylamide Gel Electrophoresis (PAGE)

3.2.3.1. Sodium Dodecyl Sulphate Polyacrylamide Gel Electrophoresis (SDS-PAGE)

Resolving and stacking gels for the SDS-PAGE gels were prepared as described in section 3.2.3.1 using ingredients and amounts outlined in table 3.1 and table 3.2.

Table 3.1**:** SDS-PAGE (0.75 mm, 12.5%) separation gel ingredients and amounts (for 1 gel)

Ingredients	**Resolving gel (ml)**
30% / 0.8% Acryl / Bis	1.518
3 M Tris pH 8.8	0.485
H_2O	1.641
10% SDS	0.091
10% APS	0.0125
TEMED	0.0025

The separation gel was left to completely polymerize in the gel cassette sandwich for about 2-3 h. The top of the separation gel was overlaid with water saturated tert-amyl-alcohol to ensure a levelled top and avoid evaporation of the added stacking gel mixture.

Table 3.2: SDS-PAGE (4%) stacking gel ingredients and amounts (for 1 gel)

Ingredients	**Resolving gel (ml)**
30% / 0.8% Acryl / Bis	0.2
3 M Tris pH 8.8	105
H_2O	1.185
10% SDS	0.015
10% APS	0.015
TEMED	0.0015

To avoid trapping air bubbles in the gel, the casting stand was gently tapped, which dislodged any trapped air bubbles. After the polymerization of the separation gel, the overlaid water saturated tert-amyl-alcohol was thoroughly washed out with distilled water. The separation gel was prepared using ingredients in the amounts presented in table 3.1. A 4% prepared stacking gel mixture with ingredients provided in table 3.2 was then overlaid separation onto the separating gel in the cassette sandwich and an appropriate comb was carefully placed in between the cassette sandwich that was clamped on the casting frame and was left to solidify for about 2 h.

The homogeneity of the proteins present in each fraction / sample was determined by electrophoresis under denaturing conditions or sodium dodecyl sulphate polyacrylamide gel electrophoresis. SDS-PAGE was performed using the Mini-Protean Tetra electrophoresis unit, from Bio-Rad, USA. The protocol used was that described by Laemmli (1970) using a 12.5% resolving gel and 4% stacking gel as set out in tables 3.1 and 3.2. Equal concentrations of samples to be analysed were mixed 1:1 with loading dye [50 µl TD and 200 µl TS (appendix E) followed by boiling for 10 min. Proteins were separated within the gels using a current of 100 V for 2 h. Page Ruler™ Pre-stained (10-170 kDa) Protein ladder (Thermal Scientific) was used as molecular weight markers in SDS-PAGE.

To visualize the protein bands, SDS-PAGE gels were stained and de-stained with Fairbank's Coomasie Blue protein staining and de-staining protocol as described by Fairbanks, (1971). Polyacrylamide gel was placed in a covered microwavable container, about 100 ml of Fairbanks A solution (0.05% Coomassie Blue R-250, 25% isopropanol, 10% acetic acid) was poured onto the gel. The gel with the solution was heated in a conventional microwave oven on full power for about 2 minutes (until solution reached boiling point). The gel with the solution was left to cool down at room temperature for about 5 minutes while gently shaking on ultra rocker rocking platform (BioRad, USA) after which the solution was discarded and gel rinsed with distilled water. About 100 ml of Fairbanks B solution (0.005% Coomassie Blue R-250, 10% isopropanol, 10% acetic acid), Fairbanks C solution (0.002% Coomassie Blue R-250, 10% acetic acid) and Fairbanks D solution (10% acetic acid) were sequentially added, boiled and discarded. The gel was rinsed with distilled water in between each Fairbanks solution change. The Fairbanks D solution changed 3 times.

3.2.3.2. Native-PAGE

Native-PAGE gels were prepared without the denaturing agent, thus analytes electrophoresed in these gels maintained their native structure and size of the folded protein assembly that governs the kinetics of the proteins in the gel. Therefore; proteins being separated by native gel electrophoresis do not only differ in their molecular mass and their cross sectional area, but also in their shape of the general structure. Native-PAGE gels allow for both conventional staining protocols and the use of specific enzyme linked stains. Resolving and stacking gels for the Native-PAGE gels were prepared as described in section 3.2.3.2 using ingredients and amounts outlined in table 3.3 and table 3.4.

Samples analyzed by Native-PAGE electrophoresis were prepared by mixing sample and Native-PAGE protein sample running buffer in a 1:1 ratio of the sample: buffer mixture.

Table 3.3: Ingredients with their corresponding amounts for the preparation of Native PAGE resolving gel.

Ingredient	Resolving gel (ml)
30% / 0.8% Acryl / Bis	1.518
3 M Tris pH 8.8	0.485
H_2O	1.641
10% APS	0.0125
TEMED	0.0025

Table 3.4**:** Ingredients with their corresponding amounts for the preparation of Native PAGE stacking gel.

Ingredient	Stacking gel (ml)
30% / 0.8% Acryl / Bis	0.2
0.5 M Tris pH 6.8	0.105
H_2O	1.185
10% APS	0.015
TEMED	0.0015

The samples were loaded into the gel wells accordingly. The electrophoresis run was performed using Mini-Protean Tetra System (Bio Rad, USA) where the gel cassette was carefully placed into the electrode assembly and was placed into the electrophoresis tank filled with 1x Native-PAGE running buffer containing 3.028 g Tris, 14.4 g glycine in 1 000 ml (between the gel cassettes and outside the frame). The electrophoresis tank was then connected to Power Pac 300 basic power supply (Bio Rad, USA), and run at 100 volts (V) for 1-2 h. The gels were visualised as described in section 3.2.3.1.

3.2.4. Protein concentration determination

Protein concentrations were determined by the use of the Bicinchoninic acid (BCA) method as first described by Smith *et al.* (1985). The commercially available kit from Thermo Scientific was used according to the manufacturer's instructions. Standard curves of protein concentration versus absorbance (figures 3.2A and B) were constructed using the absorbance values obtained for protein standards prepared with BSA, using a Spectroquant Pharo 300 spectrophotometer (Merck, Germany) at 562 nm. Fifty micro litres of the standards and the unknown samples were first pipetted into a 1.5 ml Eppendorf tube and 1 ml of the working reagent was added and gently

vortexed. Assay tubes were incubated at 37°C (figure 3.1 A) and 60°C (figure 3.1 B) for 30 minutes. Standard curves were plotted using Graph Pad prism, version 5.03 (figures 3.1 A and B). Protein concentrations between 250 and 1000 μg.ml^{-1} could be detected using the incubation at 37°C (figure 3.1A), while protein concentrations between 0 and 250 μg.ml-1 could be detected using the 60°C incubation (figure 3.1B).

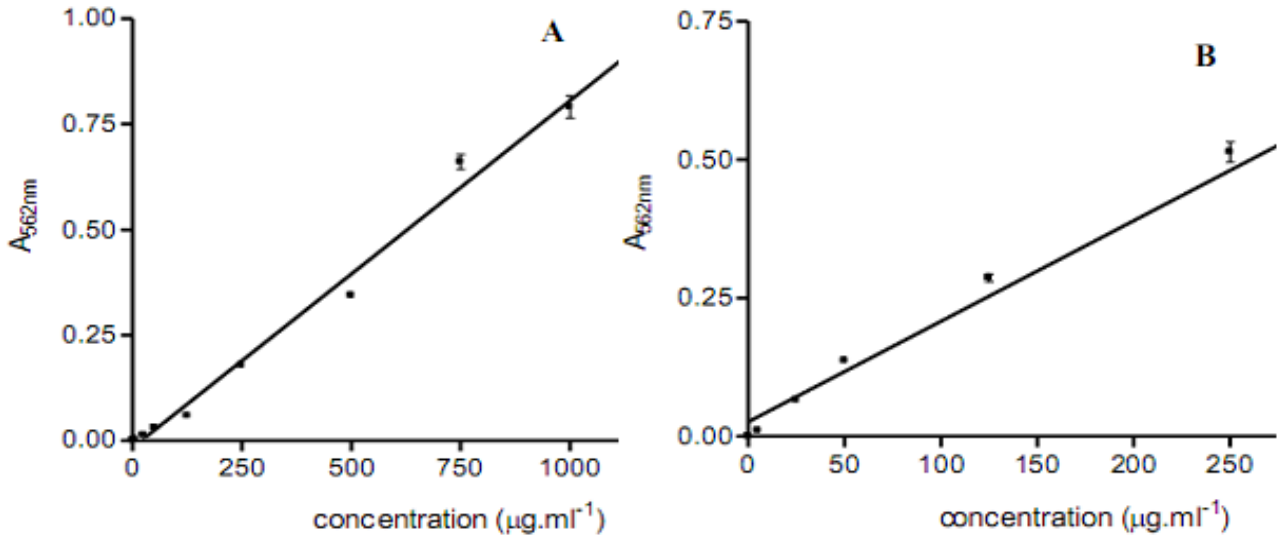

Figure 3.1**:** Standard curves for BCA protein assay using BSA protein standard incubated at (A) 37°C and (B) 60°C. Absorbance readings were taken at 562 nm.

3.2.5. Assays

3.2.5.1. Hexokinase assay

The hexokinase assay reaction is presented in equation 1.2 (section 1.6.1). Glucose, in the presence of ATP, is converted to glucose-6-phosphate and ADP by hexokinase. The glucose-6-phosphate is oxidized by glucose-6-phosphate dehydrogenase in the presence of NAD^+ to form 6-phosphogluconolactone, H^+ and NADH. The hexokinase assay, adapted from Worthington enzyme manual (2012), detects the increase in NADH which is determined spectrophotometrically by measuring the increase in absorbance at 340 nm at 30°C through a coupled reaction with glucose-6-phosphate dehydrogenase.

Table 3.5: Hexokinase assay ingredients and quantities.

Ingredients	Volume (ml)
50 mM Tris-HCL, pH 8.0 containing 13.3 mM MgCl2	210
0.67 M Glucose	50
16.5 mM ATP	10
6.8 mM NAD	10
300 U/ml Glucose-6-phosphate dehydrogenase	10
Enzyme extract	10

To determine hexokinase activity, the hexokinase assays were performed in 96 well microtiter plates containing the ingredients and amounts as presented in table 3.5 and made-up to a final reaction volume of 300 µl with assay buffer (50 mM Tris-HCl, pH 8.0 containing 13.3 mM $MgCl_2$). All assay ingredients except the enzyme extract were added into wells on a 96 well microtiter plate. Gen 5.0, version 1.10, software was used to compile/program the hexokinase assay protocol: 5 minutes incubation at 30°C to equilibrate the reaction mixture, addition of the enzyme solution followed by mixing for 5 sec by shaking. Upon addition of the enzyme solution, the mixture was incubated for an additional 5 min and the absorbance read at 20 sec intervals using a Synergy-MX microtiter plate reader (Biotek, USA).

3.2.5.2. Enzyme activity calculations

Enzyme activity was using equation 3.1.

Equation 3.1:

$$\text{Activity} = (\Delta abs.Vt) / (\varepsilon.t.Ve)$$

Where ΔAbs is the change in absorbance; Vt is the total reaction volume (300 µl); ε = extinction coefficient of NAD/H (6.22 ml^{-1}. μmol^{-1}.); t is time in minutes; Ve is the volume of enzyme extract which was added into the reaction mixture (10 µl). The calculated results were expressed in $\mu mol.ml^{-1}.min^{-1}$ or U. ml^{-1}. One unit of activity reduces 1 µmol of substrate (glucose) per minute at 30°C and pH 8.0. A negative control was run alongside the enzyme assay and was set up the same as in table 3.5 with the exception that the 10 µl enzyme solution was replaced with assay buffer. To confirm that the assay was able to quantify hexokinase activity a commercial

hexokinase from *S. cerevisiae* (Sigma) was used as a positive control. The reaction was set up as described in table 3.5.

3.2.6. Trichloroacetic acid (TCA) protein concentration

A TCA protein concentration procedure was carried out on the samples that had very low concentrations before preparation for SDS-PAGE run. Samples were mixed with 30% w/v TCA in a 1:1 ratio. The mixture was incubated on ice for 15-30 minutes followed by centrifugation (12 000 *x*g*;* 4°C; 15 min) in mini spin micro-centrifuge (Eppendorf, Germany) to collect the precipitated proteins. The supernatant was discarded and the pellet was rinsed by re-suspending the pellet in 1 ml ice cold isopropanol. The suspension was centrifuged (10 000 *x*g*;* 4°C; 5 min) and the supernatant removed and the pellet dried using a Labconco speed-vac system (Vacutec, USA) at 65°C for 30 minutes. Samples were stored for SDS-PAGE analysis as described in section 3.2.3.1.

3.2.7. Characterization studies

3.2.7.1. Temperature stability studies

The thermal stability studies were conducted using temperatures ranging from 20°C to 70°C (20°C , 25°C , 30°C , 37°C , 40°C , 55°C and 70°C) at an assay pH of 8.0 (50 mM Tris-HCl) and incubated in digital dry bath incubators (Bio Rad, USA). The hexokinase assay parameters and ingredients were as outlined in section 3.2.5.1, but scaled-up to a reaction volume of 2 ml. An aliquot from each assay mixture was collected at specific time intervals (0, 15, 30, 45, 60, 90 and 120 minutes) and the activity determined as described in section 3.2.5.1. Experiments were conducted on 3 different days in triplicate. Negative controls were run simultaneously with the characterization study assays at individual temperature and time intervals. Enzyme activity was calculated as described in section 3.2.5.2 and expressed as percentage relative activity, where 100% activity was calculated using the highest activity at a given time across the temperature range.

3.2.7.2. pH stability studies

pH stability characterization studies were performed by subjecting the recombinant enzymes to different buffer conditions over a set period of time. Hexokinase assays were run as described in

Section 3.2.5.1, in triplicates and on 3 different days. A three component equimolar buffer cocktail ranging from pH 5.5 to 9.0 (5.0, 5.5, 6.0, 6.5, 7.0, 7.5, 8.0, 8.5, 9.0) were prepared. The components were 50 mM sodium acetate, 50 mM Tris-HCl and 50 mM 2 (N-morpholino) ethanesulfonic acid (MES). Sodium acetate buffer had the lower pH range (up to 5.0) and was adjusted using acetic acid to the required pH. MES buffer covered the pH range of pH 5.5 to 6.5, and was adjusted by either HCl or NaOH. Tris-HCl buffers covered the pH range between 7 and 9, and were adjusted with HCl or NaOH.

The purified *Tb*HK and *h*GCK proteins obtained as described in sections 3.2.2 were prepared by serially diluting to appropriate concentrations and analyzed for their highest enzymatic activity using the hexokinase assay, and proteins were then concentrated to twice the obtained concentration that exhibited highest enzyme activity. The protein concentrates were then diluted with the individual pH buffers in a 1:1 protein to buffer cocktail ratio. Mixtures were incubated in a digital dry bath (Bio Rad, USA) at the optimum temperature obtained during the temperature stability characterization studies (section 3.2.7.1). Hexokinase assay readings were taken at 0, 15, 30, 45, 60, 90 and 120 minute intervals. Experiments were conducted on 3 different days and in triplicate. Negative controls were run simultaneously with the characterization study assays at individual pH and time intervals. Enzyme activity was calculated as described in section 3.2.5.2 and expressed as percentage relative activity, where 100% activity was calculated using the highest activity at a given time across the pH range.

3.2.7.3. Stability study under optimum conditions

The ability of the expressed *Tb*HK and *h*GCK to maintain basal enzymatic activity over a longer period of time was studied at the optimal conditions (section 3.2.7). The purified *h*GCK and *Tb*HK proteins were diluted with Tris-HCl buffer pH 7.5 and 8, respectively (section 3.2.7.2) to concentrations that exhibited highest enzymatic activity, and incubated at 37°C and 40°C, respectively. Hexokinase assay readings were conducted at 0, 0.25, 0.5, 1, 1.5, 2, 3, 5, 24, 36 and 52 h intervals. Hexokinase assay parameters and ingredients were as outlined in section (3.2.5.1). Assay blanks were incubated and run simultaneously with the protein samples. Enzyme activity calculations were conducted as stated in section 3.2.5.2. Assay data was obtained from three independent readings and the assays performed in triplicates.

3.2.8. Kinetic studies

In order to obtain the kinetic properties for the two expressed and purified proteins (section 3.2.2), the *Tb*HK and *h*GCK were subjected to varying concentrations of glucose using the standard hexokinase assay (section 3.2.5.1 and table 3.5), while keeping all other hexokinase assay parameters and conditions constant (table 3.6). Kinetic assays were performed at optimal pH, temperature and time interval as obtained in section 3.2.7. K_m and V_{max} properties of the expressed enzymes were calculated using a variation of the Michaelis-Menten equation (equation 3.2), namely, the Hanes-Woolf.

Equation 3.2: $$V=Vmax\ (S)/\ [Km + (S)]$$

The following substrate concentrations were used for *Tb*HK; 4, 8, 16, 33, 67, 100, 133, 167, 233 and 333 µM. For *h*GCK the following substrate concentrations were used; 0.1, 1, 2.5, 5, 10, 15, 20, 25, 30, 40, 50 and 100 mM.

Table 3.6. Hexokinase assay ingredients and amounts for kinetic studies.

Ingredients	**Volume (ml)**
50 mM Tris-HCL, pH 8.0 containing 13.3 mM $MgCl_2$	210
Varying substrate concentration (Glucose)	50
16.5 mM ATP	10
6.8 mM NAD	10
300 U/ml Glucose-6-phosphate dehydrogenase	10

Final kinetic parameters were determined from three independent readings and hexokinase assays were performed in triplicates. Enzyme activity calculations were conducted as stated in section 3.2.5.2.

3.2.9. Zymography

Zymography is the detection of enzyme and activity based on the substrate specificity using an electrophoretic technique. *In situ, in vivo* and *in gel* zymographic techniques are in practice. *In gel* zymography is centered on the SDS-PAGE run under non-denaturing conditions in which a specific enzyme substrate can be co-polymerized in the gel, after the run, enzymes can be

refolded and SDS removed by washing the gel in 2.5% Triton. Zymographic development mixture is applied onto the gel to enhance visualization (Yu and Woessner Jr, 2001) Frankowski. In gel zymographic analysis of *Tb*HK and *h*GCK was performed as described by Jelnes (1971). Samples were prepared and run on two Native-PAGE gels (section 3.2.3.2). One of the duplicate gels was stained with coomassie (Section 3.2.3.1) and the other used for the zymogram study.

To enhance visualization, the native gel was soaked in a developing reagent containing; 50 ml 50 mM Tris.HCl pH 8, 25 mM $MgCl_2$, 100 mg glucose, 25 mg ATP, 0.5 ml MTT, 0.5 ml $NADP^+$ and 0.25 PMS. The developing solution was pre-mixed thoroughly and poured onto the native gel. The native gel was incubated in the developing solution for 1 hour at 37°C, protected from obvious light. The reaction was terminated by washing the gel with distilled water thrice.

3.3. Results and discussions

The most important aim of the current chapter was to over-express both *Tb*HK and *h*GCK proteins in a bacterial expression system and to purify them to homogeneity.

3.3.1. Recombinant protein over-expression by auto-induction

Chemically competent *E. coli* BL21(DE3) cells with p-RARE 2 that were transformed with pET28b(+) and pET22b(+) plasmids, harbouring *Tb*HK and *h*GCK genes (Chapter 2, section 2.2.2) respectively, were over-expressed by auto-induction technique (section 3.1.1).

3.3.2. Auto-induction study samples

The auto-induction samples (500 µl) for both *Tb*HK and *h*GCK, including the auto-induction negative controls, were collected and immediately centrifuged as described in section 3.2.1.4. Samples were prepared for SDS-PAGE analysis and run as described in section 3.2.3. An obvious increase in the intensity of the colour and size of the protein band at 25 kDa (figure 3.2 A) indicates the increase in the expressed *Tb*HK protein over time. As compared to the negative control SDS-PAGE image (figure 3.2B), which has no obvious band that increases in its intensity at 25 kDa.

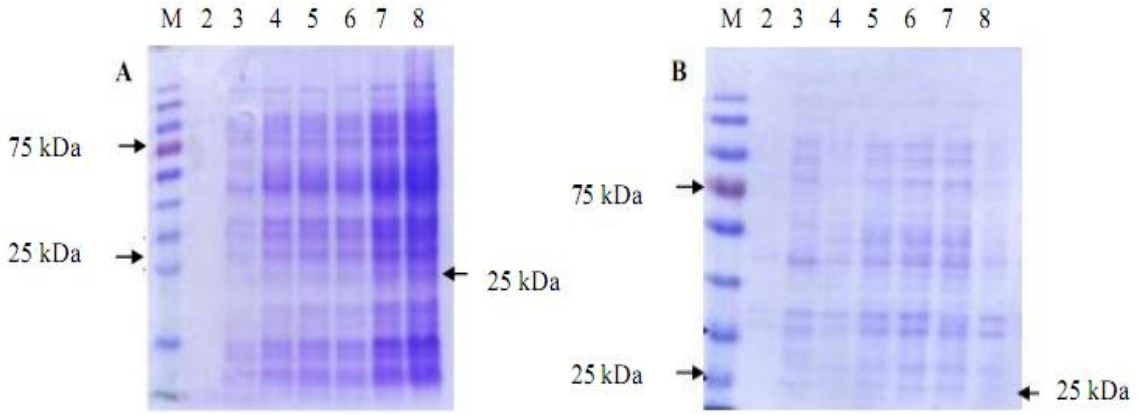

Figure 3.2: SDS-PAGE analysis of the samples collected at different time intervals during induction studies. Each lane was loaded with 150 µg.ml^{-1} protein. (A) pET28b(+) *Tb*HK and (B) Empty pET28b(+) . Lanes (M) marker, (2) 0, (3) 6, (4) 12, (5)18, (6) 24, (7) 30 and (8) 36 h of incubation at 20°C in auto-induction media.

For *h*GCK, there is a prominent increase in the intensity of the colour and size of the protein band at 55 kDa (figure 3.3 A), indicating an increase in the expressed human glucokinase protein over the auto-induction incubation period.

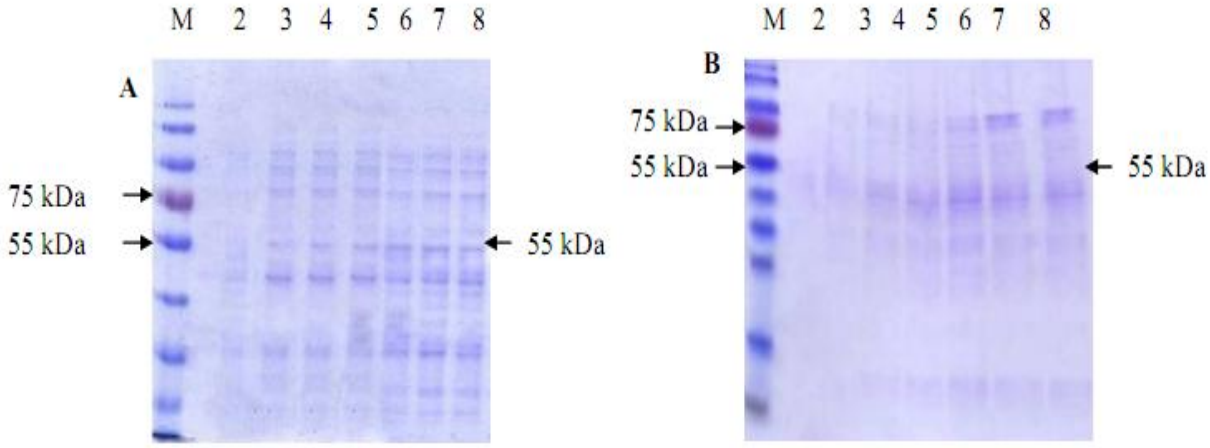

Figure 3.3: SDS-PAGE analysis of the samples collected at different time intervals during induction studies. Each lane was loaded with 100 µg.ml^{-1} protein. (A) pET22b(+) *h*GCK and (B) Empty pET22b(+). Lanes (M) marker, (2) 0, (3) 6, (4) 12, (5) 18, (6) 24, (7) 30 and (8) 36 h of incubation at 20°C in auto-induction media.

As compared to the negative control SDS-PAGE image (figure 3.3 B), there is no band that increases in its intensity at 55 kDa (Gidh-Jain *et al*., 1993; Tiedge *et al*., 1996; Ronimus and Morgan, 2001).

3.3.3. Protein purification studies

After the removal of the cell debris by centrifugation and separation of the soluble fractions from the membrane fraction by ultracentrifugation (section 3.2.2.2), the over-expressed proteins were purified. Section 3.2.2 describes the strategies employed to obtain the pure proteins and herewith are the outcomes of such strategies.

3.3.3.1. IMAC

Several affinity-tags have been reported to be in use in the purification of recombinant proteins. These tags share common features such as; (i) specific and easy removal of the protein tags to produce a native protein, (ii) one step purification, (iii) minimal effect on protein tertiary structure and (iv), possibility to be fused to different proteins (Terpe, 2002). The use of affinity tags have been reported to improve recombinant protein yields (Rajan *et al.*, 1998), prevent proteolysis, increase protein solubility, reduce fusion protein antigenicity and facilitate the re-folding of proteins (Hammarstrom *et al.*, 2002; Chen *et al*., 2005). Initially, IMAC was employed in the separation of proteins and peptides containing naturally present and exposed histidine residues, which were responsible for the binding of the molecules to the immobilized metal ions (Porath *et al.*, 1971). Later the principle was adopted (Hochuli *et al.*, 1987) for the purification of recombinant proteins with fused histidine residues. This approach can result in a purified recombinant protein with more than 90% purity (Arnau *et al.*, 2006). Immobilized metal affinity chromatography was employed as the first strategy in the purification of the recombinant proteins (section 3.2.2.3). The elution profiles obtained from this purification step are presented in figures 3.4 and 3.5.

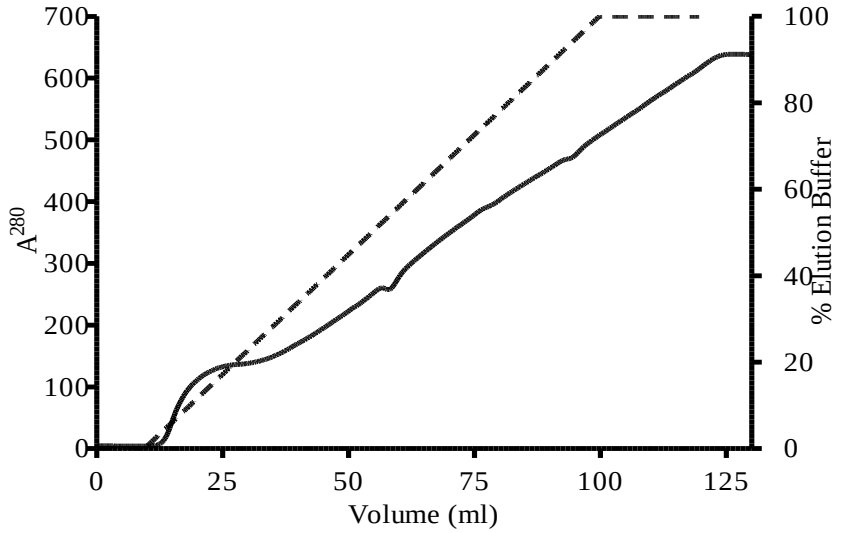

Figure 3.4: Elution profile obtained when the metal affinity resin was loaded with *Tb*HK, the solid line represents the protein samples and the dashed line represents the percentage elution buffer. Fraction collection started at the beginning of the gradient (20 ml).

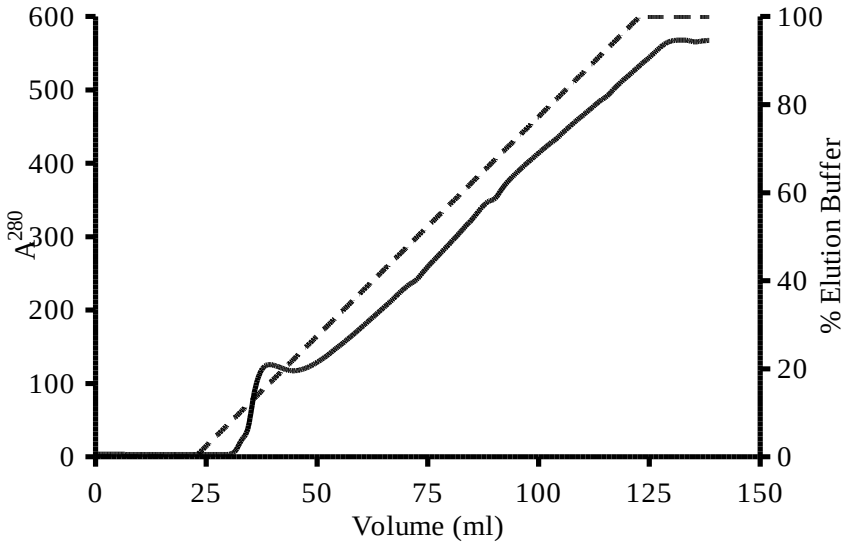

Figure 3.5: Elution profile obtained when the metal affinity resin was loaded with *h*GCK, the solid line represents the protein samples and the dashed line represents the percentage elution buffer. Fraction collection started at the beginning of the gradient (30 ml).

Both figures 3.4 and 3.5 show that as the percentage elution buffer increases, the bound proteins start to elute. The protein peak is observed when the elution buffer reaches 5% and continues until 25% is reached. This percentage of elution buffer (Fig 3.4 and 3.5, right y-axis) represents the concentration of imidazole in the elution buffer. Therefore 5-25% of the elution buffer represents 25-125 mM imidazole. Therefore it can be concluded that the bound *Tb*HK and *h*GCK, including all other bound proteins, elute from the column at an imidazole concentration ranging from 25 mM to125 mM. The intensity of the ultraviolet light absorbance peak gives a rough indication of the concentration because of the aromatic amino acids; tryptophan, tyrosine and phenylalanine absorbing ultraviolet light at a wavelength of 280 nm (Held, 2003). The UV absorbance peak of about 150 milli-absorbance units (mAU) of *Tb*HK and *h*GCK observed in figures 3.4 and 3.5 indicate that both proteins express in low concentrations that could be ascertained by BCA assay (section 3.2.4).

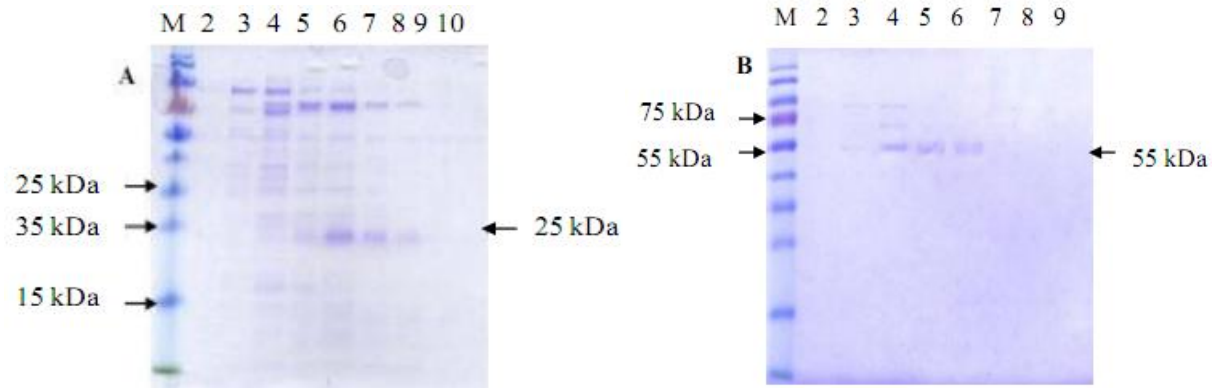

Figure 3.6: SDS-PAGE presenting the protein profiles of the selected fractions (corresponding to the elution volumes presented in figure 3.5 of the absorbance peak. (A) *Tb*HK and (B) *h*GCK. Lanes (1) marker, (2) fraction 2, (3) fraction 3, (4) fraction 4, (5) fraction 5, (6) fraction 6, (7) fraction 7 and (8) fraction 8. Showing the proteins of interest at (A) 25 kDa for *Tb*HK and (B) 55 kDa for *h*GCK.

Despite the selective affinity for His-tagged proteins of the IMAC resin, contaminating proteins and other non-protein contaminants may bind to the beads in the metal affinity column or on the tagged protein itself, these contaminants may be eluted together with the protein of interest. This phenomenon is observed on the SDS-PAGE analysis of fractions selected from the absorbance peak regions (figure 3.6) where there are other visible protein bands other than the 25 kDa *Tb*HK protein band and the 55 kDa *h*GCK protein band protein of interest.

3.3.3.2. Size exclusion chromatography

In order to remove the persistent contaminating proteins, imidazole and other contaminating molecules eluted in the IMAC fractions (for *Tb*HK and *h*GCK), the pooled samples (section 3.2.2.3) were subjected to size exclusion chromatography as described in 3.2.2.4. The elution profiles obtained from this purification step are presented in figure 3.7 and figure 3.8.

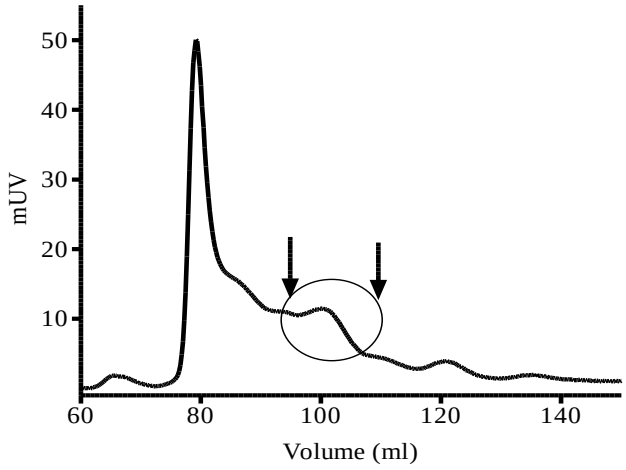

Figure 3.7: An elution profile obtained for Sephacryl S-100 HR resin when loaded with *Tb*HK. The area between the two arrows represents the region that was pooled for downsteream purification.

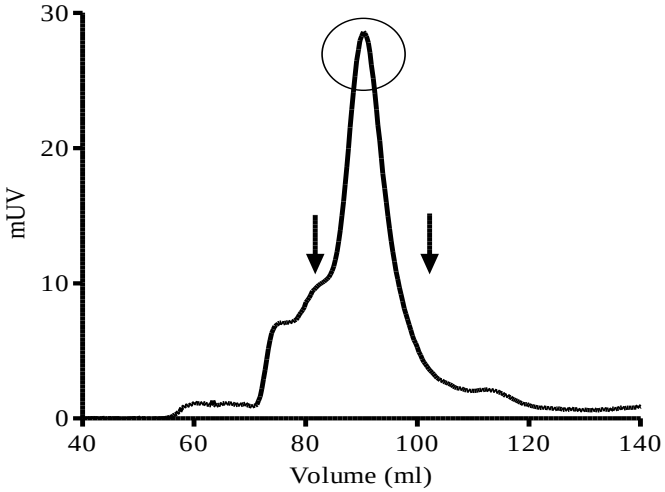

Figure 3.8: An elution profile obtained from Sephacryl S-100 HR resin when loaded with *h*GCK. The area between the two arrows represents the region that was pooled for downsteream purification.

The *Tb*HK elution profile (figure 3.7) showed 5 distinct peaks and the SDS analysis of the selected fractions (figure 3.9A) showed that the circled peak (figure 3.7) represents the recombinant protein (25 kDa) which was also confirmed by the presence of hexokinase activity (section 3.2.5.1). The *h*GCK elution profile (figure 3.8) also has five peaks with one prominent peak. SDS-PAGE analysis (figure 3.9B) of the peak fractions showed that the prominent peak (circled on figure 3.7) was the peak that contained the recombinant human glucokinase protein (25 kDa). Fractions from this peak also exhibited hexokinase enzymatic activity (section 3.2.5.1).

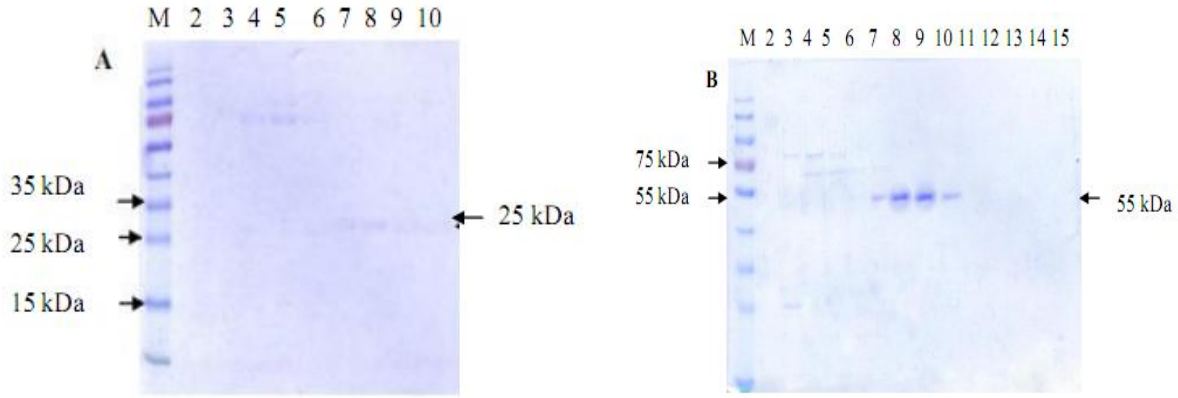

Figure 3.9: SDS-PAGE gels representing the protein profiles of the size exclusion chromatography. (A) *Tb*HK (25 kDa) - Lane (1) Marker, lanes (2-10) fractions number 12-19. (B) *h*GCK (55 kDa) - Lane (1) Marker, lanes (2-14) fractions 11-23.

The peaks, when overlaid by the hexokinase activity, peaks between the arrows on figure 3.7 and figure 3.8 corresponded to the 25 kDa protein bands on the SDS-PAGE gels (figure 3.9). These fractions were pooled for further purification procedures. Comparing the intensities of the elution peaks (figure 3.9 A lanes 7 to 8 and figure 3.9 B lanes 5 to 9), it is evident that *Tb*HK eluted in small quantities, unlike *h*GCK which had slightly higher protein concentrations. This comparison is based on the observed thickness and colour intensity of the protein bands on the SDS-PAGE gel. SDS-PAGE analysis (figure 3.9A and B) of both the recombinant proteins indicated that size exclusion chromatography eliminated most of the contaminating proteins visible in figure 3.7 (SDS PAGE of IMAC); however, there are low levels of contaminating proteins (figure 3.9) that co-eluted with the proteins of interest,therefore, further purification steps were necessary.

3.3.3.3. Dialysis

Results obtained from the *Tb*HK and *h*GCK size exclusion chromatography elution profiles (figures 3.7 and 3.8) and SDS-PAGE gels (figure 3.9A and B) were used to select the fractions to be pooled for dialysis. Pooled fractions corresponded to the activity peaks which overlapped with a protein peak. After two buffer changes, samples were retrieved from the dialysis tube and protein concentrations were determined using the BCA protein assay as described in section 3.2.4. The protein concentrations and volume of samples obtained after each step of purification were used to construct the purification tables (tables 3.7 and 3.8).

To assess the purification of the protein during the purification strategies, 2x 500 µl samples were collected at each strategy (section 3.2.2). One of the samples was subjected to SDS-PAGE analysis (section 3.2.3.1), and the second for protein and enzyme activity. The purification table obtained for the recombinant *Tb*HK is given as table 3.7. Total protein obtained after purification from one liter of auto induction media was 1.2 mg and had a purification fold of 27. The final percent yield was 11% with a specific activity of 0.041µmol.min^{-1}.mg^{-1}. These values are comparable to values reported in literature (Morris *et al.,* 2006, Chambers *et al.,* 2008).

Table 3.7: Purification table for *Tb*HK

Fraction	**Volume** (ml)	**Total protein** (µg.ml^{-1})	**Total protein** (mg)	**Activity** (µmol.min^{-1}.ml^{-1})	**Total activity** (µmol.min^{-1})	**Specific activity** (µmol.min^{-1}.mg^{-1})	**Purification fold**	**Yield** (%)
Crude	165	1766	291	0.00268	0.44212	0.00151	1	100
IMAC	30	245	7.3	0.00161	0.04823	0.00661	4	11
100HR	25	56	1.4	0.00161	0.04019	0.02871	19	9
Dialysis	23	54	1.2	0.00214	0.00214	0.04109	27	11

The purification table obtained for the recombinant human glucokinase is given as table 3.8. Total protein obtained after purification from one liter of auto induction media was 3 mg and had a purification fold of 24. A final yield of 6% was obtained with a specific activity of 0.225 µmol.min^{-1}.mg^{-1}. Each step given in the purification tables (tables 3.9 and 3.10) was also subjected to SDS-PAGE analysis as described in section 3.2.3.1. Figure 3.10 represents the SDS-PAGE results and indicates that the purification strategies were successful.

Table 3.8: Purification table for human glucokinase

Fraction	**Volume** (ml)	**Total protein** (µg.ml^{-1})	**Total protein** (mg)	**Activity** (µmol.min^{-1}.ml^{-1})	**Total activity** (µmol.min^{-1})	**Specific activity** (µmol.min^{-1}.mg^{-1})	**Purification fold**	**Yield** (%)
Crude	250	5095	1274	0.04823	12.0579	0.00947	1	100
IMAC	25	1501	38	0.01447	0.36174	0.00964	1	3
100HR	30	281	8	0.01447	0.43408	0.05149	6	4
Dialysis	28	125	3	0.02412	0.67524	0.22508	24	6

The IMAC step proved to be a powerful tool among purification strategies as this step was responsible for removing most of the undesired proteins and non-protein compounds. The final step in purification of the *Tb*HK (dialysis) resulted in a protein sample with high purity contained only one visible band (figure 3.10A lane 6).

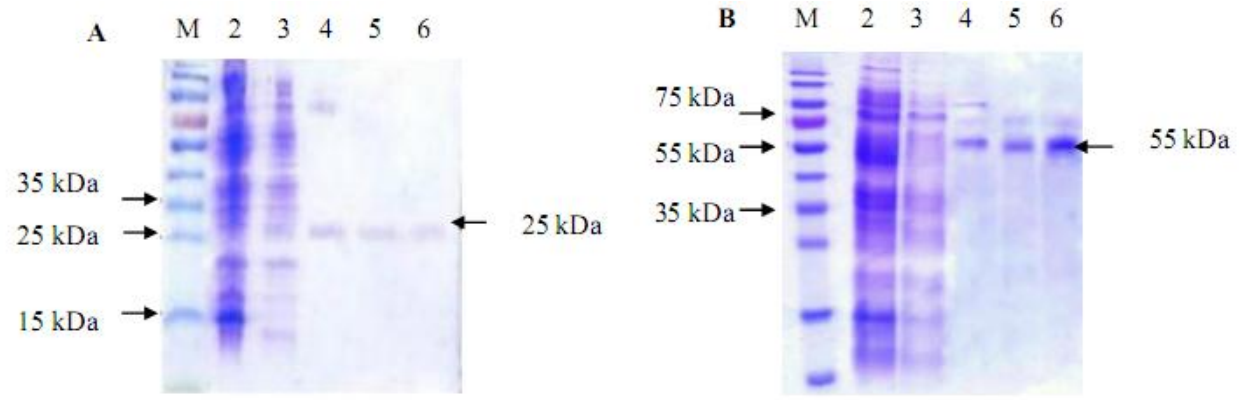

Figure 3.10: SDS-PAGE analysis of (A) *Tb*HK and (B) *h*GCK purification strategies. On both images (M) Marker, (2) lysate (3) soluble fraction, (4) IMAC, (5) SEC, (6) Dialysis; showing the 25 kDa and 55 kDa purified *Tb*HK and *h*GCK proteins, respectively.

The SDS-PAGE image obtained for the human glucokinase (figure 3.10 B), shows constant co-purification of contaminating proteins ranging from 60 to 70 kDa even in the final step of the purification strategy (dialysis, figure 3.10 B, lane 6). During the immobilized metal affinity chromatography, concomitant expressed *E. coli* proteins that exhibit high affinity to the metal chelating resin may be co-eluted with the proteins of interest. These contaminating proteins have been classified into three classes (table 3.9). Class I, which are proteins that require >80 mM imidazole buffer for their elution, Class II proteins require 55 mM to 80 mM imidazole for

elution and class III proteins that need between 30 mM and 55 mM imidazole for their elution. Class III includes heat shock proteins (HSP60) with molecular weight of 60 kDa.

Table 3.9: Classes of native *E. coli* proteins which have the ability to co-purify with His-tagged proteins during IMAC (adapted from Balanos *et al.*, 2006)

Class	***E. coli* protein**	**Molecular mass (kDa)**	**% Histidine residue**
Class I	Cu-Zn-SODM	17.6	4.0
	ArgE	42.3	4.4
	Hfq	11.1	4.9
	Fur	16.7	8.1
Class II	YadF	25.0	5.5
	GlgA	51.7	3.4
	GlmS	66.8	3.9
	CAT	22.5	5.5
Class III	Hsp60	57.0	0.2
	ODOI	10.5	3.6

Despite its co-elution, the contaminating protein may not have an influence on the hexokinase activity of the target proteins (hexokinase assay) because of the differences in the modes of actions between *Tb*HK, *h*GCK and HSP60 (Bork *et al*., 1992). However, this hypothesis presents a viable area of further studies in assessing the effects of the contaminating *E. coli* proteins on the properties of the recombinant proteins expressed in *E. coli.*

3.3.4. Characterization studies

The purified *Tb*HK and *h*GCK (section 3.2.2) were characterized to determine their optimum thermal and pH stability and this section provides the outcomes of these studies.

3.3.4.1. Temperature stability studies

The temperature at which the expressed and purified *Tb*HK and *h*GCK exhibited the highest activities over time was determined as described in section 3.2.5.1. For *Tb*HK, the optimum incubation time was 90 min (figure 3.11) and the optimum temperature was 40°C (figure 3.11).

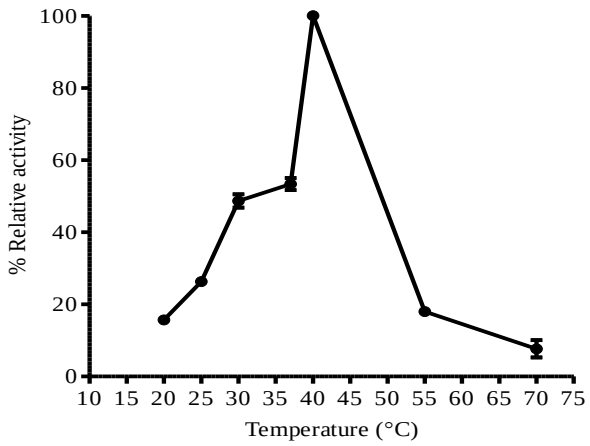

Figure 3.11: Graphical presentation of temperature stability study of *Tb*HK.

For *h*GCK, the optimum incubation time was 90 min (figure 3.12) and the optimum temperature was 37°C (figure 3.12). The enzyme velocities at the respective temperature and time interval (for *Tb*HK and *h*GCK) were used to calculate percentage relative activities. The percent relative activity for the individual temperature ranges and time intervals for *Tb*HK and *h*GCK were calculated relative to the activity obtained at the optimum incubation time and temperatures. See appendix F for individual results obtained for the percentage relative activity at different time intervals.

The thermal stability outcomes for human glucokinase are very similar to values reported in literature. Recombinant pancreatic β-cell glucokinase fused to GST tag exhibited higher relative enzymatic activity at temperatures ranging from 30°C to 50°C after incubating the expressed enzyme for a period of 30 minutes (Galan *et al.,* 2006).

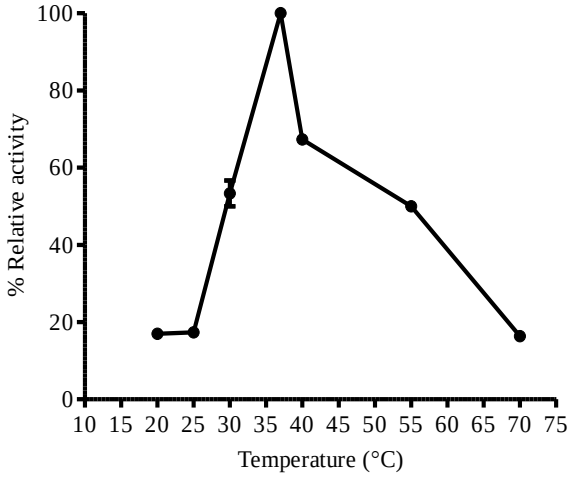

Figure 3.12: Graphical presentation of temperature stability study of *h*GHK.

In 1999, Davis *et al.* (1999) reported on the expression of a wild type glucokinase in *E. coli* (DH5α strain) that showed increasing relative activity at 37°C after 20 minutes incubation.

3.3.4.2. pH stability studies

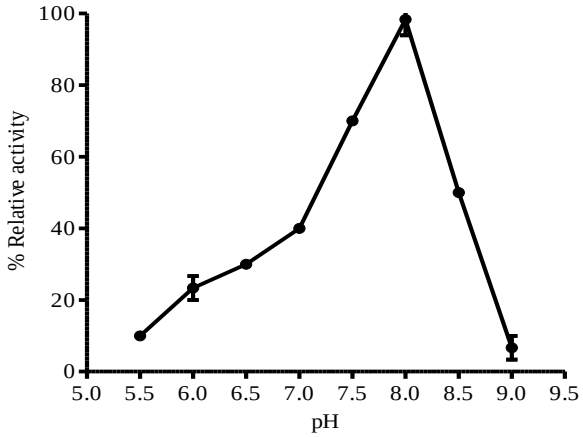

Figure 3.13: Graphical presentation of pH stability study of *Tb*HK.

The pH level at which the expressed *Tb*HK and *h*GCK exhibited the highest enzymatic activity over time was determined as described in section 3.2.7. For *Tb*HK, the protein exhibited high

enzyme activity over a fairly wide pH ranging from 7.5 to 8.5 with pH 8.0 at 90 minutes (T90) exhibiting the highest activity (figure 3.13). Dodson *et al.* (2011) reported an optimum pH of 7.5. Nwagwu and Opperdoes (1982) reported an optimum pH value of *Tb*HK activity of 7.8, which is comparable to our study.

For *hGCK*, the optimum incubation time was 60 min (figure 3.14) and the optimum pH was 7.5 (figure 3.14). The results obtained were used to calculate percentage respective relative activity and are graphically presented in figure 3.14. The percent relative activities for the individual pH ranges and time intervals for *Tb*HK and *h*GCK were calculated relative to the activity obtained at 90 min, pH 8.0 and 60 min, pH 7.5 respectively. Results obtained for the percentage relative activity different time interval are presented in appendix F.

The pH value obtained for the recombinant human glucokinase in this study is closely comparable to reports by Van dercammen and Van Schaftingen (1990) where they observed that *h*GCK exhibited an increase in enzymatic activity at pH values ranging from 6.55 to 8.15, measured at 5 mM glucose. Grossbard and Schimke (1966) investigated the optimum pH for the hexokinase isoenzymes (I, II, III) and reported that the highest enzyme activity was observed at pH values ranging from 7.8 to 8.8.

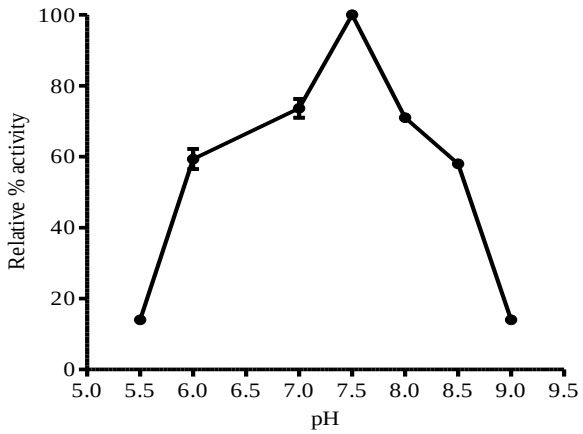

Figure 3.14: Graphical presentation of pH stability study of *h*GHK at T60.

3.3.4.3. Stability study under optimum conditions

The final stability conditions were used to determine how stable the enzyme activity for both proteins. *Tb*HK and *h*GCK were diluted in Tris. HCl, pH 8.0 and incubated at 40°C (*Tb*HK) and 37°C (*h*GCK). Standard hexokinase assays at specific time intervals over 52 hours were conducted as described in section 3.2.5.1. Hexokinase assay reading at time zero incubation was used as the reference result for the calculations of percent relative activity. *Tb*HK was the more stable protein as it maintained a relatively high activity of about 75% and above for a period of up to 36 h with a decrease in relative activity to approximately 25% at 52 h (figure 3.15 A). Recombinant *h*GCK has a unique pattern of enzymatic activity. As shown in figure 3.15 B, it exhibits a steady increase in its relative activity from 30 minutes to about 90 minutes, where its activity spontaneously drops in activity to about 60%. However this relative enzyme velocity is maintained up to 36 h. No activity was observed at 52 h.

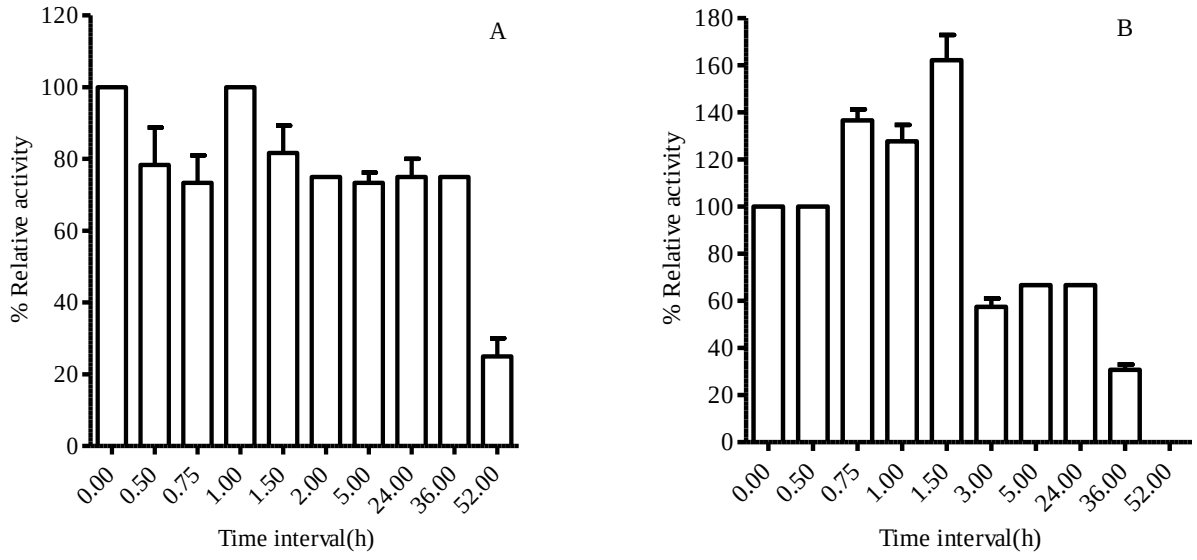

Figure 3.15: Graphical presentation of stability of (A) *Tb*HK and (B) *h*GCK.

3.3.5. Kinetic studies

Enzymes with multiple binding sites may exhibit either a positive or a negative cooperativity to its substrate. In positive cooperativity, the formation of the complex increases the affinity of the binding of the second substrate molecule. In negative cooperativity, the binding of the first substrate to its active site reduces the affinity of the enzyme to the second substrate. Sigmoidal

behaviour of an enzyme indicates substrate cooperativity which is a deviation from the conventional Michaelis-Menten kinetics. Its substrate saturation curve exhibits a palm shape as compared to the hyperbolic curve observed in Michaelis-Menten (Kamata *et al.,* 2004). The magnitude of the Hill coefficient is derived from the slope of the Hill plot that indicates the extent and direction of cooperativity. Thus, enzymes with consented enzyme kinetics (no cooperativity) will have an *h* value of 1; enzymes with negative cooperativity to its substrate will have an *h* value of less than 1; enzymes with positive cooperativity will have an *h* value of greater than 1. Therefore, enzymes that exhibit sigmoidal behaviour will have a Hill coefficient value of >1 (Roders and Gibson, 2004).

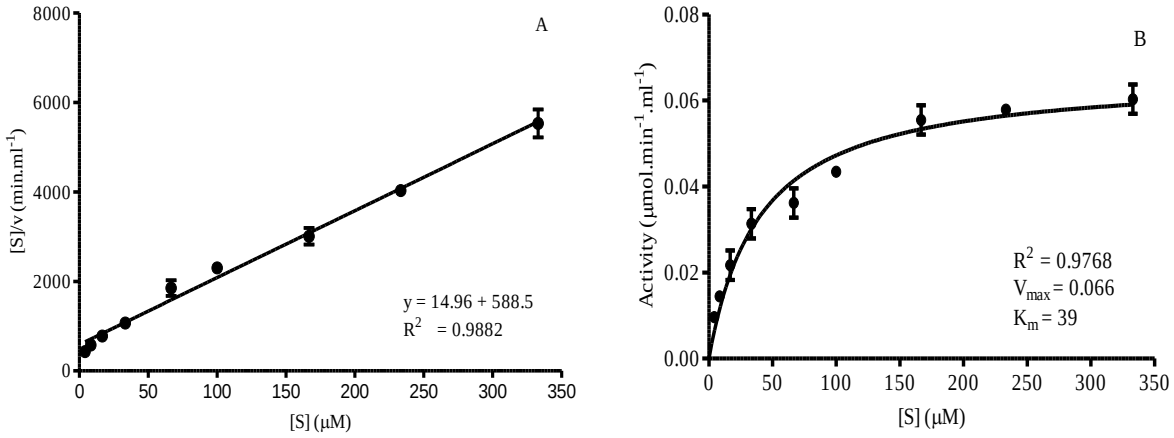

Figure 3.16: *Tb*HK enzyme kinetic plots (A) Hanes-Woolf plot and (B) Michaelis–Menten plot.

The kinetic study experiments were carried out as presented in section 3.2.8 to determine the kinetic properties of *Tb*HK and *h*CGK. Experimental data was analyzed using Hanes-Woolf (HW) and Michaelis-Menten (MM) plots. Figure 3.16 represents the obtained MM and HW plots. The K_m and values read from the MM graph were 39.3 µM and 0.066 µmol.min^{-1}.ml^{-1}, respectively, which were comparable to the K_m and values read from the HW plot of 39 µM and 0.066 µmol.ml $^{-1}$.min^{-1}, respectively. The Hanes-Woolf enzyme kinetic analysis is a more precise method for the calculation of the enzymatic parameters (Ritchie and Prvan, 2006). The obtained K_m and V_{max} for *Tb*HK in the current study are strongly comparable to those reported in literature (Nwagwu and Opperdoes, 1982; Morris *et al.,* 2006, Chembers *et al.,* 2007; Chembers *et al.,* 2008). For example, K_m values for *Tb*HK are reported to be 43 µM (Caceres, 2002).

Experimental kinetic data obtained for *h*GCK was analyzed using the Michaelis-Menten equation (Equation 3.2) and the Hanes-Woolf plot (figure 3.17). The K_m and V_{max} values read from the HW graph were 4.5 mM and 0.032 µmol.min^{-1}.ml^{-1} respectively, which is comparable to the K_m and V_{max} values read from the MM plot 4 µM and 0.032 µmol.min^{-1}.ml^{-1} respectively.

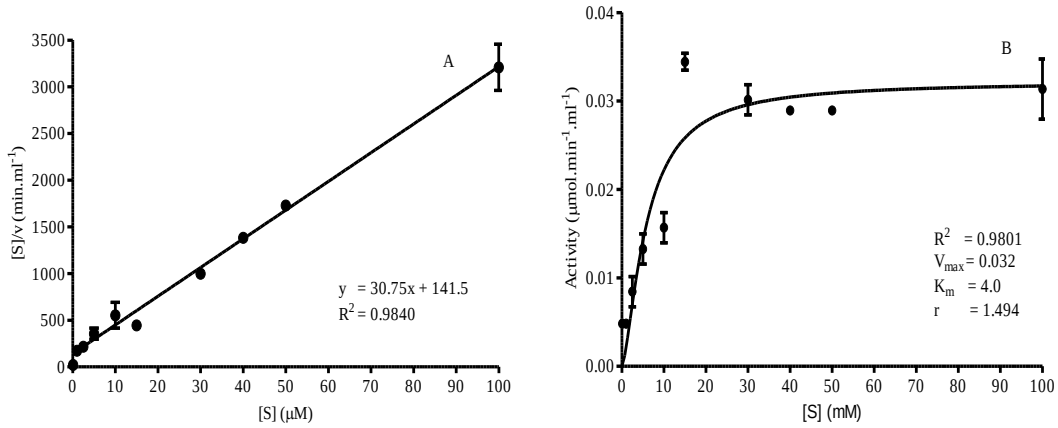

Figure 3.17: *h*GCK enzyme kinetic plots (A) Hanes-Woolf plot and (B) Michaelis–Menten plot.

The Hill coefficient value of 1.5 obtained for the recombinant human glucokinase in this project agrees with the sigmoidal behaviour of the enzyme which displays positive cooperativity (Gidh-Jain *et al.*, 1992; Matschinsky *et al.*, 1993; Stoffel *et al.*, 1993; Davis *et al.*, 1999; Kamata *et al.*, 2004). Table 3.10 is a summary of the V_{max} and K_m values obtained using the different kinetic equations/plots and can be used to draw a comparison between the human and *Tb* proteins. When comparing K_m values it is evident that the human protein has a lower affinity for the substrate than the trypanosome protein. This can be concluded based on the catalytic turnover rate and efficiency of proteins. *Tb*HK has a higher turnover rate (K_{cat}) of its enzyme-substrate complex (2.05 min^{-1}) as opposed to the turnover rate of human glucokinase (11.25 min^{-1}); the human glucokinase exhibits a lower efficiency (2.5 min^{-1}.µmol^{-1}) as compared to *Tb*HK efficiency (0.0526 min^{-1}.µmol^{-1}).

Table 3.10: Kinetic properties of the recombinant human glucokinase with the hill coefficient and *Tb*HK proteins

Plot type	***Tb*HK**				***h*GCK**				
	K_m (µM)	**V_{max}** (µmol.min^{-1}.mg^{-1})	**K_{cat}** (min^{-1})	**K_{cat}/K_m** (mol^{-1}.min^{-1})	**K_m** (mM)	**V_{max}** (µmol.min^{-1}.mg^{-1})	**h**	**K_{cat}** (min^{-1})	**K_{cat}/Km** (mol^{-1}.min^{-1})
Michaelis-Menten	39.3	0.066	2.05	0.0522	4	0.032		11.25	2.813
Hanes-Woolf	39	0.066		0.0526	4.5	0.032	1.5		2.5

Glucokinase (Hexokinase IV) an isoform of hexokinase enzymes (I, II, III and IV) in humans is reported to have significantly different kinetic properties. Despite glucokinase being a monomeric enzyme it exhibits a sigmoidal dependency to glucose as compared to the conventional Michaelis-Menten glucose dependency exhibited by its isoforms (I, II, III). Despite the differences in their substrate dependency, the hexokinase isotypes share common features, including the presence of large and small domains (figure 3.18) that are connected by an α-helix interconnecting region (Kamata *et al*., 2004; Molnes *et al.*, 2011).

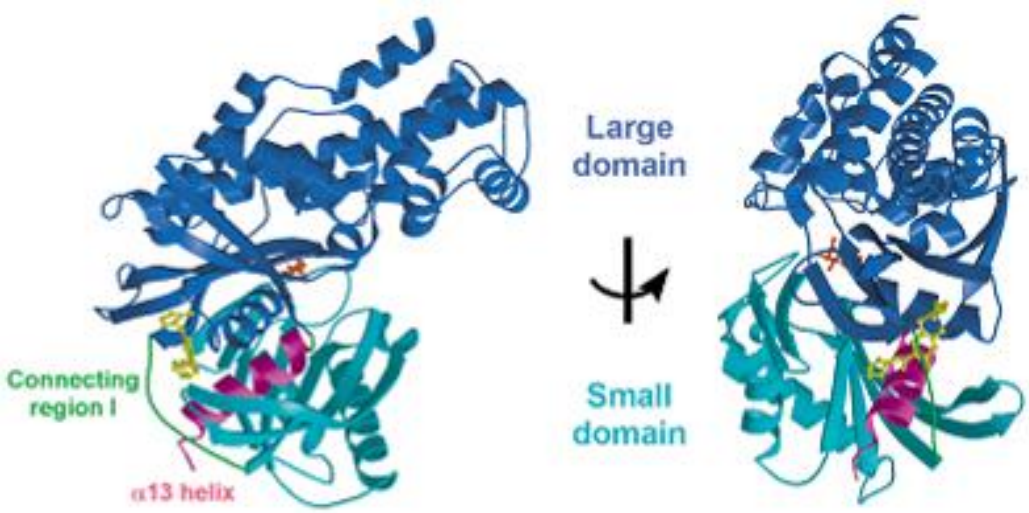

Figure 3.18: Human glucokinase structure complexed with a compound (yellow) showing the closed substrate bound state (taken from Kamata *et al*., 2004).

There are two reported possible explanations for the substrate cooperativity of glucokinase. Firstly, as explained by Cornish-Bowden and Storer, (2004) the mnemonical mechanism is proposed where there is a selectively slow inter-conversion between two free forms of the

enzyme, secondly; Patterson (1986) attributed the deviation from the Michaelis-Menten kinetics to a random order of binding of the substrate. However, based on various kinetic studies and crystal structure analysis of glucokinase, the global conformation conversion and the kinetic cooperativity upon binding to substrate may be summarized in equation 3.4, where GCK represents the substrate free, inactive enzyme, GCK-Glc is the enzyme-substrate complexes of low activity (thus lower substrate affinity), GCK*-Glc is the highly active (thus higher substrate affinity) enzyme state (figure 3.19) (Cornish-Bowden and Storer, 1977; Storer and Cornish-Bowden, 1986; Patterson, 1986; Kamata *et al.,* 2004; Molnes *et al.,* 2011). *Tb*HK follows classic Michaelis-Menten kinetics (Nwagwu and Opperdoes, 1982; Seyfang and Duszenko, 1991).

Equation 3.4:

$$GCK + Glc \underset{k_{-1}}{\overset{k_1}{\longleftrightarrow}} GCK \,.\, Glc \underset{k_{-2}}{\overset{k_2}{\longleftrightarrow}} GCK^* \,.\, Glc$$

3.3.6. Zymography

Zymographic studies were conducted as described in section 3.2.9, development of purplish discoloration was observed, although too faint to determine if activity was being displayed. For this reason, western blotting was performed and the interpretation of the obtained results is presented in appendix A.

3.3.7. Conclusions

The main objectives of the current chapter were to express, purify and characterize recombinant *Tb*HK and *h*GCK. *Tb*HK and *h*GCK proteins were readily over-expressed in an *E. coli* expression system as soluble proteins by using auto induction media. The expressed proteins maintained their enzymatic activity throughout the purification strategies (centrifugation, IMAC, SEC and dialysis). Although the finally purified proteins (*Tb*HK and *h*GCK) co-purified with other non specific proteins (figure 3.10A and B), these proteins did not significantly affect the characterization studies. Protein characterization studies revealed that *Tb*HK is stable at temperatures ranging from 37°C to 45°C with and an optimum of 40°C and a pH range of 7.0 to

8.5 with an optimum of 8.0. The recombinant human glucokinase exhibited stability at temperatures and pH ranging from 30°C to 40°C with an optimum of 37°C and 7.0 to 8.5 with an optimum of 7.5. At optimum conditions the recombinant *Tb*HK maintained activity of up to 75% for up to 36 h. Similarly, recombinant human glucokinase maintained enzymatic activity of up to 65% for up to 24 h at optimum conditions.

Studies of the kinetic parameters of the enzymes revealed that *Tb*HK had a K_m of 39 µM, V_{max} of 0.066 µmol.min^{-1}.ml^{-1} and k_{cat} of 2.05 min^{-1} and a K_{cat} / K_m of 0.0526 (min^{-1}.µmol^{-1}) as determined by Hanes-Woolf. Human glucokinase enzyme kinetic studies revealed a K_m of 4.5 mM, V_{max} of 0.032 µmol.min^{-1}.ml^{-1}, K_{cat} of 11.25 min^{-1} and a K_{cat} / K_m of 2.5 (min^{-1}.µmol^{-1}) using the Hanes-Woolf plot. The human hexokinase has a Hill coefficient of 1.5, confirming the sigmoidal behaviour and unique characteristic of the enzyme. However the expressed proteins have slightly lower maximal velocity (V_{max}), turnover rate (K_{cat}) and less efficiency (Gidh-Jain et al., 1993; Km et al., 2007; Molnes et al., 2011). These may be attributed to the expression of the protein with the N-terminal (*Tb*HK) and C-terminal His-tag (*h*GCK). When determining enzymatic kinetic parameters for the enzyme-nanoparticle interaction studies (Chapter 4), the K_m and V_{max} values determined from the Hanes-Woolf plots will be employed. The His-tag may have affected the folding and unfolding of the protein, As this is hypothetical , it presents a feasible research route to express the proteins either without the His-tag or to remove the tag and compare the their characteristics to the ones presented here and to research work found elsewhere in literature. The parameters determined from the optimization and characterization of the two enzymes was used in chapter 4 where *Tb*HK and *h*GCK were interacted with chemically synthesized silver NPs.

Chapter 4

Metallic silver NPs synthesis characterization and interactions with hexokinase

4.1. Introduction

Nanotechnology is an emerging and an important field of current research. This field focuses on the design, synthesis of nano-scale particles (1-100 nm), and their manipulation. Metallic NPs, including silver NPs, have shown importance in many areas of research due to their size and shape dependent optical, electrical and magnetic properties (The royal society, 2004). Silver NPs (AgNPs) have been synthesized using chemical (Pal *et al.*, 2008; Patil *et al*., 2011) and biological methods (Galvez *et al.*, 2008; Krutyakov *et al.*, 2008; kasthuri *et al.*, 2009; Das *et al*, 2011Huang *et al*., 2013).

4.1.1. Chemical methods

The citrate and the sodium borohydride methods are two of the most commonly used chemical methods for synthesizing silver nanomaterials (Krutyakov *et al*., 2008). The citrate method was originally used for the synthesis of metallic gold NPs (the Turkevich method) of gold nanoparticle synthesis (Krutyakov *et al*., 2008). Guzman *et al.* (2009) used the principles of the citrate method to synthesize spherical silver NPs, where 1 mM – 6 mM of silver nitrate ($AgNO_3$) was reduced to silver NPs by a combination of sodium citrate (1 mM - 2 mM) and hyrdazine hydrate (2 mM - 12 mM) as reducing agents. The NPs were stabilized by 8% (w/w) sodium dodecyl sulphate at room temperature. Elsewhere silver NPs have been synthesized using the citrate method (Fang *et al*., 2005; Šeikate *et al*., 2006).

One of the most common methods for synthesizing silver NPs is the use of sodium borohydride as a reducing agent of silver nitrate. Sodium borohydride has also been used as both the reducing and stabilizing agent (Mavani and Shah, 2013). In this method 2 ml of 1 mM silver nitrate is added to 2 mM sodium borohydride cooled in an ice bath, at a rate of 1 drop per second while stirring (Dong *et al*., 2012; Mavani and Shah, 2013). Song *et al*. (2008), reported on the synthesis of silver NPs using the sodium borohydride method with the addition of sodium dodecyl sulphate

as a stabilizer. Silver NPs of controlled size and shape can be prepared by laser irradiation of an aqueous solution of silver salt and surfactants. Microwave assisted synthesis of silver NPs employing silver nitrate solution (Pal *et al.*, 2008), carboxymethyl cellulose sodium (Chen *et al.*, 2008), silver nitrate-ethylene-glycol-H_2-[$PtCl_6$]-polyvinylpyloridone solution (Tsuji *et al*., 2008) have been reported.

Silver NPs can be synthesized using polysaccharides as both a reducing agent and as a capping agent (Korberkandi and Iravan, 2012). Raveendran and Wallen (2003) reported on the synthesis of starch – silver NPs using the polysaccharide method where α-D-glucose was used as a reducing agent and starch as a capping agent. Huang and Yang (2004) experimented on the synthesis of silver NPs by the use of negatively charged heparin as a reducing agent, stabilizing agent and a nucleation controller. Tollens method is another simple one step process that has recently been used to make silver NPs where the size is controlled (Kaler *et al*., 2010). This method involves the reduction of diaminosilver [$Ag(NH_3)_2$] (The Tollens reagent) by an aldehyde. Silver ions are reduced by saccharides in the presence of ammonia, yielding silver NPs with sizes ranging from 50 to 200 nm. It has been reported that glucose, galactose, maltose and lactose can also be used as reducing agents in the synthesis of silver NPs (Korberkandi and Iravan, 2012).

4.1.2. Biological synthesis

Biological synthesis of silver NPs with desired morphology and sizes have been achieved by the use of natural reducing, capping and stabilizing agents. Biological method of synthesizing silver NPs have become a major focus of research since in this method there is very limited or no use of harsh, highly toxic and expensive chemical substances. Extracts from proteins, enzymes, amino acids, vitamins polysaccharides, plants, bacteria, fungi, yeast, viruses and actinomycetes have been employed as bio-reducing agents (Huang *et al*., 2007; Korbekandi and Iravan, 2012).

Silver NPs synthesis using bacteria, a mechanism that utilizes the presence of nitrate reductase enzyme is widely accepted where nitrate reductase converts nitrate into nitrite. During the reduction it is proposed that an electron is transferred to the silver ion Ag^+, reducing the silver ion to Ag^0 (Prahbu and Poulose, 2012). This was observed in *Bacillus licheniformis* (figure 4.1)

which secretes NADPH and NADPH-dependent enzymes such as nitrate reductase that effectively convert Ag^+ to Ag^0 (Vaidyanathan *et al.*, 2007). Anil Kumar *et al.* (2006) further reported the synthesis of silver NPs by using purified nitrate reductase from *Bacillus subtilis*, *Corynebacterium* and Lactobacillus have also been used to induce the formation of silver NPs (Mouxing *et al*., 2006; Saifuddin *et al*., 2009; Korbekandi and Iravani, 2012). Haefeli *et al.* (1984) reported the synthesis of silver NPs by *Pseudomonus stutzeri*. Culture supernatants of *Escherichia cloacae*, *Klebsiella pneumonia* and *E. coli* (Shahverdi *et al*., 2007; Gurunathan *et al.*, 2009), *Bacillus licheniformis*, *Staphylococcus aureas* (Nanda and Saravanan, 2009) are all able to cause rapid formation of silver NPs.

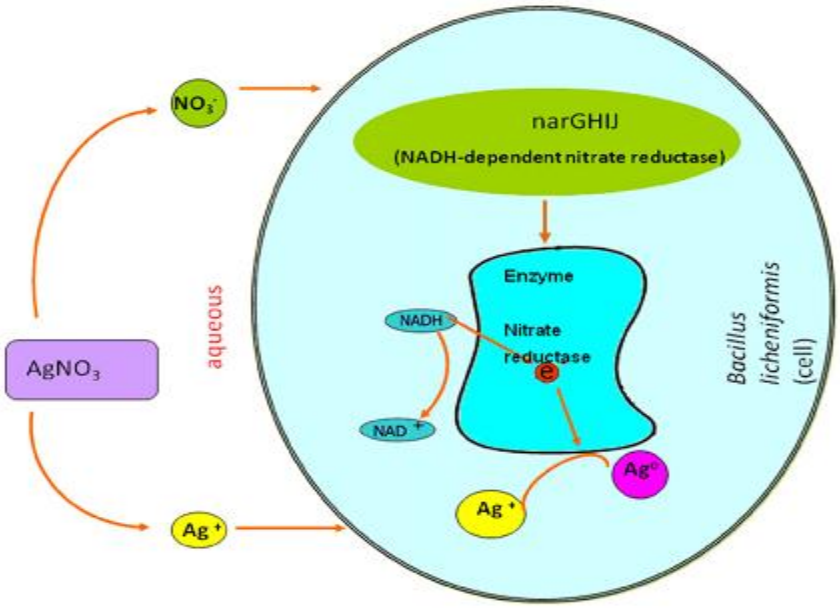

Figure 4.1: Possible mechanism for silver NPs synthesis involving nitrate reductase that may convert Ag^+ to Ag^0 through electron transfer mechanism (adapted from Kalimuthu *et al*., 2008).

Another method of synthesizing silver NPs is by using fungi. Ahmed *et al.* (2003) experimented with the extracellular synthesis of silver NPs ranging in size from 5 to 50 nm. In their findings they discussed the action of an NADH-dependent reductase that was thought to be responsible for the reduction of Ag^+ and the subsequent formation of silver NPs. Ingle *et al.* (2008) managed to extracellulary prepare AgNPs with an average size of 19 nm by *F. solani*. Bhainsa and Souza in 2006 employed the fungus *Aspergillus fumigatusin* to synthesis silver NPs. Kathiresan *et al.* (2009) produced AgNPs using a marine fungus *Penicillium fellutanum* isolated from coastal

mangrove sediments. Other fungal strains used to synthesize silver NPs include; *P. chrysosporium* (Vigneshwaran *et al.*, 2006*); Phanerochaete boryanum* (Lengke *et al*., 2007); *Cladosporium cladosporiodes* (Balaji *et al*., 2009) and *Coriolus versicolor* (Sanghi and Verma, 2009). Plants and plant extracts have also been employed in the synthesis of AgNPs. *Camelia sinensis* and black tea leaf extracts have been used as reducing agents in the synthesis of AgNPs (Vilchis – Nester *et al*., 2008; Begum *et al*., 2009). Song and Kim, (2008) reported the rapid biological formation of silver NPs using *Pinus desiflora*, *Diospyros kaki, Ginko biloba, Magnolia kobas* and *Platanus orientalis* leaf broths that produced AgNPs of between 15 and 500 nm.

4.1.3. Potential uses for silver NPs

AgNPs have attracted the attention of researchers due to their dynamic and extensive applicability over a broad range of disciplines that includes but not limited to; sensors, bio-labelling, filters, antimicrobial deodorant fibres, low cost paper batteries, and antimicrobials. AgNPs have been used widely as antimicrobial agents hence their usage in health, textile coating, food storage and a number of environmental areas (Korbekandi and Iravani, 2012). Cho *et al.* (2005) as well as Duran *et al.* (2005) reported on the antimicrobial effects of AgNPs on *E. coli, V. cholera*, *B. subtilis* and *P. aerogenosa*. Due to their antimicrobial effects, silver NPs have been used in various applications including disinfecting medical devices, home appliances and in water treatment, and as additives to some medical devices i.e. polymethylmetacrylate bone cement, surgical masks and implantable devices. Roe *et al.* (2008) reported on the antimicrobial properties of silver NPs coated on plastic catheters against *E. coli, S. aureas, Enterococcus, C albicans, P. aerogenosa* and *Staphylococcus*. HIV-1 virus infected cells (Hut/CCR5) undergo a HIV-associated apoptosis due to the inhibition of the viral replication by silver NPs, further AgNPs antiviral effects were reported where they successfully prevented the binding of the virus to the host cell (Sun *et al*., 2005). The prevention of cell free and cell associated transmission of HIV-1 and the pressure that AgNPs exerts in the early viral replication steps prevent CD4-dependent viral binding, fusion and ultimate infectivity (Lara *et al*., 2010). Lu *et al*. (2011) reported on the possibility of silver NPs inhibiting *in vitro* assembly of hepatitis B virus. Xiang *et al*. (2011) reported on the inhibitory effects of silver NPs against H1N1 influenza-A virus. Silver NPs also have notable effects on various viruses including; *Respiratory syncytial virus, Monkeypox virus, Tacaribe virus (TCRV), Herpes simplex virus type-1* (HSV-1) (Galdiero *et al*

2011) Singh *et al.* (2008) reported that AgNPs have also been used in the diagnosis and treatment approaches in cancer and Alzheimer's patients.

There is increase in AgNP consumer products, which has increased research in order to understand the correlation between the unique properties of AgNPs and their risk to human health and to the environment. There is inadequate information on the serious effects of silver NPs to humans that have so far been reported. As articulated by Lubick, (2008), it is not known whether the cytotoxicity is a result of the effects from NPs, or by Ag^{+} released by the AgNPs, or possibly both. Negative effects of silver NPs include argyria, a skin condition that results from a prolonged ingestion of silver NPs (Korbekandi and Iravani, 2012). Haase *et al*. (2011) demonstrated the cytotoxic effects of silver NPs on human macrophages and liver cells' oxidative stress dependent cytotoxicity was reported by Kim *et al*. (2009). Furthermore, Park *et al.* (2011) reported the size dependent cell toxicity and inflammatory response in human cells.

The main aims of the current chapter are;

1. Chemical synthesize silver NPs
2. Characterization of the synthesized silver NPs
3. Assessment of the effects of silver NPs on the activity of *Tb*HK and *h*GCK

4.2. Materials and methods

4.2.1. Silver NPs synthesis

In order to synthesize silver NPs, 100 mM sodium nitrate solution was prepared (16.988 mg silver nitrate dissolved in 1 ml of distilled water), and 200 µl of this solution was then added to 10 ml of 1% ethanolic polyvinylpyrrolidone (PVP) (100 mg PVP dissolved in 10 ml of 95% ethanol) in a total volume of 25 ml. The solution was microwaved for 5 sec at full power (Defy, 700W MD 0348 model microwave).The solution was left at room temperature and the colour change, from clear to pale yellow, which denoted the formation of the silver NPs. The sample was stored in a glass bottle in the dark for further experimental procedures. In this AgNPs synthesis, ethanol and heat acted as reducing agents while polyvinylpyrrolidone was used as stabilizing agent (Pal *et al*., 2009).

4.2.2. Silver nanoparticle characterization

The final concentration of the prepared AgNPs solution (section 4.2.1) was estimated to be 64 mM. The NPs were characterized in terms of size, morphology and distribution using transmission electron microscopy and UV-visible spectroscopy.

4.2.2.1. Transmission Electron Microscopy

The transmission electron microscopy (TEM) samples were prepared 24 h in advance of viewing in order for the sample to completely dry. A drop of the AgNPs solution was placed on Formvar/carbon film on 200 mesh copper grids (Agar Scientific) and sample was allowed to settle for 20-30 sec. The excess sample was removed by touching the edges of the copper TEM grid with a filter paper. The TEM grid was left overnight to completely dry. Micrographs were obtained using Zeiss Libra 120 Transmission Electron Microscope operating at 120 keV.

4.2.2.2. Ultra-violet visible spectroscopy

Ultra-violet visible spectroscopy also referred to as absorption or reflectance spectroscopy within the Ultraviolet-visible region was used to characterize the optical properties of the synthesized AgNPs. The synthesized silver nanoparticle samples (section 4.2.1) analyzed using a wave scan at a wavelength range from 300 -700 nm using a Spectroquant Pharo 300 (Merck, Darmstadt, Germany) UV-Visible spectrophotometer to obtain the surface plasmon resonance (SPR) of the silver NPs.

4.2.2.3. Silver NPs stability

The synthesized NPs (section 4.2.1) were assessed for their stability at different storage conditions and the effects of light on storage. Two 10 ml samples were aliquoted into screw capped bottles and wrapped with tin foil (Morales-Sanchez *et al.*, 2011). One nanoparticle sample bottle was kept at room temperature and the other was kept at 4°C over a period of one month. Samples collected at the beginning and end of the incubation period after which the samples were analyzed using TEM (section 4.2.2.1) and ultra-violet visible spectroscopy (section 4.2.2.2).

4.2.3. Interaction of G6PDH with AgNPs

To assess the effect of AgNPs on the hexokinase assay (section 4.2.4) used to determine activity of the *Tb*HK and *h*GCK, different concentrations of AgNPs were incubated with the assay components (table 3.5 Chapter 3). AgNP concentrations evaluated ranged from 0.1 to 100 µM. As described in section 3.2.5.1 the hexokinase assay is a coupled assay and the coupling enzyme (G6PDH) was assayed independently to evaluate the effect of the AgNPs using the Worthington G6PDH assay. The G6PDH assay components are given in table 4.1. The G6PDH assay was adapted from the Worthington glucose-6-phosphate dehydrogenase assay, with changes made in order to replicate the reaction mixture conditions used in the standard hexokinase assay. A normal G6PDH assay (without added NPs) was performed in parallel to the interaction assay and this was used as a reference to calculate the percent relative activity as described in section 3.2.5.2.

Table 4.1: G6PDH and silver NPs interaction assay components.

Ingredients	**G6PDH (µl)**	**G6PDH / AgNPs (µl)**	**AgNPs (µl)**
Tris-HCl reaction buffer, pH 8.0	270	260	260
16.8 mM NAD	10	10	10
100 mM G6P	10	10	10
300 U G6PDH	10	10	0
AgNPs (0.1 to100µm)	0	10	10

In the standard coupled hexokinase assay, G6PDH was a pre-added ingredient in the reaction mixture and reaction is initiated by the addition of hexokinase (section 3.2.5.1). In order to replicate this in the current assay; all assay ingredients were pre-added, including the different AgNP concentrations and the reaction was initiated by the addition of the G6PDH. Enzyme activity calculations were conducted as the standard coupled hexokinase assay (section 3.2.5.2), since in both assays the production of NADH is monitored at 340 nm.

4.2.4. Silver NPs interaction with *Tb*HK and *h*GCK (NP range finding)

In order to obtain the appropriate nanoparticle concentration for the enzyme-silver nanoparticle kinetic studies; various nanoparticle concentrations were prepared and interacted with the expressed enzymes using the standard hexokinase assay (section 3.2.5.1). The initial silver nanoparticle concentrations ranged from 0.1 to 100 µM. Ethanol/PVP (1%) solution was used as

negative control, and was diluted by the same procedure as the nanoparticle solution. Assay additive concentrations and assay parameters are given in table 4.2 which is an adaptation of the conditions described in section 3.2.5.1. A standard coupled hexokinase assay for *Tb*HK and *h*GCK was performed simultaneously with the interaction assays and their outcomes were used as the 100% relative activity values.

Table 4.2: Silver NPs range finding interaction hexokinase assay components (adapted from table 3.5).

Ingredients	**Protein (µl)**	**Protein AgNPs (µl)**	**EtOH.PVP Control (µl)**	**Assay Control (µl)**
Tris-HCl reaction buffer, pH 8.0	210	200	200	220
0.67 M Glucose	50	50	50	50
16.5 ATP	10	10	10	10
6.8 mM NAD	10	10	10	10
300 U G6PDH	10	10	10	10
*Tbr*HK/*h*GCK	10	10	10	0
AgNP ranges	0	10	0	0
EtOH.PVP	0	0	10	0

4.2.5. Enzymes (*Tb*HK and *h*GCK) and AgNPs interaction studies kinetics

In order to evaluate the type of effect the silver NPs have on *Tb*HK and *h*GCK, a full set up of kinetic experiments were performed that were similar to the kinetic experiments described in section 3.2.8. A nanoparticle concentration of 0.1 µM was selected for the interaction studies (sections 4.3.6.1) for both the *Tb*HK and *h*GCK NPs interaction kinetic studies. The substrate concentration used for the *Tb*HK/AgNP kinetics were 4 µM, 8 µM, 16 µM, 33 µM, 67 µM, 100 µM, 133 µM, 167 µM, 233 µM, 333 µM and for the *h*GCK interaction kinetic studies the substrate concentrations used were 0.1 mM, 1 mM, 2.5 mM, 5 mM, 10 mM, 15 mM, 20 mM, 25 mM, 30 mM, 40 mM, 50 mM and 100 mM. The standard hexokinase assay (section 3.2.5.1) was employed with appropriate modifications, after optimum incubation at 40°C for *Tb*HK and 37°C for *h*GCK (section 3.2.7), respectively. Kinetic data was recorded at 60 minutes (T60) for *Tb*HK and at 90 minutes (T90) for *h*GCK. The experimental data for the enzyme and silver NPs interaction kinetics obtained for *Tb*HK and *h*GCK were analyzed using Michaelis-Menten and Hanes-Woolf plots. The enzyme and silver NPs interaction hexokinase assays were performed concurrently with the assay negative control and a normal kinetic run.

4.3. Results and Discussion

4.3.1. Silver nanoparticle synthesis

Silver NPs were prepared using a microwave assisted method (Pal *et a*l., 2009) as described in section 4.2.1. Immediately after adding $AgNO_3$ into the ethanolic PVP solution, no obvious discoloration was observed (figure 4.2A). Heating the $AgNO_3$ / ethanolic-PVP solution for 5 seconds in the microwave led to a colour change from colourless to pale yellow (figure 4.2B), indicating the formation of silver NPs (Solomon *et al.*, 2007; Pal *et al*., 2009; Vaidyanathan *et al.*, 2010; Patil *et al*., 2011).

Overnight storage of the microwaved solution at room temperature in the dark resulted in the development of an intense orange/yellow colour (figure 4.2C). This observation can be contributed to the seeding phenomenon, which is explained as the maturation (growth) of the initial nanoparticle seeds formed upon microwaving (Šileikaite *et al.*, 2009).

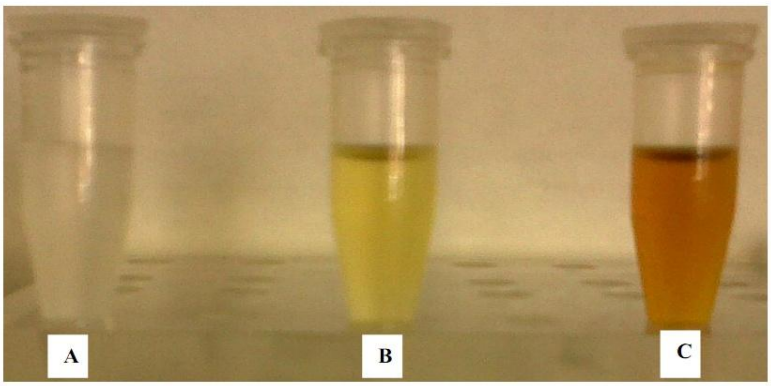

Figure 4.2: Microwave assisted silver NPs synthesis. (A) Solution prior to microwaving, (B) Solution immediately after microwaving, showing slight colour formation (C) 24 hours after microwaving, showing intense colour formation.

4.3.2. Transmission Electron Microscopy

Silver NPs synthesized as described in section 4.2.1 were visualized using TEM as described in section 4.2.2 to determine nanoparticle sizes, shape and distribution. Three hundred NPs were counted and the sizes were determined using Image J software (version 1.42). Figure 4.3A is representative of the nanoparticle morphology immediately after synthesis, while figure 4.3B represents the nanoparticle counts and size distribution plot. The size of the NPs immediately

after synthesis ranged from 2-18 nm and was consistently spherical in morphology. The average size was 6 nm. These observations are similar to those reported in the literature (Pal *et al*., 2009; Singh *et al.*, 2009; 2009; Hsu and Wu, 2011). At 24 h post synthesis nanoparticle morphology was still spherical but there was a slight shift in the size distribution.

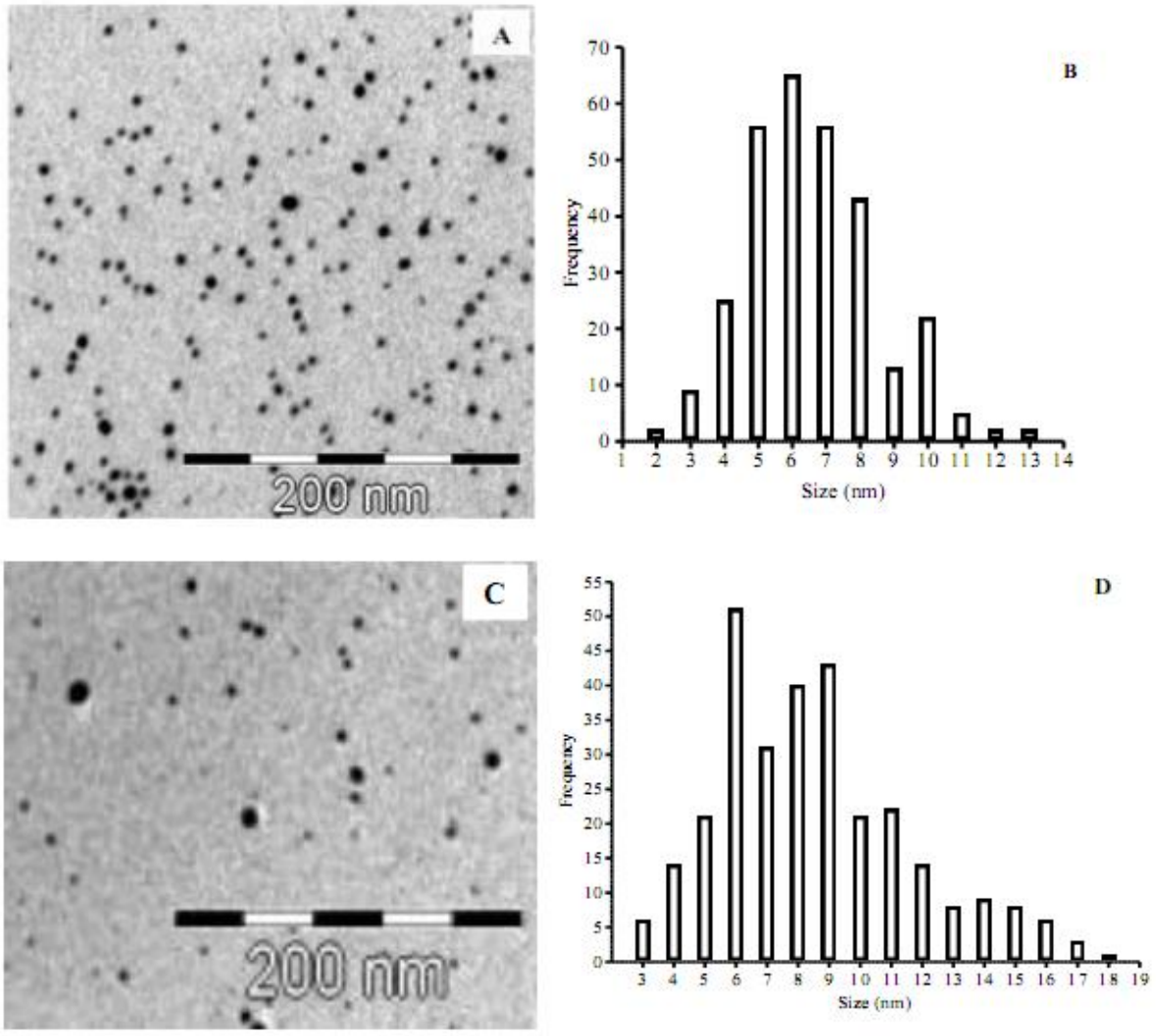

Figure 4.3: TEM micrographs of silver NPs and their size distribution. (A and B) AgNPs morphology and sized distribution immediately after synthesis. (C and D) AgNPs morphology and size distribution 24 h after synthesis.

Figure 4.3B showed a narrow size distribution with particles mostly between 5 and 8 nm. While figure 4.3D shows a slight increase in nanoparticle size but still with an average size of 6 nm.

With the observation made, it is recommended to use freshly prepared NPs for experiments for any slight change in their sizes may bring changes in their size dependent properties.

4.3.3. Ultra-Violet visible spectroscopy

A characteristic UV light absorbance wavelength of silver NPs synthesized is shown in figure 4.4 is consistent with reported spectrums (Gusman *et al*., 2009; Nanda and Siravanan, 2006; Kalimuthu *et al.*, 2008; Gurunathan *et al*., 2009; Viadyanathan *et al.*, 2010; Patil *et al*., 201l; Hsu and Wu, 2011).

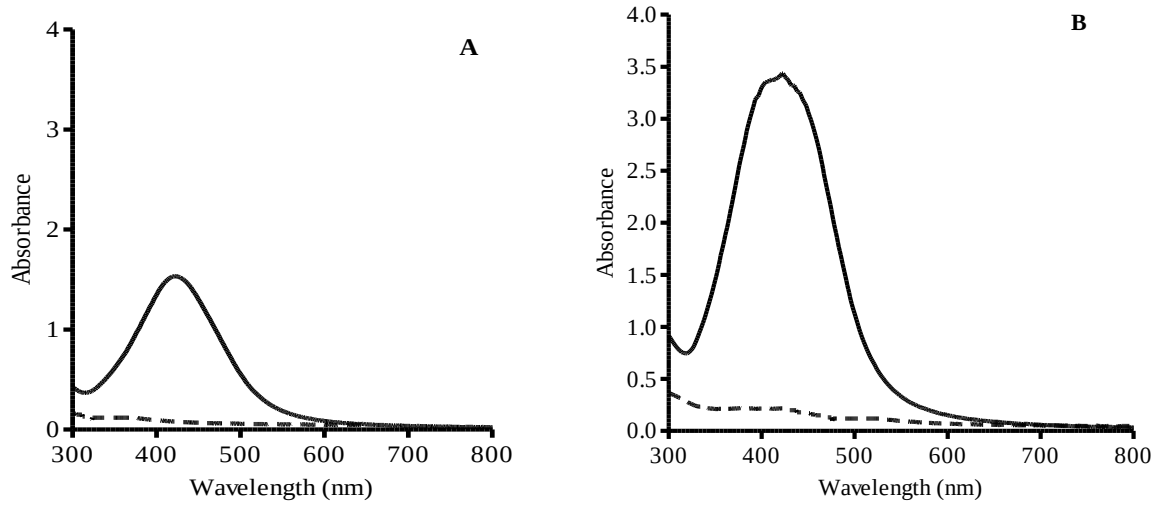

Figure 4.4: Silver NPs spectrophotometric analysis. (A) Silver NPs exhibiting a strong peak at 421 nm (solid line) at time 0 h and a negative control (dashed line) showing no apparent peak. (B) Silver NPs with a peak at 423 nm 24 hour after synthesis (solid line) and a negative control (dashed line) showing no peak.

4.3.4. Nanoparticle stability

Retaining nanoparticle stability is of vital importance in the study of NPs since they are prone to aggregation under varying conditions (Huang *et al*., 2010). Silver NPs synthesized as described in section 4.2.1 were stored under varying conditions. After one month of storage at room temperature and in the dark the NPs still had a spherical morphology (figure 4.5A) and a similar size distribution pattern (figure 4.5B) to the 24 h synthesized nanoparticle solution (figure 4.3D) with average nanoparticle size of 9-10 nm. When the nanoparticle solution was store at 4°C, the AgNPs tended to form aggregates (figure 4.5C) and had a slight increase in size, from 6 nm to 18

nm. This may imply that nanoparticle stability is temperature dependent, and for this reason, NPs stored at room temperature and obscured from direct light were used for the enzyme interaction studies (section 4.3.6). This is in line with reports in literature (Morales-Sanchez *et al.*, 2011).

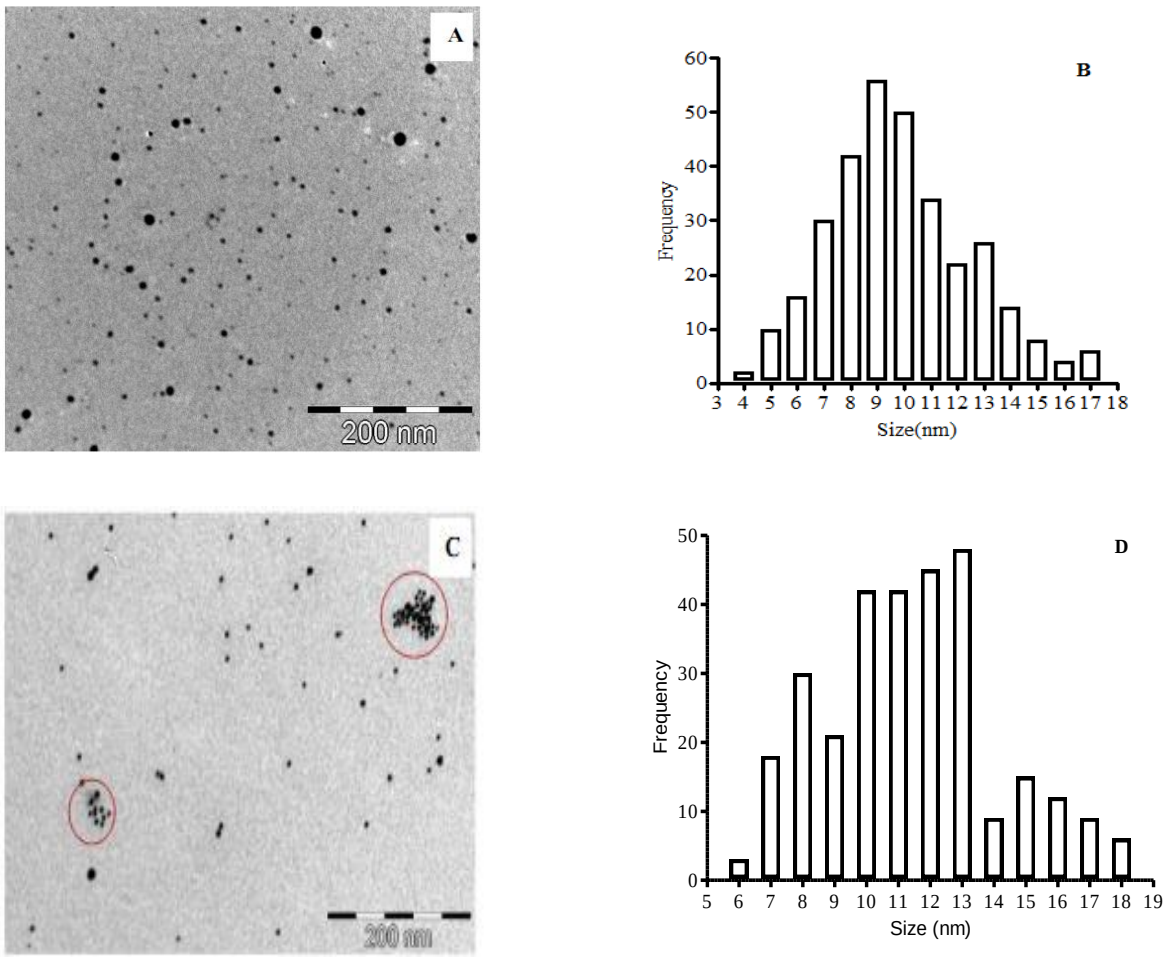

Figure 4.5: Silver nanoparticle stability under different conditions for 8 weeks. (A and B) TEM micrograph and size distribution graph of the sample stored at room temperature in the dark, (C and D) TEM micrograph and the size distribution graph of silver nanoparticles stored a 4°C in the dark.

4.3.5. Interaction of G6PDH with AgNPs

The effect of silver NPs on the enzymatic activity of the coupling enzyme (G6PDH) in the standard hexokinase assay (section 3.2.5.1) was investigated as described in section 4.2.3. G6PDH activity was determined in the presence of various concentrations of silver NPs. Figure

4.6 represent the results obtained and indicates that the lower concentration range had the least effect on the assay. AgNP concentrations of 0.1 and 0.25 μM only inhibit G6PDH activity by 35 and 41%, respectively, and concentrations of 0.5, 1, 5, 20, 50, 100 μM inhibit *Tb*HK by 63 %, 65%, 80%, 75%, 70% and 82%, respectively. The latter concentrations inhibit the enzyme activity in higher magnitudes and therefore were not ideal concentrations for the interaction studies. Therefore the final concentration of 0.1 μM silver NPs was chosen for the enzyme-silver nanoparticle interaction kinetics.

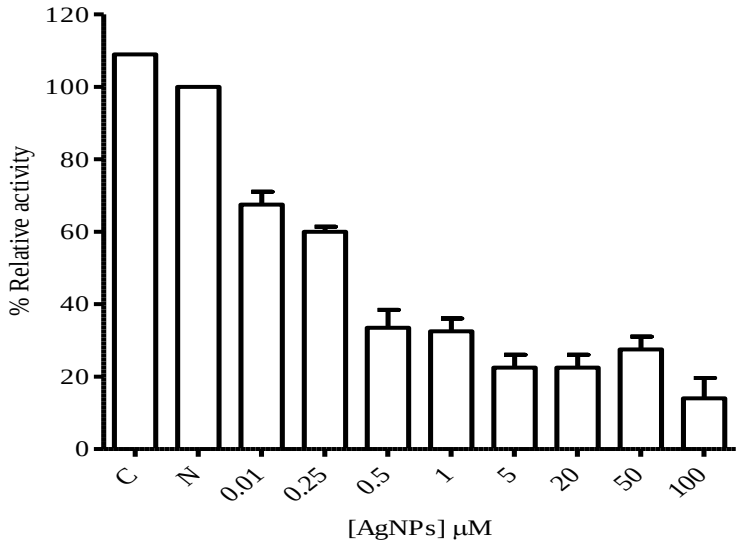

Figure 4.6: A bar graph of different AgNP concentrations vs percent relative activity of G6PDH. (C) represents a control assay containing 1% ethanol.PVP and (N) represents a standard HK assay (100% activity).

4.3.6. Silver nanoparticle interaction studies with *Tb*HK and *h*GCK

*Tb*HK and *h*GCK were subjected to varying silver nanoparticle concentrations both to determine the concentration of nanoparticle that would present desired outcomes of minimal inhibition and allow the determination of the enzymes' kinetic behaviour under the influence of silver NPs.

4.3.6.1. Silver nanoparticle range finding

*Tb*HK and *h*GCK were subjected to varying concentrations of silver NPs (0.1-100 μM) as described in section 4.2.4. Figure 4.7A illustrates that Ethanol.PVP has no apparent effect on the *Tb*HK enzymatic activity. Silver nanoparticle concentrations of 0.1 μM and 0.25 μM inhibited

the enzyme activity by approximately 10% and 30%, respectively. A 40% inhibition to the *Tb*HK activity was observed with silver nanoparticle concentrations of 0.5 µM and 1 µM. AgNP concentrations of 5 µM , 20 µM and 100 µM exhibited more than 50% inhibition of the enzyme activity, making them not ideal for the interaction kinetics as they inhibited the enzyme activity by too a higher margin. Therefore a concentration of 0.1 µM was selected and used in the enzyme-nanoparticle interaction kinetics.

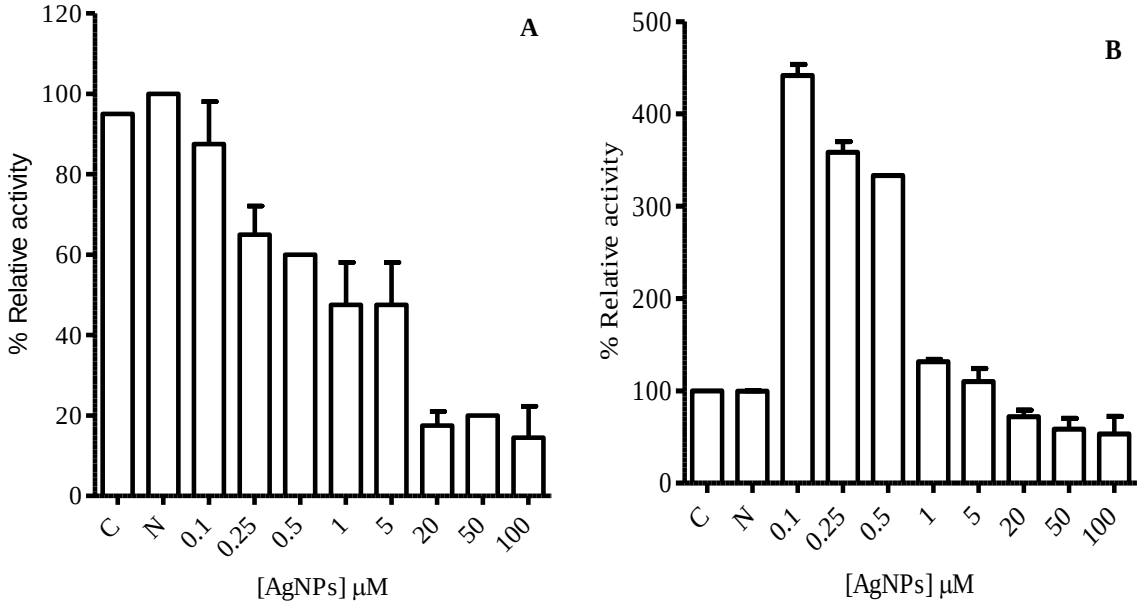

Figure 4.7: Silver nanoparticle range finding interaction assays for (A) *Tb*HK and (B) *h*GCK

Figure 4.7B illustrates that silver nanoparticle concentrations of 0.1 µM, 0.25 µM and 0.5 µM exponentially increased the enzymatic activity of the human glucokinase (up to 4 fold) as compared to the hexokinase assay without silver NPs. Silver nanoparticle concentrations of 1 µM and 5 µM activated the enzyme by approximately 20% and concentrations of 20 µM, 50 µM and 100 µM of silver NPs inhibited the enzyme by approximately 20%. The interaction negative control (Ethanol.PVP) had negligible effect on the assay as it showed the same percent relative activity as the reference assay. When a molecule is bound to an enzyme, it has a negative or a positive effect on the activity of the enzyme. Some molecules increase the enzyme activity (enzyme activators) and others inhibit the activity of the enzyme (enzyme inhibitor).In the

current work, the synthesized enzyme *Tb*HK and *h*GCK (chapter 3) and their changes in activity will be assessed after being interacted with silver NPs (section 4.2.5).

Enzyme inhibition can be divided into 2 main types, reversible and irreversible inhibition. The reversible enzyme inhibition is further typified into 4, these includes: (i)Competitive inhibition: in this type of inhibition, the inhibitor competes with the substrate in binding to the active site of the enzyme, thereby negatively affecting the affinity of the enzyme for its apparent substrate. However, further increase in substrate concentration alleviates the inhibitory effect. Therefore in competitive inhibition there is an increase in the apparent K_m and with a constant V_{max}; (ii) Un-competitive inhibition: an uncompetitive inhibitor binds to the enzyme only after the enzyme has forms an enzyme-substrate complex.

The binding of the inhibitor to the enzyme decreases the enzyme's ability to remain bound to the substrate. This result in the decrease of both K_m and V_{max} values, an effect brought about by the elimination of the enzyme-substrate complexes, the increased binding efficacy as the enzyme develops a new reaction equilibrium state in counteracting the imposing effect (Le Chateliars principle) and as a result of removing the activated complexes respectively; (iii) Non-competitive inhibition: in this type of inhibition, the inhibitor can bind to both complexed and free enzyme. The binding of the inhibitor to the enzyme reduces the enzymatic activity but it does not affect the substrate binding affinity; therefore the V_{max} decreases while the K_m may remain constant; (iv) Mixed inhibition: in this type, the inhibitor can bind the enzyme at the same time as the substrate binds to the enzyme. The binding of the inhibitor may cause the enzyme to have less affinity to its substrate. This inhibition may be reduced but not overcome by an increase in substrate concentration. The induced inhibition is generally a result of the inhibitor binding to an allosteric site that triggers the enzyme's conformational change with a concomitant reduction in the affinity of the enzyme active site to its substrate. Therefore, mixed inhibition results in an increased K_m and reduced V_{max} (Stryer, 1995; and Voet, 2004). With irreversible inhibition the enzyme usually gets modified when the inhibitor binds to the enzyme. Irreversible inhibitors usually interact with serine, threonine, tyrosine and cysteine amino acid side chains (hydril and sulfhydril groups) and form covalent bonds.

4.3.6.2. Effect of silver NPs on *Tb*HK and *h*GCK

The effects exerted by silver NPs on the *Tb*HK and *h*GCK enzymes activity were investigated as described in section 4.2.5. A complete set of enzyme kinetics (chapter 3) and enzyme-NPs (chapter 4) interaction kinetics were carefully performed using 0.1 µM silver NPs as inhibitor/activator. The kinetic data was analyzed by Michaelis-Menten and Hanes-Woolf plotting. The comparison of the kinetic *Tb*HK and *h*GCK studies to those of *Tb*HK and *h*GCK under the influence of 0.1 µM silver NPs is presented in figures 4.8 and figure 4.9.

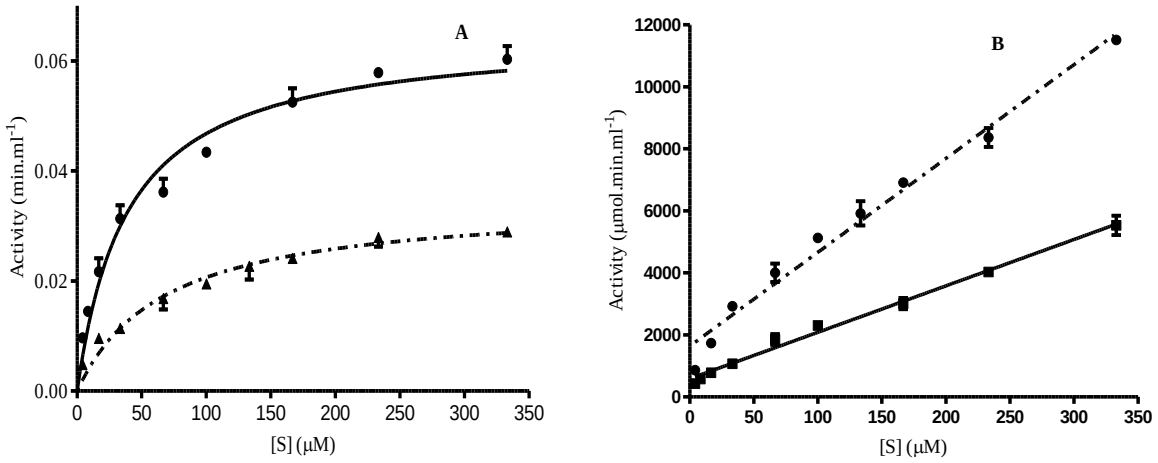

Figure 4.8: Hanes-Woolf and Michaelis-Menten of *Tb*HK kinetics (solid lines) and *Tb*HK kinetics under the influence of silver NPs (dashed lines).

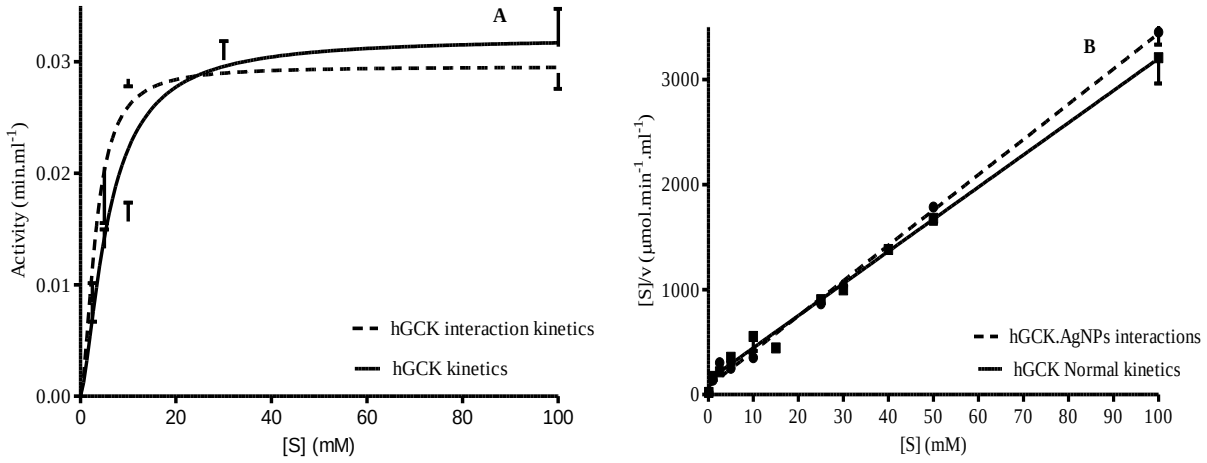

Figure 4.9: Hanes-Woolf and Michaelis-Menten of the normal *h*GCK kinetics (solid lines) *h*GCK kinetics under the influence of silver NPs (dashed lines).

As illustrated in table 4.3, *Tb*HK and silver NPs interaction kinetic parameters using Hanes-Woolf plotting indicates an increase in the K_m value, from 39 µM to 54 µM with an apparent reduction in V_{max} from 0.066 µmol.min^{-1}.ml^{-1} to 0.033 µmol.min^{-1}.ml^{-1} and K_{cat} / K_m value from 0.0526 min^{-1}.µmol^{-1} to 0.0380 min^{-1}.µmol^{-1} This represents a 38% reduction in the enzymes affinity to its substrate, 50% reduction in its activity and a 28% reduction in the enzyme efficiency. Although Hanes-Woolf plotting was the analysis choice in the interaction kinetic studies, Michaelis Menten analysis of the kinetic data revealed a similar pattern of the kinetic parameters, where an increase in the K_m value from 39 µM to 68 µM was determined, representing a 74% reduction in the enzyme's affinity to its substrate. There was an observed decrease in the V_{max} value from 0.066 µmol.min^{-1}.ml^{-1} to 0.035 µmol.min^{-1}.ml^{-1}, representing a 47% decrease the enzyme's activity, a 42% reduction in the enzyme efficiency from 0.0522 min^{-1} to 0.0303 min^{-1}. There is a close similarity in the change of the activity when the interaction data is analyzed by both Michaelis-Menten and Hanes-Woolf, but the change in K_m provides different outcomes of 74% and 50%, respectively. However Hanes-Woolf results were accepted for this project for its accuracy. The inhibition pattern obtained for *Tb*HK (increased K_m and reduced V_{max}) falls under the mixed type of inhibition where there is a resultant decrease in the affinity of the enzyme to its substrate with a concomitant reduction in the overall enzyme activity. A phenomenon that is caused by the enzyme inhibitor and the substrate binding to the enzyme simultaneously, thereby reducing the affinity of the enzyme to its substrate and thus reducing its activity.

Table 4.3: A comparison of *Tb*HK to silver nanoparticle and *Tb*HK interaction kinetics parameters.

Plot type	***TbHK kinetics***				**AgNPs/*Tbr*HK interaction kinetics**			
	K_m (µm)	V_{max} (µmol.ml^{-1}.min^{-1})	K_{cat} (min^{-1})	K_{cat}/K_m (mol^{-1}.min^{-1})	K_m (µm)	V_{max} (µmol.ml^{-1}.min^{-1})	K_{cat} (min^{-1})	K_{cat}/K_m (mol^{-1}.min^{-1})
Michaelis-Menten	39.3	0.066	2.05	0.0522	68	0.035	2.05	0.0302
Hanes-Woolf	39.	0.066		0.0526	54	0.033		0.0380

Table 4.4: A comparison of *h*GCK to silver nanoparticle and *h*GCK interaction kinetics parameters.

Plot type	***h*GCK kinetics**					**AgNPs/*h*GCK interaction kinetics**				
	K_m (μm)	**V_{max}** ($\mu mol.min^{-1}.ml^{-1}$)	**h**	**K_{cat}** (min^{-1})	**K_{cat}/K_m** ($min.\mu mol^{-1}$)	**K_m** (mM)	**V_{max}** ($\mu mol.min^{-1}.ml^{-1}$)	**h**	**K_{cat}** (min^{-1})	**K_{cat}/K_m** ($min^{-1}.\mu mol^{-1}$)
Michaelis-Menten	4.0	0.032		11.25	2.813	3	0.028		11.25	3.75
Hanes-Woolf	4.5	0.032	1.5		2.5	3	0.029	1.8		3.75

As illustrated in table 4.4, when the human glucokinase is interacted with silver NPs, a unique pattern is revealed when the kinetic data is analyzed by Hanes-Woolf plotting. There is a significant decrease in the K_m value from 4.5 mM to 3 mM representing a 33% increase in the affinity of the enzyme to its substrate (glucose). There is a notable slight decrease in the V_{max} value from 0.032 $\mu mol.min^{-1}.ml^{-1}$ to 0.029 $\mu mol.min^{-1}.ml^{-1}$ representing 9% decrease in the maximal enzyme activity (V_{max}), and an apparent increase in the enzyme efficiency from 2.5 min^{-1} to 3.75 min^{-1}, representing a 50% increase. Michaelis-Menten analysis of the interaction kinetic data reveals a similar change in the K_m value, from 4.0 to 3 mM, a 13% reduction in maximal enzyme activity (V_{max}) and 34% increase in the enzyme efficiency (K_{cat}/K_m).

This inhibition pattern falls under the un-competitive inhibition. This type of inhibition is as a result of the inhibitor binding to the enzyme after the enzyme has already formed a complex with its substrate, resulting in the release of the initially formed enzyme-substrate complex and the enzyme binds to a new substrate, thereby reducing the enzyme activity but increasing the substrate affinity.

In general, designed hexokinase or glucokinase inhibitors should possess features that include; (i) compounds should be derivatives of glucosamine that facilitates a high similarity to the enzyme substrate (glucose), (ii) C-2 position should be the substituted atom, (iii) the presence of an aryl group is required to promote the binding of the compound to the enzyme through an amidic bond, (iv) the length of the aryl substituent should be varied to maximize contact with the enzyme, (v) substituent molecule on the aromatic ring should be alternated according to their

ability to release or withhold electrons, (vi) the ortho and meta positions of the aromatic ring should be varied so that the space within the active site may be explored by ring rotation (Wilson *et al*., 2002). Silver NPs have no similarities to the designed glucosamine inhibitors that inhibit *Tb*HK (Wilson *et al.,* 2002) and the reported mechanism of inhibition of the glucosamine compounds cannot possibly apply in to the mixed inhibition model of *Tb*HK obtained in this research project. Joyce *et al.* (2013) reported on the most implausible mechanism of the *Tb*HK by Ebselen, selenium containing variant of isobenzothiazolinone (Shallow *et al*., 2010). Ebselen forms a seleno-sulfide bond with cysteine residues and its resultant oxidation, rather than modification, thereby significantly decreases the enzymatic activity of *Tb*HK.

Silver NPs have been reported to interact with the thiol groups of the amino acid cysteine (Shen *et al.*, 2007; Galdeiro *et al*., 2011). The tertiary structure of *Tb*HK has free cysteine residues proximal to the active site at positions C103, C212, C242, C327, C369, C386, C401, C402 and C445. Oxidation of cysteine residues C327 and C386 effectively decreases the activity of *Tb*HK (Joyce *et al.,* 2013). Therefore, it is possible to speculate that the mixed inhibitory effects that silver NPs have on *Tb*HK observed in this research may be a result of the AgNP interacting with one or more of the cysteine residues found on distant positions to the active site. The NPs may have either oxidized or modified the cysteine residues that resulted in the decrease in enzyme activity and the reduction in the substrate affinity.

The interaction of silver NPs with human glucokinase may have been facilitated by the presence of free cysteine residues; *h*GCK has five cysteine residues on positions C213, C220, C230, C233, C252 that assume a ring surrounding the enzyme's active site, and cysteine residues at positions C364, C371, C382 proximal to the active site. The oxidation of cysteine residue C364 and C371 by a pyrimidine derivative glucokinase inhibitor alloxan result in the reduction of glucokinase activity (Tiedge *et al.*, 2000).

With the above information, it is possible to suggest that silver NPs interact with the proximal cysteine residues, regarding the uncompetitive effects of the NPs. Thus having a resultant release of the pre formed enzyme-substrate complex and a decrease in enzyme activity. As the enzyme adjusts to a new state it forms a new enzyme-substrate complex with higher affinity. The uncompetitive inhibition pattern observed was also reported by Storer and Cornish-Bowden (1977) with the use of MgATP as the inhibitor and glucose as a variable substrate of rat liver

glucokinase (Monasterio and Cardenas, 2003). The hill coefficient for the *h*GCK and AgNPs interaction sigmoidal kinetic analysis reveals an increase from 1.5 to 1.8 representing a 2% increase in the enzyme cooperativity to glucose.

4.4. Conclusions

The principle objectives of this chapter were to synthesize, characterize and assess the effects of silver NPs on the activity of *Tb*HK and *h*GCK respectively.

Silver NPs were successfully synthesized using a microwave assisted method with ethanol and PVP as reducing and stabilizing agent, respectively. TEM and wavescan spectroscopy revealed that the silver NPs had a characteristic spherical shape, an average size of 6 nm with an absorption peak at 422 nm. The obtained NPs maintained their size and distribution over a period of 8 weeks when store in the dark and at room temperature.

*Tb*HK and *h*GCK exhibited unique kinetic properties in the presence of 0.1 µM silver NPs. Hanes-Woolf analysis of the *Tb*HK-nanoparticle interaction kinetics revealed a mixed type inhibition with 38% reduction in the enzyme's affinity to its substrate (increase in K_m), 50% reduction in the maximal activity of the enzyme (decrease V_{max}) and a 28% reduction in its efficiency (decrease in K_{cat}/K_m). The human glucokinase interaction kinetics indicated an un-competitive inhibition pattern with a characteristic 33% increase in the enzyme's affinity to glucose, 9% decrease in the maximal enzyme activity and a 50% increase in the overall enzyme efficiency. These distinctive inhibition patterns exhibited by *Tb*HK and *h*GCK with 0.1 µM concentration silver NPs can be a result of the interaction between silver NPs and the thiol groups on cysteine amino acid residues that are situated at positions C103, C212, C242, C327, C386, C401, C403 and C445 for *Tb*HK and on position C364, C371 and C382 for human glucokinase. Oxidation of these proximal cysteine amino acids have been validated to initiate a conformational shift that may trigger a variety of enzyme activity and kinetic behaviour. The precise *Tb*HK and *h*GCK amino acid-nanoparticle interactions and their mechanisms presents a viable option for further research work in order to fully understand these aspects.

Chapter 5

General discussions, conclusions and recommended future studies

5.1. Discussions and Conclusions

HAT a much neglected disease, is a parasite borne infection with *Tb* as its causative agent. Increasing reports of drug resistant trypanosomes calls for new anti-trypanosome approaches (Rupol and Burke, 1977; Pepin *et al.*, 1994; Brun *et al.*, 2001). In its human host, *Tb* relies completely on glycolysis for its energy production. The glycolytic pathway, especially hexokinase, the first enzyme in the pathway has been validated as a viable target for anti-trypanosome agents (Morris, 2002; Chembers, 2005; Joyce *et al.*, 2013). In pursuit of more novel approaches to new anti-trypanosome agents, the current study focussed on the interaction of *Tb*HK and *h*GK with silver NPs. The changes in enzyme activities were evaluated.

The *Tb*HK (1 417 bp) and *h*GCK (1 398 bp) were PCR amplified. *Tb*HK and *h*GCK can readily be over expressed in *E. coli* (Studier, 2005) cells using auto-induction protocols. Both proteins were expressed containing a 6 histidine-tag to facility purification. Studies using the purified, recombinant proteins showed that *Tb*HK exhibited thermal stability between 30-55°C and pH stability between 7.5 and 8.5, while the *h*GCK is thermally stable between 30 and 40°C and stable between pH 7.0 and 8.0. Kinetic studies revealed that *Tb*HK and *h*GCK have K_m values of 39 µM and 4.5 mM, indicating that the *Tb*HK protein had a higher affinity for glucose as substrate. *Tb*HK has a V_{max} of 0.066 µmol.min^{-1}.ml^{-1}, while the V_{max} for the human glucokinase is 0.032 µmol.min^{-1}.ml^{-1}. The catalytic (K_{cat}/K_m) of the *Tb*HK protein was 0.0522 min^{-1}.µmol^{-1}and the *h*GCK was 2.5 min^{-1}.µmol^{-1}. *h*GCK exhibited a hill coefficient of 1.5.

Silver NPs were synthesized using the microwave assisted method (Pal *et al.*, 2009). The obtained NPs have a characteristic spherical shape with an average size of 6 nm and exhibited a plasmon resonance band at 423 nm. The nanoparticle solution was stable for one month when stored at room temperature in the dark.

Upon incubation of the recombinant proteins with AgNPs, apparent differences in the inhibition patterns were observed for *Tb*HK and *h*GCK. *Tb*HK interaction kinetic analysis showed a mixed

type of inhibition when incubated in the presence of 0.1 µM silver NPs. A 38% reduction in the enzyme's affinity to its substrate was noted and a 50% reduction in the maximal activity of the enzyme was also observed. This is turn led to a 28% reduction in enzyme efficiency. The *h*GCK interaction kinetics indicated an uncompetitive inhibition pattern with a characteristic 33% increase in the enzyme's affinity to glucose, a 9% decrease in the maximal enzyme activity and a 50% increase in the overall enzyme efficiency. From the experimental data, it was observed that 0.1 µM silver NPs selectively inhibit *Tb*HK hexokinase over *h*GCK. This observation proves the hypotheses that silver NPs selectively inhibit *Tb*HK over *h*GCK.

The inhibition of *Tb*HK by silver NPs presents an interesting possibility for its use in the development of anti-trypanosomal agents. This could be applied in two folds; firstly the NPs may be conjugated to the known anti-trypanosomal chemotherapeutic compounds. This approach may enhance targeted delivery to the brain, which is still a major challenge in the treatment of trypanosomiasis (Olbrich *et al.,* 2004). Secondly, the unconjugated NPs could be used to selectively inhibit the parasite hexokinase, which is crucial for parasite survival.

In trying to enhance the access of drugs to the central nervous system, various drug carriers and hyperosmolar solutions, such as liposomes (Bigon *et al.,* 1979), lithium chloride and sucrose have been investigated (Odika *et al.,* 1995). Another approach is the use functionalized NPs for the delivery of drugs to the CNS. Troster *et al*. (1990) reported on the accumulation of poly(methylmethacrylate) (PMMA) NPs in rat brain, demonstrating their ability to cross the blood-brain barrier. Elsewhere, anti cancer drugs dalagin and loperamide have been delivered to the brain after been functionalized to NPs (Kreuter *et al.,* 1994, Kreuter, 2001).

The second stage of HAT presents with the same problem, namely the failure to get the anti-trypanosomal agents across the blood-brain barrier. Olbrich *et al.* (2004) reported on diminazine diaceturate, an anti-trypanosomal agent which was delivered to the CNS of mice by formulating a lipid-drug conjugate (LDC)-nanoparticle complex. Daunorubicin conjugated to polycyanocrylate NPs have been shown to enter the trypanosoma parasite, and premaquine and pentamidine combined with NPs have proved useful in the experimental visceral leishmaniasis (Croft, 1999). Unconjugated NPs have also been reported to possess an anti parasitic property

(Lherm *et al.*, 1987; Golingtly, 1988; Croft, 1999). With this knowledge from literature and data obtained from this study, the inhibition of *Tb*HK by unconjugated silver NPs with an average size of 6 nm may add to the effect of the anti-trypanosomal agent that could be functionalized to the nanoparticle, doubling the efficiency in killing the parasite with limited or no negative effect to the human hosts.

Results from this study can be extrapolated to include a possible treatment for the reduction of fasting hyperglycemia observed in maturity onset diabetes of the youth (MODY) (Byrne *et al.,* 1993), as the *h*GCK efficiency was enhanced. Glucokinase have been validated to be a vital target in the treatment of diabetes, as it has high correlation to glucose levels control because of glucose sensor function in the pancreas and its involvement in decreasing high glucose levels and synthesis of glycogen in the liver (Matschinsky 2009; Matschinsky *et al.,* 2010; Matschinsky and Porte Jr, 2010; Angadi *et al.,* 2013). Studies have been conducted where solid lipid NPs (Liu *et al.,* 2007), [poly(-ɛcaprolactone)] (Damġe, 2006) and dextran NPs (Chalasani *et al.,* 2007) have been pre-loaded with insulin and used as delivery systems in the treatment of diabetes. Silver NPs have also been employed to enhance the healing of a delayed diabetic wound (Mishra *et al.,* 2008). The versatility of silver NPs and data obtained by this research project could be utilized either on their own as it has been found to increase enzyme efficiency or by functionalized to various anti-diabetic agents including insulin, thereby yielding its potential in two folds.

The highly selective inhibitory effects of AgNPs observed between *Tb*HK and *h*GCK may be attributed to the high affinity of the NPs to thiol groups in the surface cysteine amino acid residues. These residues are located away from the active sites of both proteins. The binding of AgNPs to these specific amino acids may induce changes in the protein's structure with resultant distinct changes in the properties of the proteins.

5.2. Recommended future studies

The outcomes obtained from this research project have presented platforms for various interesting possible future studies. The selective inhibitory effects of AgNPs on the studied proteins can be used in the designing of new and dynamic nanoparticle based anti-trypanosomal drugs. Since tagged recombinant proteins may have some of its properties affected (Terpe,

2002), it would be very interesting to carry out similar studies on the effects of silver NPs on wild type *Tb*HK and *h*GCK. The wild type protein can be closely mimicked by expressing the protein without an affinity tag or to cleave the tag post expression and purification. The *Tb* arm of the project could be expanded by investigating the inhibitory properties of silver NPs on hexokinase of the trypanosomes *in vitro*. This could be performed in trypomastigotes cultures, and this investigation could determine if the inhibition is dose dependent, and elucidate the internalization mechanism of the NPs into the trypanosomes and the organelle.

In silico studies could be performed on the *Tb*HK and *h*GCK to investigate if the subunits assume different orientations after binding to the NPs and also to determine which of the cysteine residues are responsible for the binding of the NPs and the change in properties. Furthermore, the cysteine residues may be mutated to other amino acids like alanine that have no affinity to silver NPs and investigate the response of the mutated proteins to the inhibitory/activating effects of silver nanoparticle.

References

- Ahmad, A., Senapati, S., Khan, M.I., Kumar, R., Ramani, R., Srinivas, V., Sastry, M. (2003). Intracellular synthesis of gold nanoparticles by a novel alkalotolerant actinomycete, *Rhodococcus* species. *Nanotech*. 14:824-828.

- Aitken, R.J., Creely, K.S., Tran, C.L. (2004). Nanoparticles: An occupational hygiene review. www.hse.gov.uk/research/rrpdf/rr274.pdf, accessed on 19/09/2012.

- Albert, M.A., Haanstra, J.R., Hannaert, V., Van Roy, J., Opperdoes, F.R., Bakker, B.M.,Michels, P.A. (2005) Experimental and in Silico Analyses of Glycolytic Flux Control in Bloodstream Form *Trypanosoma brucei. J. Biol. Chem.* 280(5): 28306-28315.

- Angadi, K.K., Gundampati, R. K., Jagannadham, M. V., Kandru, A. (2013). Molecular docking studies of guggultetrol from *Nymphaea pubescens* with target glucokinase (GK) related to type-II Diabetes. *Sci. 3*(2): 127-131.

- Allsopp, R. (2001). Options for vector control against trypanosomiasis in Africa. *Trends Parasitol.* 17:15–19.

- Anil Kumar, S., Majid K.A., Gosavi, S.W., Kulkarni S.K., Pasricha, R., Ahmad, A., Khan, M.I (2007).Nitrate reductase mediated synthesis of silver nanoparticles from $AgNO_3$. *Biotechnol. Lett*. 29:439–445.

- Arnau, J., Lauritzen, C., Petersen, G. E., Pedersen, J. (2006). Current strategies for the use of affinity tags and tag removal for the purification of recombinant proteins. *Prot. expres. purif.* 48(1):1-13.

- Ashby, J., Schachermeyer, S., Pan, S., Zhong, W. (2013). Dissociation-Based Screening of Nanoparticle−Protein Interaction via Flow Field-Flow Fractionation. *Anal. Chem.*, 85: 7494−7501.

- Baker, N., de Koning, H.P., Maser, P., Horn, D. (2013). Drug resistance in African trypanosomiasis: the Melarsprol and Pentamidine story. *Trends Parasitol. 29(3)*

- Balaji, D.S., Basavaraja, S., Deshpande, R., Bedre Mahesh, D., Prabhakar, B.K., Venkataraman, A. (2009). Extracellular biosynthesis of functionalized silver nanoparticles by strains of *Cladosporium cladosporioides* fungus. *Coll and Surf B: Biointerfaces*, 68:88-92.

- Baneyx, F. and Mujacic, M. (2004). Recombinant protein folding and misfolding in *Escherichia coli*. *Nat. Biotechnol.* 22:1399–1408.

- Baptista, P.V., Koziol-Montewka, M., Paluch-Oles, J., Doria, G., Franko, R. (2006). Gold nanoparticle-probe-based assay for the rapid and direct detection of Mycobacterium tuberculosis DNA in clinical samples. *Clin. Chem. Microbiol.*, 52(7):1433-1434.

- Barrett, M.P. (1999). The fall and rise of sleeping sickness. *Lancet,* 353(9159):1113-4.

- Barrett, M.P., Burchmore, R. J. S., Stich A., Lazzari, J. O., Frasch, A. C., Cazzulo, J. J., Krishna, S. (2003). The Trypanosomiases. *Lancet,* 1(362): 1469–80.

- Begum, N.A., Mondal, S., Basu, S., Laskar, R.A., Mandal, D. (2009). Biogenic synthesis of Au and Ag nanoparticles using aqueous solutions of Black Tea leaf extracts. *Coll and Surf B: Biointerfaces,* 71:113–118.

- Berrow, N.S., Büssow, K., Coutard, B., Diprose, J., Ekberg, M., Folkers, G. E., Levy, N., Lieu, V., Owens, R.J., Peleg, Y., Pinaglia, C., Quevillon-Cheruel, S., Salim, L., Scheich, C., Vincentelli, R., Busso, D. (2006). Recombinant protein expression and solubility screening in *Escherichia coli*: a comparative study. *Acta crystallogr. Section D, Bio. Crystal.* 62(10):1218-1226.

- Bigon, E., Boarato, E., Bruni, A., Leon, A., Toffano, G., (1979). Pharmacological effects of phosphatidylserine liposomes: regulation of glycolysis and energy level in brain, *Br. J. Pharmacol*. 66:167–174.

- Blattner, J., Dorsam, H., Clatyon, C.E. (1995). Function of N-terminal import signals in trypanosome microbodies. *FEBS Lett.* 360: 310–314.

- Block, O., Mitra, A., Novotny, L., Dykes, C. (2012). A rapid label-free method for quantitation of human immunodeficiency virus type-1 particles by nanospectroscopy. *J. of Virol. Meth.* 182(1-2):70-75.

- Bonanni, A., Pividori, M. I., Valle, M. (2010). Impedimetric detection of influenza A (H1N1) DNA sequence using carbon nanotubes platform and gold nanoparticle amplification. *Carb. Nano.* 135:1765-1772.

- Bork, P., Sander, C., Valencia, A. (1992). An ATPase domain common to prokaryotic cell cycle proteins, sugar kinases, actin, and hsp70 heat shock proteins. *Proc. Natl. Acad. Sci.* 89(16):7290-7294.

- Brown, T.A. (2010). Gene cloning and DNA analysis. An introduction, 6th Edition. Chapter 3: Vectors for gene cloning: Plasmids and Bacteriophages, pp. 13-24. John Wiley and sons, Ltd., publication, UK

- Brun, R. and Balmer, O. (2006). New developments in human African trypanosomiasis. *Curr Opin. Inf. Dis.* 19(5):415-20.

- Buffat, P.H and Borel, J.P. (1976). Size effect on the melting temperature of gold particles. *Phys. Rev.* 13(6):2287.

- Byrne, M. M., Sturis, J., Clément, K., Vionnet, N., Pueyo, M. E., Stoffel, M., Takeda, J., Passa, P., Cohen, D., Bell, G.L., Velho. G., Froguel, P and Polonsky, K.S. (1994). Insulin

secretory abnormalities in subjects with hyperglycemia due to glucokinase mutations. *J. Clin. Invest*. 93(3):1120-1130.

- Casadaban, M.J., Chou, J., Cohen, S.N. (1980). *In vitro* gene fusions that join an enzymatically active beta-galactosidase segment to amino-terminal fragments of exogenous proteins: *Escherichia coli* plasmid vectors for the detection and cloning of translational initiation signals. *J. Bacteriol.* 143(2):971-980.

- Cereghino, J.L., Cregg, J.M. (2000). Heterologous protein expression in the methylotrophic yeast *Pichia pastoris*. *FEMS Microbiol. Rev*. *24*(1):45-66.

- Chalasani, K.B., Russell-Jones, G.J., Jain, A.K., Diwan, P.V., Jain, S.K. (2007). Effective oral delivery of insulin in animal models using vitamin B12-coated dextran nanoparticles. *J. Control. Release*, 122(2):141-50.

- Chappuis, F., Loutan, L., Simarro, P., Lejon, V., Büscher, P. (2005). Options for field diagnosis of Human African Trypanosomiasis. *Clin. Microbiol. Rev.* 18(1):133-146.

- Chambers, J.W., Fowler, M.L., Morris, M.T., Morris, J.C. (2008). The anti-trypanosomal agents Lonidamine inhibit *Trypanosoma brucei* hexokinase 1. *Mol. Biol. Para*. 158:202-207.

- Chambers, J.W., Kearns, M.T., Morris, M.T and Morris, J. C. (2008) Assembly of Heterohexameric Trypanosome hexokinases reveals that hexokinase 2 is a regulable enzyme. *J. Biol. Chem.* 283(22):14963-14970.

- Chambers, J.W., Morris, M.T., Smith, K. S., Morris, J.C. (2008). Residues in an ATP binding domain influence sugar binding in a trypanosome hexokinase. *Biochem. and biophys. Res. Communic.*, *365*(3), 420-425.

- Chang-dong, Z.O.U., Yu-lai, G.A.O., Bin, Y. and Qi-jie, Z. (2009). Size-dependent melting properties of Sn nanoparticles by chemical reduction synthesis. *Transac. Nonferr. Met. Soc. China*, 20(2):*248-253*.

- Chappuis, F., Udayraj, N., Stietenroth, K., Meussen, A., Bovier, P. A., Chappuis, F., Udayraj, N. (2005). Eflornithine Is Safer than Melarsoprol of Second-Stage for the Treatment of Human *Trypanosoma gambiense* African Trypanosomiasis. *Clin. Inf. Dis.* 41(5):748-751.

- Chart, H., Smith, H. R., La Ragione, R. M. and Woodward, M. J. (2000). An investigation into the pathogenic properties of *Escherichia coli* strains BLR, BL21, DH5alpha and EQ1. *J. Appl. Microbiol*. *89*(6):1048-1058.

- Checchi, F., Filipe, J.A.N., Barrett, M.P., Chandramohan, D. (2008). The Natural Progression of Gambiense Sleeping Sickness: What Is the Evidence? PLOS *Negl. Trop. Dis.* 2(12):303

- Chen, W., Lee S.B, Bailey, J.E. (1991). Molecular Design of Expression Systems: Comparison of Different Repressor Control Configurations Using Molecular Mechanism Models. *Biotechnol. Bioeng*. 38:679-687.

- Chou, S., Jensen, B. C., Parsons, M., Alber, T., Grundner, C. (2010). The *Trypanosoma brucei* life cycle switch TbPTP1 is structurally conserved and dephosphorylates the nucleolar protein NOPP44/46. *J. Biol Chem.* 285(29):22075-22081.

- Colasante, C., Ellis, M., Ruppert, T., Voncken, F. (2006) Comparative proteomics of glycosomes from bloodstream form and procyclic culture form *Trypanosoma brucei brucei*. *Prot.* 6(11): 3275-3293.

- Corchero, L., Seras, J., García-fruitós, E., Vazquez, E., & Villaverde, A. (2010). Nanoparticle-assisted tissue engineering. *J. Biomed. Mat. Res. Part B: Applied Biomaterials*, (June) 13-15.

- Croft, S. L. (1999). Pharmacological approaches to antitrypanosomal chemotherapy. *Memórias do Instituto Oswaldo Cruz*, *94*(2):215-220.

- Damgé, C., Maincent, P., Ubrich, N. (2007). Oral delivery of insulin associated to polymeric NPs in diabetic rats. *J. Cont. Rel*., *117*(2):163-170.

- Davis, E.A., Cuesta-Munoz, A., Raoul, M., Buettger, C., Sweet, I., Moates, M., Magnuson, M. A., Matschinsky, F. M. (1999) Mutants of glucokinase cause hypoglycaemia- and hyperglycaemia syndromes and their analysis illuminates fundamental quantitative concepts of glucose homeostasis. *Diabetologia* 42:1175–1186.

- Desai, N. P., Louie, L., Ron, N., Magdassi, S., Soon-Shiong, P. Protein-based nanoparticles for drug delivery of paclitaxel. *Trans. World Biomater. Congr.* 1:199- 200.

- Despommeir, Gwadz, Hotez, Knirsch. (2005) Parasitic Diseases, Fifth Edition, Apple Trees Productions, pp 32-38. L.L.C. NY.

- Dodson, H.C., Lyda T.A., Chambers, J.W. Morris, M.T., Christensen, K.A., Morris, J.C. (2011). Quercerine, a fluorescent bioflavanoid, inhibits *Trypanosoma brucei* hexokinase 1. *Expr. Para.* 127:423-428.

- Donaldson, K, Stone, V., Tran, C. L., Kreyling, W., Borm, P. J. (2004). Nanotoxicology. *Occ. and Environ. Med.*, *61*(9), 727-728.

- Dong, P.V., Ha, C.H., Binh, L.T., Kasbohm, J. (2012) chemical synthesis and antibacterial activity of novel – shaped silver NPs. *Int. nano. let*. 2:9.

- Dolye, M.E (2006). Nanotechnology: A brief literature review. Madison: Food Research Institute, UW-Madison, 33-37. Accessed from: http://www.wisc.edu/fri/briefs.

- Dreher, K.L. (2003). Health and Environmental Impact of Nanotechnology: Toxicological Assessment of Manufactured NPs. *Toxicol. Sci.* 77(1):3-5.

- Driskell, J.D., Jones, C.A., Tompkins, S.M., Tripp, R.A. (2011). One-step assay for detecting influenza virus using dynamic light scattering and gold nanoparticles. *Analyst*, 136:3083–3090.

- Dykman, L. A and Khlebtsov, N.G. (2011). Gold nanoparticles in Biology and Medicine: *Rec. Adv Prosp. Europe,* 3(9):34-55.

- Enanga, B., Burchmore, R.J.S., Stewart, M.L., Barrett, M P. (2002). Sleeping sickness and the brain.*Cell. Mol. Life Sci.* 59 (2002) 845–858.

- Enserink M. (2007) Entomology. Welcome to Ethopia's fly factory. *Sci* 317:310-323.

- Eriksson, B.I., Ekman, S., Peter, K., Zachrisson, B., Bach, D., Close, P. (1996). Prevention of deep-vein thrombosis after total hip replacement: direct thrombin inhibition with recombinant hirudin, CGP 39393. *Lancet*, 347:635-639.

- Eschenfeldt, W. H., Maltseva, N., Stol, L., Donnelly, M. I., Gu, M., Nocek, B., Tan, K., Kim, Y., Joachimiak, A. (2011). Cleavable C-terminal His-tag vectors for structure determination. *J. Struct. Genom.* 11(1):31-39.

- Fang, J., Zhong, C., Mu, R. (2005). The study of deposited silver particulate films by simple method for efficient SERS. *Chem. Phys. Lett*, 401:271-275.

- Fèvre, E. M., Wissmann, B. V., Welburn, S. CandLutumba, P. (2008). The burden of human African trypanosomiasis. *Negl. Trop. Dis.*, 2(12):e333.

- Galan, M.,Vincent, O.,Roncero, I., Azriel, S., Boix-Pallares, P., Delgado-Alvarez, E., Diaz-Cadorniga, F., Blazquez, E., Navas, M.A. (2006). Effects of novel maturity-onset diabetes of the young (MODY)-associated mutations on glucokinase activity and protein stability. *Biochem. J.* 393:389-396.

- Galdiero, S., Falanga, A., Vitiello, M., Cantisani, M., Marra, V. and Galdiero, M. (2011). Silver nanoparticles as Potential Antiviral Agents. *Mol*.16 8894-8918.

- Gálvez, N., Sánchez, P., Domínguez-Vera, J.M., Soriano-Portillo, A., Clemente-León, M. and Coronado, E. (2006). Apoferritin-encapsulated Ni and Co superparamagnetic Nanoparticles. *J. Mat. Chem.*, 16:2757-2761.

- Hollenberg, C.P. and Gellissent, G. (1996). Production of recombinant proteins by methylotrophic yeasts. *Curr. Opin. In Biotech.* 8: 554-560.

- Gehrig, S. and Efferth, T. (2008). Development of drug resistance in *Trypanosoma brucei rhodesience* and*Ttrypanosoae brucei gambiense.* Treatment of Human African Trypanosomiasis with natural products (Review). *Int. J. of Mol. Med.* 22: 411-419

- Gidh-Jain, M., Takeda, J., Xu, L.Z., Lange, A.J., Vionnet, N, Stoffel, M., Froguel, P., Velho, G., Sun, F., Cohen, D., Froguel, P., Lo, Y.M.D., Hatters;ey, A.T., Luthman, H., Wedell, A., St. Charles, R., Harrison, R..W., Weber, I.T., Bell, G.I. and pilkis, S.J. (1993.) Glucokinase mutations associated with non-insulin-dependent (type 2) diabetes mellitus have decreased enzymatic activity: implications for structure/function relationships. *Proc. Natl. Acad. Sci*.90(5):1932–1936.

- Golightly, L, Brown, J.E., Mitchell, J.B., Brown, J.R. (1988). Trypanocidal activity of free and carrier bound daunorubicin. *Cell Biol. Int. Rep*. 12:77-83.

- Gould, S.J., Keller, G.A., Hosken, N., Wilkinson, J. and Subramani, S. (1989)**.** A conserved tripeptide sorts proteins to peroxisomes. *J. Cell Bio.* 108:1403-1411.

- Gouteux, J.P., Kounda Gboumbi, J.C., Noutoua, L., D'Amico, F., Bailly, C., Roungou, J.B. (1993). Man-fly contact in the Gambian trypanosomiasis focus of Nola-Bilolo (Central African Republic) *Trop. Med. and Para.*44:213–218.

- Granqvist, C.G., Buhrman, R.A. (1976) Far-infrared absorption in ultrafine Al particles, *Phys. Rev. Lett*. 37:625-629.

- Griffiths, A.J. (1995). Natural plasmids of filamentous fungi. These include : Natural Plasmids of Filamentous Fungi. *Microbiol*, *59*(4).673.

- Griffin, L.D., Gelb, B. D., Wheeler, D., Davison, D., Adams, V and McCabe, E. R. (1991). Mammalian hexokinase 1: evolutionary conservation and structure to function analysis. *Geno, 11*(4):1014-1024.

- Grossbard, L and Schimke, R.T. (1966). Multiple hexokinases of rat tissue. Purification and comparison of soluble forms. *J. Bio. Chem.* 241:3546-3560.

- Gurunathan, S., Kalishwaralal, K., Vaidyanathan, R., Hariharan, N. and Hyun, S. (2009). Colloids and Surfaces B : Biointerfaces Biosynthesis, purification and characterization of silver Nanoparticle using *Escherichia coli*. Growth *(Lakeland).74*:328-335.

- Guzmán, M. G., Dille, J and Godet, S. (2009). Synthesis of silver nanoparticles by chemical reduction method and their antibacterial activity. *Int. J. Chem. and Bio. Engin.* 2(3):104-111.

- Haase, A., Tentschert, J., H Jungnickel, H., Graf, *P*., Mantion, A., Draude, F., Plendl, J., Goetz1, M.E., Galla, S., A Mašić, A., Thuenemann, A.F., A Taubert, A., Arlinghaus, H.F., and Luch, A. (2011). Toxicity of silver nanoparticles in human macrophages: uptake, intracellular distribution and cellular response. *J Phys.: conf. ser.* 304 (2011)*012030*.

- Haefeli, C., Franklin, C., Hardy, K. (1984). Plasmid-determined silver resistance in Pseudomonas stutzeri isolated from a silver mine. *J. Bacteriol.* 158:389–392.

- Hammarstrom, M., Hellgren, N., van Den Berg, S., Berglund, H., Hard, T. (2002). Rapid Screening for Improved Solubility of Small Human Proteins Produced as Fusion Proteins in *Escherichia Coli*. *Protein Sci.*11:313–21.

- Hanahan, D. and Harbor, C. S. (1983). Studies on Transformation o f *Escherichia coli* with Plasmids, *J. Mol. Biol.* 166: 557-580.

- Hannig, G. and Makrides, S.C. (1998). Strategies for optimizing heterologous protein expression in *Escherichia coli*. *Trends Biotechnol*. 16:54–60.

- Hansen, L. H., Knudsen, S., Sørensen, S. J. (1998). The effect of the lacY gene on the induction of IPTG inducible promoters, studied in *Escherichia coli* and *Pseudomonas fluorescens*. *Curr. Microbiol*, 36(6):341-347.

- Hasebe, A., Tashima, H., Ide, T., Iijima, M., Yoshimoto, N., Ting, K., Kuroda, S., Niimi, T. (2012). Efficient production and characterization of recombinant human NELL1 protein in human embryonic kidney 293-F cells. *Mol. Biotech.*, *51*(1):58-66.

- Hayashi, C.H., Uyeda, R., Tasaki, A. (1997). Ultra-fine particles: exploratory science and technology Translation of the Japan report of the related ERATO Project (1981–86*). Noyes Pub.*

- Herranz, F., Almarza, E., Rodríguez, I., Salinas, B., Rosell, Y., Desco, M., Bulte, J.W., Cabelo, J.R. (2011). The application of nanoparticles in gene therapy and magnetic resonance imaging. *Microsc. Res. Tech.* 74(7):577-591.

- Hirsch, L.R., Stafford, R.J., Bankson, J.A., Sershen, S.R., Rivera, B., Price, R.E., Hazle, J.D., Halas, N.J., West, J.L. (2003). Nanoshell-mediated near-infrared thermal therapy of tumors under magnetic resonance guidance. *Proc. Natl. Acad. Sci.* 100:13549-13554.

- Holms H. (1996). Flux Analysis and Control of the Central Metabolic Pathways in *Escherichia Coli*. *FEMS Microbiol Rev*.19:85–116

- Hochuli, E., Döbeli H., Schacher A. (1987) New metal chelate adsorbent selective for proteins and peptide containing neigh- bouring histidine residues. *J. Chromatogr.* 411:177–184

- Hsu, S. L.-chung., Wu, R.-tarng, & Materials, A. (2011). Preparation of Silver Nanoparticle with Different Particle Sizes for Low- Temperature Sintering. *Int. Conf. on nanotech. and Biosens. 2*:55-58.

- Huang, X. and El-sayed, M. A. (2010). Gold nanoparticles : Optical properties and implementations in cancer diagnosis and photothermal therapy. *Nanotech.* 13-28.

- Ingle, A., Gade, A., Pierrat, S., Sönnichsen, C., Mahendra R (2008). Mycosynthesis of silver NPs using the fungus Fusarium acuminatum and its activity against some human pathogenic bacteria. *Curr. Nanosc.*, 4:141-144.

- Ikonomou, L., Schneider, Y.J., Agathos, S.N. (2003). Insect cell culture for industrial production of recombinant proteins. *Appl. Microbiol*. 62:1-20.

- Inoue, K., Takano, H., Yanagisawa, R., Hirano, S., Sakurai, M., Shimada, A., Yoshikawa, T. (2006). Effects of Airway Exposure to nanoparticles on Lung Inflammation Induced by Bacterial Endotoxin in Mice. *Environ. Health Persp.* 114(9):1325-1330.

- Iwahori, K. and Yamashita, I. (2007). Bio-template Synthesis of Nanoparticle by Cage-shaped Protein Supramolecule, Apoferritin. *J. Clust. Sci.*18 (2):358-370.

- Jacob, F. and Monod, J. (1961). Genetic Regulatory Mechanisms in the Synthesis of Proteins. *J. Mol. Biol.,* 3:318–56.

- Jelnes, J.E. (1971). Identification of hexokinases and localization of a fructokinase and a tetrazolium oxidase locus in *Drosophilia melanogaster*. *Her*. 67:291-293.

- Johannessen, C.M., Boehm1, J.S., Kim S.Y., Thomas, S.R., Wardwell, L., Johnson, L.A. Emery, C.M., Stransky, N., Cogdill, A.P., Barretina, J., Caponigro, G., Hieronymus, H., Murray, R.R., Salehi-Ashtiani, K.., Hill D.E., Vidal, M., Zhao, J.J., Yang, X., Alkan, O., Kim, S., Harris, J.L., Wilson, C.J., Myer, V.E., Finan, P.M., Root, D.E., Roberts, T.M., Golub, T., Flaherty, K.T., Dummer, R., Weber, B., Sellers, W.R., Schlege, R., Wargo, J.A., Hahn, W.C and Garraway, L.A. (2010) COT/MAP3K8 drives resistance to RAF inhibition through MAP kinase pathway reactivation. *Nat.* 468(7326): 968–972.

- Joice, A.C., Harris, M.T., Kahney, E.W., Dodson, H.C., Maselli, A.G., Whitehead, D.C., Morris, J.C. (2013). Exploring the mode of action of ebselen in *Trypanosoma brucei* hexokinase inhibition. *Int. J. for para; Drugs and Drug resistance* 3:154-160.

- Kagan, V.E., Bayir, H., Shvedova, A. (2005). Nanomedicine and nanotoxicology: two sides of the same coin. *Nanomedicine, Nanotech. Bio. and Med.* 1(4):313-6.

- Kalimuthu, K., Babu, R. S., Venkataraman, D., Bilal, M., Gurunathan, S. (2008). Colloids and Surfaces B : Biointerfaces Biosynth*esis* of silver nanocrystals by *Bacillus licheniformis. Coll and Surf*. 65:150-153.

- Kamata, K., Mitsuya, M., Nishimura, T., Eiki, J., Nagata, Y. (2004). Structural basis for allosteric regulation of the monomeric allosteric enzyme human glucokinase, *Structure* 12:429–438.

- Kasthuri, J., Veerapandian, S, Rajendiran, N. (2009). Biological synthesis of silver and gold nanoparticles using apiin as reducing agent. *Coll and surf. B, Bioint.*, *68*(1):55-60.

- Kathiresan, K., Manivannan, S., Nabeel, M.A., Dhivya, B. (2009). Studies on silver NPs synthesized by a marine fungus, *Penicillium fellutanum* isolated from coastal mangrove sediment. *Col. and Surf. B*: Biointerfaces.71:133-137.

- Klassen-fischer, M.K., Meyers, W.M., Neafie, R.C. (2011). Topics on the pathology of protozoan and invasive arthropod diseases: African Trypanosomiasis. Accessed from http//:www.WHO.org.

- Khonde, N., Pepin, J., Niyonsenga, T., De, W.P. (1997). Familial aggregation of *Trypanosoma brucei gambiense* trypanosomiasis in very high incidence community in Zaire. *Trans. R. Soc. Trop. Med. Hyg*. 91:521–524.

- Khlebtsov, N. G and Dykman, L. A. (2010). Optical properties and biomedical applications of plasmonic nanoparticles. *J. of Quant. Spect. Rad. Tran*. *111*(1): 1-35.

- Kohagne, T.L., M'eyi, M.P., Kamkuimo, R.G., Kaba, D., Louis, J.F., Mimpfoundi, R. (2011). Transmission of human African trypanosomiasis in the Komo-Mondah focus, Gabon. *Pan. Aft.*; 8:36.

- Kreuter, J. (2001). Nanoparticulate systems for brain delivery of drugs. *Adv. Drug Deliv. Rev.*, 47: 65-81.

- Krutyakov, Y.A., Kudrinskiy, A.A., Olenin, A.Y., Lisichkin, G.V. (2008). Synthesis and properties of silver NPs: advances and properties. *Russ. Chem. revew*. 77 (3):233-257.

- Kruis, F.E, Fissan, H, Peled, A. (1998). Synthesis of NPs in the gas phase for electronic, optical and magnetic applications: a review. *J. of Aero. Sci.*; 29:511- 535.

- Kuzoe F.A.S and Schofield C.J. (2004). Strategic review of traps and targets for tsetse and african trypanosomiasis control. *WHO.*

- Lam, C.W., James, J. T., McCluskey, R., Hunter, R. L. (2004). Pulmonary toxicity of single-wall carbon nanotubes in mice 7 and 90 days after intratracheal instillation. *Toxicol. Sci.*, 77(1):126-34.

- Lara, H.H., Ayala-Nuñez, N.V., Ixtepan-Turrent, L., Rodriguez-Padilla ,C. (2010) Mode of antiviral action of silver nanoparticles against HIV-1. *J. Nanobiotech:* l8:1–10.

- Lederberg, E.M. and Cohen, S.N. (1974). Transformation of *Salmonella typhirium* by plasmid deoxyribonucleic acid. *J. Bactriol*. 119 (3):1074.

- Lherm, C., Couvreur, P., Loiseau, P., Bories, C., Gayral, P. (1987). Unloaded polyisobutylcyanoacrylate nanoparticless: efficiency against bloodstream trypanosomes. *J Pharm. Pharmacol.* 39:650-652.

- Laemmli, U.K. (1970) Cleavage of structural proteins during the assembly of the head of bacteriophage T4. *Nat*. 227:680–685.

- Lengke, M.F., Fleet, M.E., Southam, G. (2007). Biosynthesis of silver NPs by filamentous cyanobacteria from a silver nitrate complex. *Langm*.23:2694 – 2699.

- Li, T., Guo, L., Wang, Z. (2008) Microarray based Raman spectroscopic detection witl gold nanoparticles probes. *Biosens. Bioelectron.,* 23:1125-1130.

- Li, T., Liu, D., Wang, Z. (2009). Microarray based Raman spectroscopic assay for kinase inhibition by gold nanoparticle probes. *Biosens. Bioelectron*., 24:3335-3339.

- Li, X., Chik, W., Choy, H., Lu, H., Sha, W. E. I., Ho, A., Ho, P. (2013). Efficiency Enhancement of Organic Solar Cells by Using Shape-Dependent Broadband Plasmonic Absorption in Metallic Nanoparticles, *Adv. Funct. Mater.* 23:2728–2735.

- Linkov, I., Satterstrom, F. K., Corey, L. M. (2008). Nanotoxicology and nanomedicine: making hard decisions. *Nanomedicine: Nanotech. Bio. and Med. 4*(2):167-171.

- Liu, C., Yang, X., Yuan, H., Zhou, Z., Xiao, D. (2007). Preparation of Silver Nanoparticle and Its Application to the Determination of ct-DNA. *Sensors (Peterborough, NH)*, 708-718.

- Liu, J., Gong, T., Wang, C., Zhong, Z., Zhang, Z. (2007). Solid lipid nanoparticles loaded with insulin by sodium cholate-phosphatidylcholine-based mixed micelles: preparation and characterization. *Int. J. of pharm*. *340*(1-2):153-162.

- Lichty, J.J., Malecki, J.L., Agnew, H.D., Michelson-Horowitz, D.J., Tan, S. (2005) Comparison of affinity tags for protein purification, *Protein Expr. Purif.* 41:98–105.

- Lubick, N. (2008) Nanosilver toxicity: ions, nanoparticles or both. *Environ. Sci. Technol*. 42:8617.

- Luther, W. (2004). Bottom-up method for making nanotechnology products; Future Technologies Division of VDI (Verein Deutscher Ingenieure). Report: Industrial Application of nanomaterialsp-Chances and Risks: Technology Analysis. http://www.azonano.com/ Details.asp?ArticleID=1079, accessed 19/09/2012.

- Lyda, T. (2009) Exploring *Trypanosoma brucei* hexokinase biology, localization and inhibition studies, Graduate school of Clemson University. DPhil Thesis. Retrieved from www.etd.lib.Clemson.edu/document/1263396314/lyda_clemson/0050d/10416.pdf. Accessed on 28/5/12.

- Madigan, M.T. and Martinko, J.M. (2006). Chapters: Bacterial Genetics, Brock Biology of Microorganisms – Principals of Microbiology, 11th edition, pp 288- 289, Pearson Education, INC, Upper Saddle River, NJ USA.

- Makrides, S. C. (1996). Strategies for achieving high-level expression of genes in *Escherichia coli*. *Microbiol. Rev*. *60*(3):512-538.

- Mann, S. (2006) "Nanotechnology and Construction". Nanoforum.org European Nanotechnology Gateway. Accessed from; http://www.nanoforum.org/dateien/temp/ Nanotech%20and%20Construction%20Nanoforum%20report.pdf?08112010050156**;** Retrieved 2012-09-18, on 10/07/2012

- Mamani-matsuda, M., Rambert, J., Malvy, D., Lejoly-Boisseau, H., Daulouede, S., Thiolat, D., Coves, S., Courtois, P., Vincendeau, P., Mossalayi, M. D. (2004). Quercetin Induces Apoptosis of *Trypanosoma brucei gambiens*e and Decreases the Proinflammatory Response of Human Macrophages. *Soc*, *48*(3):924-929.

- Matasci, M., Hacker, D. L., Baldi, L and Wurm, F. M. (2008). Recombinant therapeutic protein production in cultivated mammalian cells: current status and future prospects. *Drug Disc. Today: Technol*. *5*(2-3): e37-e42.

- Matschinsky, F. M. and Porte, D. (2010). Glucokinase activators (GKAs) promise a new pharmacotherapy for diabetics. *F1000 med. Rep. 2*(June):12-16.

- Mavani, K. and Shah, M. (2013). Synthesis of silver NPs by using sodium borohydride as a reducing agent. *Inter. J. Of Engin. Res. And Tech. 2(3):1.5.*

- McAtee, M. (2010). African sleeping sickness treatment, accessed from; http://www.livestrong.com/article/198623-african-sleeping-sickness-treatment/ accessed on 15/05/2012.

- Mendel, M. and Higa. A. (1970). Calcium-dependent bacteriophage DNA infection. *J. Mol. Biol*. 53:159-162.

- Meyer, D. E., Curran, M. A. N. N., Gonzalez, M. A., Agency, U. S. E. P., Risk, N. (2009). Policy analysis an examination of existing data for the industrial manufacture and use of nanocomponents and their role in the life cycle impact of nanoproducts. *Environ. Sci. Tech.* 43(5):1256-1263.

- Mironava, T., Hadjiargyrou, M., Simon, M., Jurukovski, V., Rafailovich, M. H. (2010). Gold nanoparticless cellular toxicity and recovery. *Cancer Res.* 3:199-201.

- Misset, O. and Opperdoes, F. R. (1987) The Phosphoglycerate kinase from *Trypanosoma brucei*, a comparison of the glycosomal and the cytosolic isoenzymes and their sensitivity towards suramin. *Eur. J. Biochem.* 144:475-483

- Mishra, M., Kumar, H., Tripathi, K. (2008). Diabetic delayed wound healing and the role of silver. *J. of Nano*. *3*(2):49-54.

- Mittra, B., Saha, A., Chowdhury, A. R., Pal, C., Mandal, S., Mukhopadhyay, S., Bandyopadhyay, S., Majumder H.K. (2000). Luteolin, an abundant dietary component is a potent anti-leishmanial agent that acts by inducing Topoisomerase II-mediated Kinetoplast DNA Cleavage Leading to Apoptosis. *Para. 6*(6): 527-541.

- Molnes, J., Teigen, K., Aukrust, I., Bjørkhaug, L., Søvik, O. (2011). Binding of ATP at the active site of human pancreatic glucokinase – nucleotide-induced conformational changes with possible implications for its kinetic cooperativity. *FEBS J. 278*: 2372-2386.

- Monasterio, O. and Cardenas, M.L. (2003) Kinetic studies of rat liver hexokinase D (glucokinase) in non-co-operative conditions show an ordered mechanism with MgADP as the last product to be released. *Biochem. J.* 371:29–38.

- Morales-sánchez, E., Guajardo-pacheco, J., Noriega-treviño, M. (2011). Synthesis of Silver nanoparticles using Albumin as a reducing agent. *Coll and Surf.* 2: 578-581.

- Morris, M. T., DeBruin, C., Yang, Z., Chambers, J. W., Smith, K. S., Morris, J. C. (2006). Activity of a second *Trypanosoma brucei* hexokinase is controlled by an 18-amino-acid C-terminal tail. *Eukar. cell*. *5*(12):2014-2023.

- Mouxing, F.U., Qingbiao, L.I., Daohua, S., Yinghua, L.U., Ning, H., Xu, D. (2006). Rapid preparation process of silver nanopartcles by bioreduction and their characterizations. Chinese *J. Chem. Engin.* 14(1):114–7.

- Mukherjee, P., Ahmad, A., Mandal, D., Senapati, S., Sainkar, S.R., Khan, M.I., Ramani, R., Parischa, R., Ajayakumar, P.V., Alam, M., Sastry, M., Kumar, R. (2001). Bioreduction of AuCl4- ions by the fungus, Verticillium sp. and surface trapping of the gold Nannoparticles formed. *Angewandte Chemie- Internat edition*, 40(19):3585-3588.

- Murakami, A., K. Matsumoto, K. Koshimizu., H. Ohigashi. 2003. Effects of selected food factors with chemopreventive properties on combined lipo-polysaccharide and interferon-γ-induced IκB degradation in RAW264.7 macrophages. *Cancer Lett.* 195:17–25.

- Murray, C.B., Norris, D.J., Bawendi, M.G. (1993). Synthesis and characterization of nearly monodisperse CdE (sulfur, selenium, tellurium) semiconductor nanocrystallites. *J. Am. Chem. Soc.*, 115(19):8706-8715.

- Nanda, A. And Saravanan, M. (2009). Biosynthesis of silver nanoparticless from *Staphylococcus aureas* and its antimicrobial activity against MRSA and MRSE. *Nanomed*. 5; 425 - 456

- Narayanan, K.B. and Sakthivel N. (2010). Biological synthesis of metal microbes by microbes. *Adv. Colloid Interface. Sci.* 156:1-13

- Neumann, E., Schaefer-Ridder, M., Wang, Y., Hofschneider, P.H. (1982). Gene transfer into mouse lyoma by electroporation in high electric fields. *The EMBO J.* 7. 841-845

- Nguyen, K. T. (2012). Photothermal Therapy and Nanomaterials. *J. Bioeng. Biomed. Sci.* 2(4): e112*2*.

- Nwagwu, M., opperdoes F.R. (1982). Regulation of glycolysis in *Trypanosoma brucei*: hexokinase and phosphofructokinase activity. *Acta Tropica*. 39:61-72.

- Nowack, B. and Bucheli, T. D. (2007). Occurrence, behavior and effects of nanoparticles in the envir*onment. Environ. Poll.* 150(1):5-22.

- Oba, A., Gahtse, A., Ekouya Bowassa, G., Nika, E., Obengui. (2011). [Congenital human African trypanosomiasis: an observation at the University Hospital of Brazzaville (Congo)]. *Archives de pédiatrie: organe officiel de la Sociéte française de pédiatrie*, *18*(10), 1114-1115.

- Oberdörster, G., Maynard, A., Donaldson, K., Castranova, V., Fitzpatrick, J., Ausman, K., Carter, J., Karn B., Kreyling W., Lai D., Olin S., Riviere N.M., Warheit D., Yang H. (2005). Principles for characterizing the potential human health effects from exposure to nanomaterials: elements of a screening strategy. *Part. Fibre Toxicol.* 2: 8.

- Odiit, M., Kansiime, F., Enyaru, J.C. (1997). Duration of symptoms and case fatality of s*leeping sickness caused by Trypanosoma brucei rhodesiense* in Tororo Uganda. *East Afr. Med. J.,* 74:792-795.

- Odika, I.E, Asuzu I.U, Anika, S.M (1995). The effects of hyperosmolar agents lithium chloride and sucrose on the brain concentration of diminazene aceturate in rats. *Acta Trop* 60:119-125

- Oldenburg, J., Dolan, G., Lemm, G. (2009). Haemophilia care then, now and in the future. *Haemoph. 15 Suppl.* 1: 2-7.

- Olbrich, C., Gessner, A., Schröder, W., Kayser, O., Müller, R. H. (2004). Lipid-drug conjugate nanoparticles of the hydrophilic drug diminazene-cytotoxicity testing and mouse serum adsorption. *J. Control. Release.: 96*(3):425-35.

- Opperdoes, F. R. and Szikora, J. P. (2006). In silico prediction of the glycosomal enzymes of *Leishmania major* and trypanosomes. *Mol. Bio. Para.* 147(2):193-206.

- Overney, R. (2010). Nanothermodynamics and Nanoparticle synthesis, lecture 4, from; http://courses.washington.edu/overney/NME498_Material/NME498_Lectures/Lecture4-Overney-nanoparticles-Synthesis.pdf accessed on 19/09/20122.

- Pal, A., Shah, S., Devi, S. (2009). Microwave-assisted synthesis of silver nanoparticless using ethanol as a reducing agent. *Mat. Chem. Phys.* 114:30-532.

- Pepin, J., Milord, F., Guern, C. (1989). Trial of prednisolone for prevention of melarsoprol-induced encephalopathy in gambiense sleeping sickness. *Lan*cet, 1(8649):1246-50.

- Patil, R. S., Kokate, M. R., Salvi, P. P., Kolekar, S. S. (2011). Comptes Rendus Chimie A novel one step synthesis of silver nanoparticles using room temperature ionic liquid and their biocidal activity. *Comptes rendus - Chimie*, 14(12):1122-1127.

- Perez Martin, O., Lastre Gonzalez, M., Urban, M., Shwalbach, J. (1991). In vivo resistance to strains to *Trypanosoma rhodesience*, Mozambique, 1985. *Rev. Cub. de Med. Trop.* 43:189-193.

- Perez-Morga, D. (2006). Trypanolytic factor of human serum. *Bulletin et mémoires de l'Académie royale de médecine de Belgique*, *161*(5):309-315.

- Phung, O. J., Coleman, C. I., Baker, E. L., Scholle, J. M., Girotto, J. E., Makanji, *S. S., Che*n, *W.* T., Talati, R., Kluger, J., White, C.M. (2010). Recombinant human growth hormone in the treatment of patients with cystic fibrosis. *Pediatrics*, *126*(5): e1211-e1226.

- Pitsillides, C.M, Joe, E.K, Wei, X, Anderson, R.R, Lin, C.P. (2003). Selective cell targeting with light-absorbing microparticles and NPs. *Biophys J*. 84:4023–4032.

- Poltera, A.A. (1985). Pathology of human African trypanosomiasis with reference to experimental African trypanosomiasis and infections of the central nervous system; *Br. Med Bull*, *41*(2), 169-74.

- Poltera, A. A., Owor, R., Cox, J. N. (1977). Virclwws Archiv A Pathological Aspects of Human African Trypanosomiasis (HAT) in Uganda, *Virchows Arch. A Path. Anat. Histol*. 373:249-265.

- Porath, J., Janson, J.C., Liis, T. (1971). Agar derivatives for chromatography, electrophoresis, and gel-bound enzymes. 1. Desulphated and reduced crosslinked agar and agarose in spherical bead form. *J. Chromatogr.* 60:167-177.

- Prabhu, S. and Poulose, E. K. (2012). Silver nanoparticless : mechanism of antimicrobial action, synthesis, medical applications and toxicity effects. *Pub Health. 2*(1):1.

- Pullen T. J., Ginger M. L., Gaskell S. J., Gull K. (2004). Protein targeting of an unusual, evolutionarily conserved adenylate kinase to a eukaryotic flagellum. *Mol. Biol. Cell.* 15(7):3257-3265.

- Quesada, J. R., Hersh, E. M., Manning, J., Reuben, J., Keating, M., Schnipper, E. (1986). Treatment of hairy cell leukemia with recombinant alpha-interferon. *Blood*, *68*(2), 493-497.

- Rabeth, W.M., Zhu, H., Nedyalkova, L., Temple, W., Wasney, Landry, G.R., Vedadi, M., Arrowsmith, C.H., Edwards, A.M., Sundstrom, M., Weigelt, J., Bochkarsv., Park, A.H. (2006). Structure details, Human hexokinase 2, accessed from http://www.thesgc.org/structures/.

- Rahimnejad, M., Mokhtarian, N. and Ghasemi, M. (2009). Production of protein nanoparticles for food and drug delivery system, *Afr. J. Biotech.*, 8(19):4738-4743.

- Rai, M. and Padh, H. (2001). Expression systems for production of heterologous proteins. *Current Science*, 80(9):1121-1128.

- Ramakrishnan, R., Buckingham, W., Domanus, M., Gieser, L., Klein, K., Kunkel, G., (2004). Sensitive assay for identification of methicillin-resistant *Staphylococcus aureus* based on direct detection of genomic DNA by use of gold nanoparticle probes. *Clin. Chem*; 50:1949-1952.

- Rajan, S.S., Lackland, H., Stein, S., Denhardt, D.T. (1998). Presence of an N- terminal polyhistidine tag facilitates stable expression of an other- wise unstable N-terminal domain of mouse tissue inhibitor of metalloproteinase-1 in Escherichia coli, *Prot Expr. Purif.* 13:67–72.

- Raveendran, P., Fu, J., Wallen, S.L. (2003). Completely "green" synthesis and stabilization of metal nanoparticles. *J. Am. Chem. Soc*. 125:13940-13941**.**

- Riddin, T.L., Gericke, M., Whiteley, C.G. (2006). Analysis of the inter- and extracellular formation of platinum nanoparticles by *Fusarium oxysporum* f.sp. Lycopersici using surface response methodology. *Nanotech*, 14:3482-3489.

- Roe, D., Karandikar, B., Bonn-savage, N., Gibbins, B., Roullet, J. (2008). Antimicrobial surface functionalization of plastic catheters by silver nanoparticles. *J. Antimicrob. Chemo.*, 869-876.

- Rocha, G., Martins, A., Gama, G., Brandao, F., Atouguia, J. (2004). Possible cases of sexual and congenital transmission of sleeping sickness. *Lan*cet, 363:247.

- Ronimus, R. S., and H. W. Morgan. 2001. The biochemical properties and phylogenies of phosphofructokinases from extremophiles. *Extremophiles* 5:357–373.

- Ross, M., Molhoek, P., Lundergan, C., Knudtson, M., Draoui, Y., Regalado, L., Le Louer, V. (2001). Randomized comparison of Enoxaparin, a low-molecular-weight Heparin, with unfractionated heparin adjunctive to recombinant tissue plasminogen activator thrombolysis and aspirin: Second Trial of Heparin and Aspirin Reperfusion Therapy (HART II). *Circ.* 104(6), 648-652.

- Rosser, M. P., Xia, W., Hartsell, S., McCaman, M., Zhu, Y., Wang, S., Harvey, S., Bringmann, P., Cobb, R.R. (2005). Transient transfection of CHO-K1-S using serum-free medium in suspension: a rapid mammalian protein expression system. *Prot Expr. Purif., 40*(2):237-43.

- Ruppol, J.F and Burke, J. (1977). Follow-up des traitements contre la trypanosomiase experimentes a Kimpangu (Republic du Zaire). *Ann. de la Soc. Belge de la Med. Trop.* 57:481-491.

- Saiki, R.K.; Scharf, S.J.; Faloona, F.; Mullis, K.B.; Horn, G.T.; Erlich, H.A., Arnheim, N. (1985). Enzymatic amplification of beta-globin sequences and restriction site analysis for diagnosis of sickle cell anemia. *Sci*. 230:1350-1354.

- Samra, Z.Q., Ahmad, S., Javeid, M., Dar, N., Aslam, M.S., Gull, I., Ahmad, M.M. (2013). Anticancer medicine (Doxorubicin and Methotrexate) conjugated with magnetic nanoparticles for targeting drug delivery through iron. *Prep. Biochem. Biotech*. 43 (8):781-797.

- Santra, S., Tapec, R., Theodoropoulou, N., Dobson, J., Hebard, A., Tan, W. (2001). Synthesis and Characterization of Silica-Coated Iron Oxide Nanoparticles in microemulsion : The Effect of Nonionic Surfactants. *Soc*. 18:2900-2906.

- Savage N and Diallo, M.S. 2006. Nanomaterials and water purification: opportunities and challenges. *J. Nano. Res.* 7:331–342.

- Robays, J., Nyamowala, G., Sese, C., Betu, V., Mesu, K., Lutumba, P. (2008). High Failure Rates of Melarsoprol for Democratic Republic of Congo. *Emer. Inf. Dis.*, 14(6): 966-967.

- Sadanandan, N. (2011), Nanomedicine-The basics, *West London Med J.* 3(3): 11-14

- Sambrook, J., Russell, D.W. (2001) Molecular Cloning: a Laboratory Manual, 3rd edn. Cold Spring Harbor Laboratory Press, New York.

- Saifuddin, N., Wong, C.W., Nur Yasumira, A.A (2009). Rapid biosynthesis of silver NPs using the culture supernatant of bacterial with microwave irradiation. *E-J. Chem.* 6: 61-70.

- Sanghi, R. and Verma, P. (2009). Biomimetic synthesis and characterisation of protein capped silver nanoparticless. *Bioresour. Tech.* 100:501-504.

- Sanger, F. and Coulson, R. (1975). A rapid method for determining sequences in DNA by primed synthesis with DNA polymerase. *J. Mol.Bio*. 94(3):441-8.

- Scown, T. M., Aerle, R. V., Johnston, B. D., Cumberland, S., Lead, J. R., Owen, R., Tyler, C. R. (2009). High Doses of Intravenously Administered Titanium Dioxide nanoparticles Accumulate in the Kidneys of Rainbow Trout but with no Observable Impairment of Renal Function. *Ultrapure Water*, 109(2): 372-380.

- Sellebjerg, F., Krakauer, M., Limborg, S., Hesse, D., Lund, H., Langkilde, A., Søndergaard, H.B., Sørensen, P.S. (2012). Endogenous and recombinant type I interferons and disease activity in multiple sclerosis. *PloS one*, 7(6):e35927.

- Šileikaitė, A., Prosyčevas, I., Puišo, J., Juraitis, A., Guobienė, A. (2006). Analysis of Silver nanoparticles Produced by Chemical Reduction of Silver Salt Solution. *Mat. Sci.*, 12(4):287-291.

- Sennuga, A.T. (2011). Biological synthesis of metallic nanoparticles and their interactions with various biomedical targets. PhD Thesis, Rhodes; Retrieved from; http://eprints.ru.ac.za/3049/ accessed on 15/08/2012

- Seyfang, A. and Duszenko, M. (1991). Specificity of glucose transport in *Trypanosoma brucei*. Effective inhibition by phloretin and cytochalasin. *B. Eur. J. Biochem*., 202:191-196.

- Sreenath, H.K., Bingman, C.A., Buchan, B.W., Seder, K.D., Burns, B.T., Geetha, H.V., Jeon W.B., Vojtik, F.C, Aceti D.J., Frederick, R.O., Phillips, G.N., Jr, Fox, B.G. (2005). Protocols

for Production of Selenomethionine-Labeled Proteins in 2-L Polyethylene Terephthalate Bottles Using Auto-Induction Medium. *Prot. Expr. Purif.* 40:256–67.

- Sinha, R., Kim, G. J., Nie, S., Sinha, R., Kim, G. J., Nie, S. (2006). Nanotechnology in cancer therapeutics : bioconjugated NPs for drug delivery Review Nanotechnology in cancer therapeutics : bioconjugated nanoparticles for drug delivery. *Mol. Cancer Ther.* 5(8): 1909-1917.

- Sharlow, E. R., Lyda, T., Dodson, H. C., Mustata, G., Morris, M. T., Leimgruber, S. S., Lee, K.H., Kashiwada, Y., Close, D., Lazo, J.S., Morris, J.C. (2010). A target-based high throughput screen yields *Trypanosoma brucei* hexokinase small molecule inhibitors with antiparasitic activity. *PLoS negl. trop dis*, *4*(4):e659.

- Sharma, R., Gluenz, E., Peacock, L., Gibson, W., Gull, K., & Carrington, M. (2009). The heart of darkness: growth and form of *Trypanosoma brucei* in the tsetse fly. *Trends in para.*, *25*(11): 517-24.

- Shahverdi, A. R., Fakhimi, A., Shahverdi, H. R., Minaian, S. (2007). Synthesis and effect of silver nanoparticles on the antibacterial activity of different antibiotics against S*taphylococcus aureus* and *Escherichia coli*. Nanomedicine: NBM, 3: 168-171. doi:10.1016/j.nano.2007.02.001

- Shemen Industries (2007). Canola active oil. http://www.nanotechproject.org/cpi/ products/canola-active-oil/, accessed on 28/09/2012.

- Shen, W., Feng, L., Feng, H., Kong, Z., Guo, M. (2011). Ultrafine silver (II) oxide particles decorated porous ceramic composites for water treatment. *Chem. Eng. J.175*: 592-599.

- Schreiber, S., Howaldt, S., Schnoor, M., Nikolaus, S., Baudits, J., Gasche, C., Lochs, H., Raedler, A. (1996). Recombinant erythropoietin for the treatment of anaemia in inflammatory bowel disease. *Bowel dis.* 334 (10):619-623.

- Silvestrini, B. (1991). Lonidamine: an overview. *Semin Oncol* 18(2 Suppl 4): 2-6.

- Silvestrini, B., Palazzo, G., De Gregorio, M. (1984) Lonidamine and related compounds. *Prog. Med. Chem.* 21: 110-35.

- Simarro, P.P., Cecchi, G., Franco, J.R., Paone, M., Fèvre, E.M., Diarra, A., Postigo, J.A.R., Mattioli, R.C., Jannin, J.G. (2012). Risk for human African trypanosomiasis, central Africa, 2000-2009. *Emer. Inf. Dis*;17(12):2322-4.

- Simarro, P. P., Jannin, J., Cattand, P. (2008). Eliminating human African trypanosomiasis: where do we stand and what comes next? *PLoS Med.*, *5*(2):e55.

- Sinha, A., Grace, C., Alston, W.K. (1999). African trypanosomiasis in two travelers from the United States. *Clin Inf. Dis*; 29(4):840-844.

- Singh, M., Singh, S., Prasad, S., Gambhir, I.S (2008). Nanotechnology in medicine and antibacterial effect of silver nanoparticles. *J. Nano. Biostr.* 3..(3):115-122

- Sivaraman, S.K., Elago, I., Kumar, S., Santhanam V. (2009). A green protocol for room temperature synthesis of Silver nanoparticles in seconds. *Curr. Sci.*, 97 (7), 1055-2059.

- Sivaraman, S.K., Elago, I., Kumar, S., Santhanam, V. (2010). Room-temperature synthesis of gold nanoparticles-size control by slow addition. *Gold Bul.* 43: 275-286.

- Speers, D. J. (2006). Clinical applications of molecular biology for infectious diseases. The Clinical biochemist. Reviews */ Austr. Asso. Clin. Biochem.*, 27(1): 39-51.

- Smith, A. W. and Iglewskil, B. H. (1989). Nucleic Acids Research Transformation of *Pseudomonas aeruginosa* by electroporation, Aston Univ. 17(24), 25669.

- Smith, R.A., Duncan, M.J., Moir, D.T. (1985) Heterologous protein secretion from yeast. *Sci* 229:1219-1224

- Solomon, S.D., Bahadory M., Jeyarajasingam A.V., Rutkowsky M., Borits C., Mulfinger L., (2007) Synthesis and study of silver nanoparticles. *J. Chem. Edu.*, 84:322-325.

- Sørensen, H.P. and Mortensen, K.K. (2004) Advanced genetic strategies for recombinant protein expression in *Escherichia coli. J. Biotech*, 115:113–128.

- Steverding, D. (2008).The history of African trypanosomiasis. *Para. Vectors*.1:3.

- Stoffel, M., Bell, K. L., Blackburn, C. L., Powell, K. L., Seo, T. S., Takeda, J. U. N., Vionnet, N., Xiang, K., Godh-Jain, M., Pilkis, S.J., Ober, C., Bell, G.I.. (1993). Identification of Glucokinase Mutations in Subjects with Gestational Diabetes Mellitus, *42*(June): 937-940.

- Stryer, L. (1995). Biochemistry. 4th Edition. Chapter 8. Enzymes: Basic concepts and kinetics, pp 181-206. Freeman and Company. NY.

- Studier, F.W. (2005). Protein Production by Auto-Induction in High Density Shaking Cultures. Protein Expression *Purif.* 41:207-34.

- Sun, R.W., Chen, R., Chung, N.P., Ho, C.M., Lin, C.L., Che, C.M. (2005). Silver nanoparticles fabricated in Hepes buffer exhibit cytoprotective activities toward HIV-1 infected cells. *Chem. Commun.* (Camb), 40: 5059–5061.

- Sun, L., Singh, A.K., Vig, K., Pillai, S., Shreekumar, R., Singh, S.R. (2008). Silver nanoparticles inhibit replication of respiratory sincitial virus. *J. Biomed. Biotechnol*. 4:149–158.

- Tanizawa, Y., Koranyi, L. I., Welling, C. M., Permutt, M. A. (1991). Human liver glucokinase gene: cloning and sequence determination of two alternatively spliced cDNAs. *Proc. of the Nat. Acad. of Sci. of the U.S.A. 88*(16), 7294-7297.

- Terpe K. (2002). Overview of Bacterial Expression Systems for Heterologous Protein Production: From Molecular and Biochemical Fundamentals to Commercial Systems. *Appl Microbiol Biotechnol.* 72:211–22

- Thakkar, K.N., Mhatre, S.S., Rasesh, M.S., Parikh, Y. (2010) Biological synthesis of metallic NPs. *Nano. Biol. Med*. 6, 257-262.

- Theodore, L. and Kunz, R.G. (2005). Nanotechnology: Prime Materials and Manufacturing Methods. In: Theodore L. and Kunz R.G Nanotechnology: Environmental implications and solutions. Hoboken, New Jersey: John Wiley& Sons, Inc. 70-79.

- The royal society. (2004) Nanoscience and nanotechnologies: opportunities and uncertainities, RS policy document 19/04 London, p5; accessed from: http://www.nanotec. org.uk/finalReport.htm; on 19/09/2012

- Thomas, T., Thomas, K., Sadrich, N., Savage, N., Adair, P., Bronaugh. R. (2006). Research strategies for safety evaluation of nanomaterials, Part VII: Evaluating consumer exposure to nanoscale materials. *Toxicol. Sci.* 91:14–19.

- Tiedge, M., Krug, U., Lenzen, S. (1997). Modulation of human glucokinase intrinsic activity by SH reagents mirrors post-translational regulation of enzyme activity. *Bio. Et Phys. Acta.*1337 (1997): 175-190.

- Tiedge, M., Richter, T., Lenzen, S. (2000). Importance of cysteine residues for the stability and catalytic activity of human pancreatic beta cell glucokinase. *Arch. Biochem Biophys,* 375(2):251-60.

- Troster, S.D., Muller, U., Kreuter, J. (1990). Modification of the body distribution of poly(methyl methacrylate) nanoparticles in rats by coating with surfactants, *Int. J. Pharm*. 61:85–100.

- Trinquier, M., Perie, J., Callens, M., Opperdoes, F., Willson, M. (1995). Specific inhibitors for the glycolytic enzymes of *Trypanosoma brucei*. *Bioorg. Med.Chem.* 3(11): 1423-1427.

- Truc, P., Lando, A., Penchenier, L., Vatunga, G., Josenando, T. (2012). Human African trypanosomiasis in Angola: clinical observations, treatment, and use of PCR for stage determination of early stage of the disease. *Trans. R Soc. Trop. Med. Hyg.*; 106(1):10-14.

- Tsuji, M., Matsumoto, K., Jiang, P., Matsuo, R.., Tang, X., Kamarudin, K. (2008). Roles of Pt Seeds and Chloride Anions in the Preparation of Silver Nanorods and Nanowires by Microwave- *Polyol method.Colloids surf.* A. 266–277.

- Turrens, J.F, Cazzulo, J.J. (1987). Inhibition of growth and respiration of *Leishmania mexicana* by the antitumor agent lonidamine. *Comp Biochem Physiol C*.88:193-6.

- Tyler, R.C., Sreenath, H.K., Singh, S., Aceti, D.J., Bingman, C.A., Markley, J.L., Fox, BG. (2005). Auto-Induction Medium for the Production of [U-^{15}N]- and [U-^{13}C, U-^{15}N]-Labeled Proteins for NMR Screening and Structure Determination. *Pro Exp. Purif.* 40:268-78.

- Urbina, J.Crespo, A. (1984). Regulation of energy metabolism in *Trypanosoma (Schizotrypanum) cruzi* epimastigotes. I. Hexokinase and phosphofructokinase. *Mol. Biochem. Parasitol*., 11:225-39.

- Vaidyanathan, R., Gopalram, S., Kalishwaralal, K., Deepak, V., Ram, S., Pandian, K., Gurunathan, S. (2010). Colloids and Surfaces B : Biointerfaces Enhanced silver nanoparticle synthesis by optimization of nitrate reductase activity, *Coll. and Surf. B: Biointerfaces.* 75:335–341.

- Vandercammen, A., Van Schaftingen, E. (1990). The mechanism by which rat liver gluco-kinase is inhibited by the regulatory protein. *Eur. J. Biochem*.191:483–489.

- Verlinde, C. L., Hannaert, V., Lonski, C., Willson, M., Perie, J.J., Fothergill-Gilmore L. A., Opperdoes R. R., Gelb M. H., Hol W. G., Michels P. A. (2001) Glycolysis as a target for the design of new anti-trypanosome drugs. *Drug Resist. Updat.* 4: 50-65.

- Vaidyanathan, R., Gopalram, S., Kalishwaralal, K., Deepak, V., Pandian, S.R., Gurunathan, S (2010)Enhanced silver nanoparticle synthesis by optimization of nitrate reductase activity. *Colloids Surf. B Biointerfaces*. 75:335–341.

- Vigneshwaran, N., Kathe, A.A., Varadarajap, P.V., Nachane, R.P., Balasubramanya R (2006). Biomimetics of silver nanoparticles by white rot fungus, Phaenerochaete chrysosporium. *Coll and Surf B: Biointerfaces*.53:55-59.

- Vilchis-Nestor, A.R., Sánchez-Mendieta, V., Camacho-López, M.A., Gómez-Espinosa, R.M., Camacho-López, M.A., Arenas-Alatorre, J. (2008 S)solventless synthesis and optical properties of Au and AgNPs using Camellia sinensis extract. *Mate.r Lett.*.62:3103–310.

- Voet, D and Voet, J.G. (2004) Biochemistry, 3rd Edition. Chapter 14, Enzyme Kinetics. pp 477-491 NY, Wiley.

- Waugh, D.S. (2005). Making the most of affnity tags, *Trends Biotech*. 23:316–320.

- Williams, S., Saha, L., Singha, U. K., Chaudhuri, M. (2008) *Trypanosoma brucei:* differential requirement of membrane potential for import of proteins into mitochondria in two developmental stages. *Exp. Parasitol.* 118(3):420- 433.

- Wilson, J. E. (2003). Isozymes of mammalian hexokinase: structure, subcellular localization and metabolic function. *J. Exp. Bio.*, *206*(12):2049-2057.

- Willson, M., Sanejouand, Y. H., Perie, J., Hannaert, V., Opperdoes F. (2002) Sequencing, modeling, and selective inhibition of *Trypanosoma brucei* hexokinase. *Chem. and Bio.* 9(7): 839–847.

- Wirth, R., Friesenegger, A., Fiedler, S. (1989). Transformation of various species of gram-negative bacteria belonging to 11 different genera by electroporation. *Mol. Gen. Genet: MGG*, *216*(1):175-7.

- Wong, P, Gladne, S, Keasling, J.D. (1997). Mathematical Model of the Lac Operon: Inducer Exclusion, Catabolite Repression, and Diauxic Growth on Glucose and Lactose. *Biotechnol. Prog*. 13:132–143

- World Health Organization. Control and surveillance of African trypanosomiasis. Report of a WHO Expert Committee. *World Health Organ Tech. Rep. Ser*. 1998; 881: I-VI, 1-114.

- World Health Organization. WHO fact sheet on African Trypanosomiasis. WHO fact sheets;Fact sheet 259: Retrieved from: http://www.who.int/mediacentre/ factsheets/fs259/en/ : on 29 July, 2014.f

- Wurapa, F.K., Dukes, P., Njelasani, E.K., Boatin, B.A., (1984). Healthy carrier of *Trypanosoma rhodesiense*: a case report. *Trans R. Soc. Trop. Med. Hyg*. 78: 349-350.

- Wurm, F. and Bernard, A. (1999). Large-scale transient expression in mammalian cells for recombinant protein production. *Curr. opinion in biotech*, *10*(2):156-9

- Yang, J., Pu, Y.G., Zeng, Z.-M., Yu, Z.-J., Huang, N., Deng, Q.-W. (2009). Interferon for the treatment of genital warts: a systematic review. *BMC Inf. dis*. *9*:156.

- Yang, M., Li, J., Lin, F., Zhu, X. (2013). Absorption Enhancements in Plasmonic Solar Cells Coated with Metallic nanoparticles. *Plasm.* 877-883.

- Xiang, D.-xi, Chen, Q., Pang, L., Zheng, C.-long. (2011). Inhibitory effects of silver nanoparticless on H1N1 influenza A virus in vitro. *J. Viro.l Meth.*, 178(1-2): 137-142.

- Xu, J, Craig, S.L. (2005) Thermodynamics of DNA hybridization on gold-Nanoparticles. *J Am. Chem. Soc*. 127:13227–31.

- Ye, J., Wang, Q., Zhou, X., Zhang, N. (2007). Injectable actarit-loaded solid lipid Nanoparticles as passive targeting therapeutic agents for rheumatoid arthritis. *Blood*, 352, 273-279.

- Yu, W. H. and Woessner, J. F., Jr. (2001). Heparin-enhanced zymographic detection of matrilysin and collagenases. *Anal. Biochem.,* 293:38-42.

- Zharov, V.P., Galitovsky, V., Viegas, M. (2003). Photothermal detection of local thermal effects during selective nanophotothermolysis. *Appl. Phys. Lett*., 83(24):4897-4899.

- Zamboni, W. C., & Zamboni, W. C. (2005). Liposomal, Nanoparticle, and Conjugated Formulations of Anticancer Agents. *Clin. Cancer Res*. 11:8230-8234.

Appendices

A. Chemiluminescence-based Western analysis

A.1. Method

The proteins (*Tb*HK and *h*GCK) separated by SDS-PAGE (chapter 3, section 3.2.3.1) were transferred onto nitrocellulose membrane, pre-soaked in distilled water and transfer buffer [13 mM Tris-HCl, 100 mM glycine and 20% (v/v) methanol] for 10 minutes each, using a semi-dry Transblot (LASEC, USA) at a constant amplitude of 400 mA for 50 minutes (Towbin *et al*, 1979). The transferred proteins were confirmed by Ponceau staining [0.5% (w/v) Ponceau S in 1% (v/v) glacial acetic acid]. Nitrocellulose membrane with transferred proteins was blocked with 1% Blotto [non-fat dry milk (Sant Cruz Biotechnology) in Tris-buffered saline-Tween (TBST; 50 mM Tris, pH 7.5, 150 mM NaCl, 1% {v/v} Tween20)] for 30 minutes and incubated with His-probe [Rabbit polyclonal; Santa Cruz Biotechnology (sc-8040)] at 4°C overnight with agitation, diluted 1:1000 in 1% Blotto. The membrane was rinsed four times in TBST for 15 minutes replacing the TBST each rinse. The membrane was incubated with species-specific anti-Rabbit IgG conjugated to horseradish peroxidase [HRP] (AbCAM, ab6802) at 1:5000 dilution in 1% Blotto for 45 minutes at room temperature with agitation. After the incubation with the secondary antibody, the membrane was rinsed with TBST four times 15 minutes each rinse. Protein bands were detected using the Clarity Western ECL Substrate kit (Biorad; UK) with visualization of chemi-illuminescence on x-ray film (AGFA, USA).

A.2. Results and discussions

Western blot analysis of the recombinant proteins (*Tb*HK and *h*GCK) is presented in figure A1.

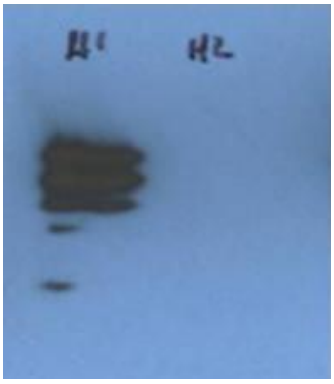

Figure A1: Western blot image showing the presence of His-tagged human glucokinase loaded in lane (H1). *TbHK* was loaded in lane H2.

The western blot results (figure A1) show that His-tagged human glucokinase can be detected by the use of the anti-His antibody. However, His-tagged *Tb*HK could not be detected by anti-His antibodies used in the current procedure. This could be attributed to sub-potential protein transfer that could come about due to the low quality membranes, improper western transfer procedure and incorrect SDS-PAGE gel preparation and/or run (Gomez A.V. 2009).

B. Virtual PCR products for *Tb*HK and *h*GCK

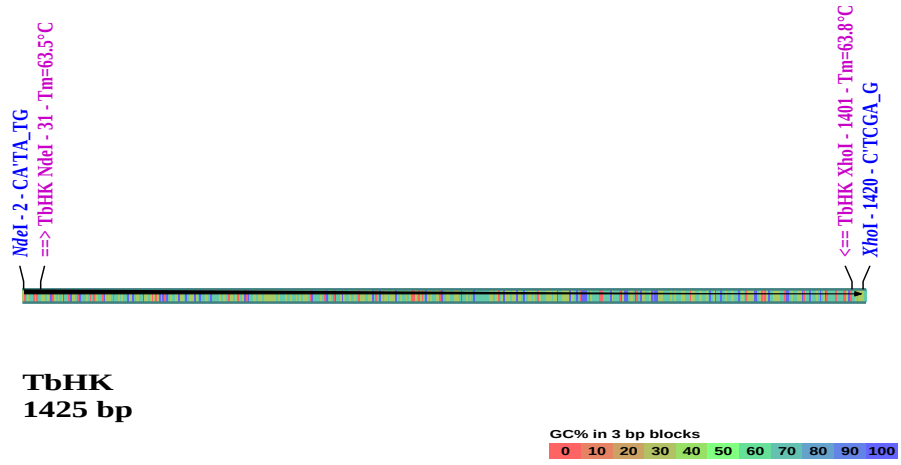

Figure B1: *Tb*HK virtual PCR product, showing the *NdeI* and *XhoI* primers

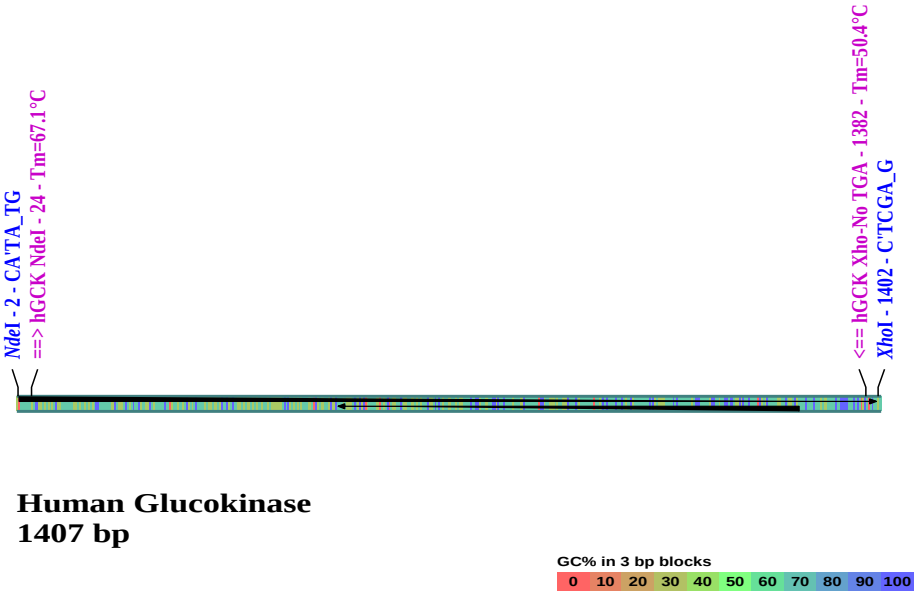

Figure B2: *hGC*K virtual PCR product, showing the *NdeI* and *XhoI* primers

C. Rubidium Chloride method for preparing competent *E. coli* cells.

C.1. Reagents and solutions

C.1.1. Psi broth / liter

5g Yeast extract

20g Tryptone

5g magnesium sulphate

pH 7.6 adjusted with potassium hydroxide.

C.1.2. TfbI Buffer

30mM Potassium acetate

100mM rubidium chloride

10mM Calcium chloride

50mM manganese chloride

15% glycerol v/v

pH 5.8 adjusted with acetic acid

C.1.3. TfbII Buffer

10mM 3-(N-morpholino)propanesulfonic acid (MOPS)

75mM Calcium chloride

10mM rubidium chloride

15% glycerol v/v

pH 6.5 adjusted with diluted sodium hydroxide

C.2. Procedure:

- Inoculate 1ml from overnight culture into 100ml Psi broth (scale up or down as required)
- Incubate at 37^{o}C with aeration to A550 =0.48
- Incubate on Ice for 15 minutes
- Pellet cells in appropriate centrifuge tube 3-500 *x*g for five minutes (about 5000 rpms)

- Discard supernatant and add 0.4 volume (i.e. of original volume, here it is 40 ml) TfbI, re-suspend and incubate on ice for 15 minutes
- Discard supernatant and re-suspend in 0.04 volume of TfbII
- Incubate on ice for 15 minutes and either use immediately of quick freeze at -70^{o}C for storage. Store in 0.1ml aliquots
- Quick freeze in ethanol-dry ice or liquid nitrogen prior to storage in a -70^{o}C to -80^{o}C freezer
- Thaw on ice just before using in a transformation experiment.

D. TCA protein concentration protocol

- Mix the sample with the 30% Trichloroacetic acid and the sample in 1:1 ratio
- Incubate on ice for 15-30 minutes
- Spin in microcentifuge at 4^{0}C for 15 minutes
- Rinse pellet with ice cold Isopropanol
- Centrifuge at 10,000g for 5 minutes at 4^{0}C
- Remove the supernant and dry the pellet using speed-vac system at 65 for 30^{0}C minutes
- If the sample is to be run on SDS, re-suspend the dried pellet in required amount of SDS loading buffer.

E. PAGE protocols

E.1. SDS-PAGE Running Buffer (10x)
30.3 g Tris-base
144.0 g glycine
10.0 g SDS
completely dissolve in about 800 ml dH_2O and then more dH_2O up to 1 liter.

E.2. Staining solutions and procedure

E.2.1. Coomassie staining

E.2.1.1. Fairbanks A

0.5g Coomassie Blue R-250

250ml Isopropanol

100ml Acetic acid

650ml distilled water

E.2.1.2. Fairbanks B

0.05g Coomassie Blue R-250

100ml Isopropanol

100ml Acetic acid

800ml distilled water

E.2.1.3. Fairbanks C

0.02g Coomassie Blue R-250

100ml Acetic acid

900ml distilled water

E.2.1.4. Fairbanks D

100ml Acetic acid

900ml distilled water

E.3. Silver staining

E.3.1. Reagents and solutions

E.3.1.1. 1.5mM Sodium dithionite (m.r. 174.10) 100 ml

- 26.115mg weigh and dissolve in 100 ml of distilled water

E.3.1.2. 5% silver nitrate

- 0.02g dissolved in 100 ml of distilled water.

- Cover the stock bottle with foil paper of prepare into a brown bottle to avoid exposure to direct sun light.

E.3.1.3. Sodium thiosulfate (2 µM)

- Prepare 2mM Sodium thiosulfate (Mr. 158.11) and dilute to 2 µM
- Weigh 31.622 mg, dissolve in 10 ml of distilled water
- Dilution of 2 mM Sodium thiosulfate to 2 µM;
- 10 µl into 90 µl of distilled water

E.3.1.4. Silver staining developer

6% Sodium carbonate in 2 µM Sodium thiosulfate**.**

Weigh 6g of sodium carbonate and dissolve it in 100 ml of 2µM Sodium thiosulfate

E.3.1.5. Silver staining stop reagent (5% Acetic acid)

2.5 ml of acetic acid into 97.5 ml of distilled water

E.3.2. Protocol for silver-staining

As described by Rabilloud *et al*. (1988)

E.3.2.1. Materials

- Complete destain solution (40% EtOH and 10% acetic acid)
- 1.5mM Sodiumdithionite (25mg/10ml)
- 5% silver nitrate
- Developer
    - 6% Sodium carbonate (Na_2CO_3); 2ul anhydrous sodium thiosulfate ($Na_2S_2O_3$)
- Stop reagent: 5% Acetic acid

E.3.2.2. Method

- After migration the gel is fixed with 10% Acetic acid- 30% ethanol overnight or stained with Coomassie brilliant blue and destained. Use the complete destain solution to destain gel for silver staining
- Wash gel 2x for 15 min with distilled water
- Leave in sodiumdithionite for 1 minute
- Wash the gel 2x for 29 seconds with distilled water
- Leave in silver nitrate for 20-30 minutes
- Wash gel for 5 minutes in distilled water
- Leave in developer for 5 minutes
- Discard developer and put gel into 50 ml developer with 200ul Formaldehyde (Mix before adding to gel)
- Stop the reaction by adding acetic acid solution directly to the developer mixture
- Wash the gel with distilled water to remove background.
- Dry the gel or store in 20% ethanol at 4^{o}C

F. *Tb*HK and *h*GCK temperature and pH stability studies.

F.1. Temperature stability studies for *Tb*HK

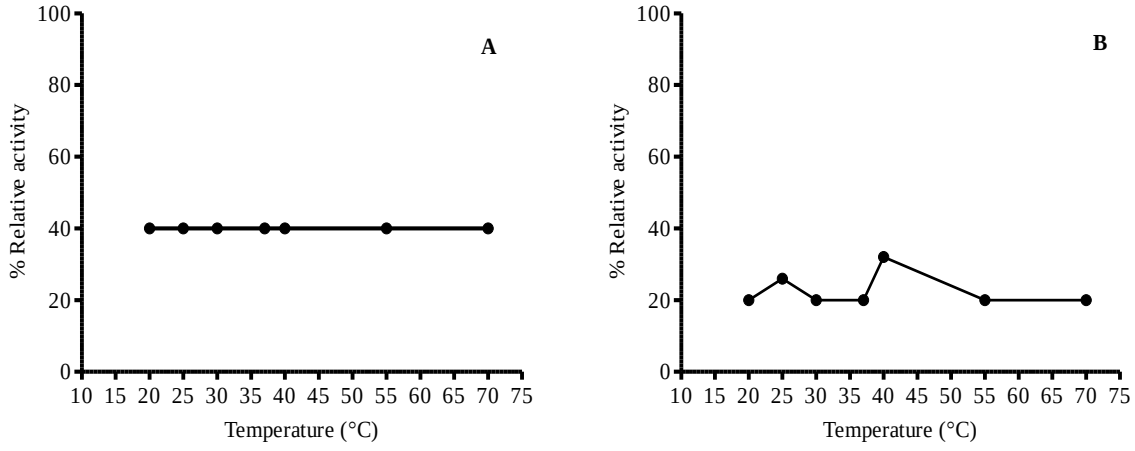

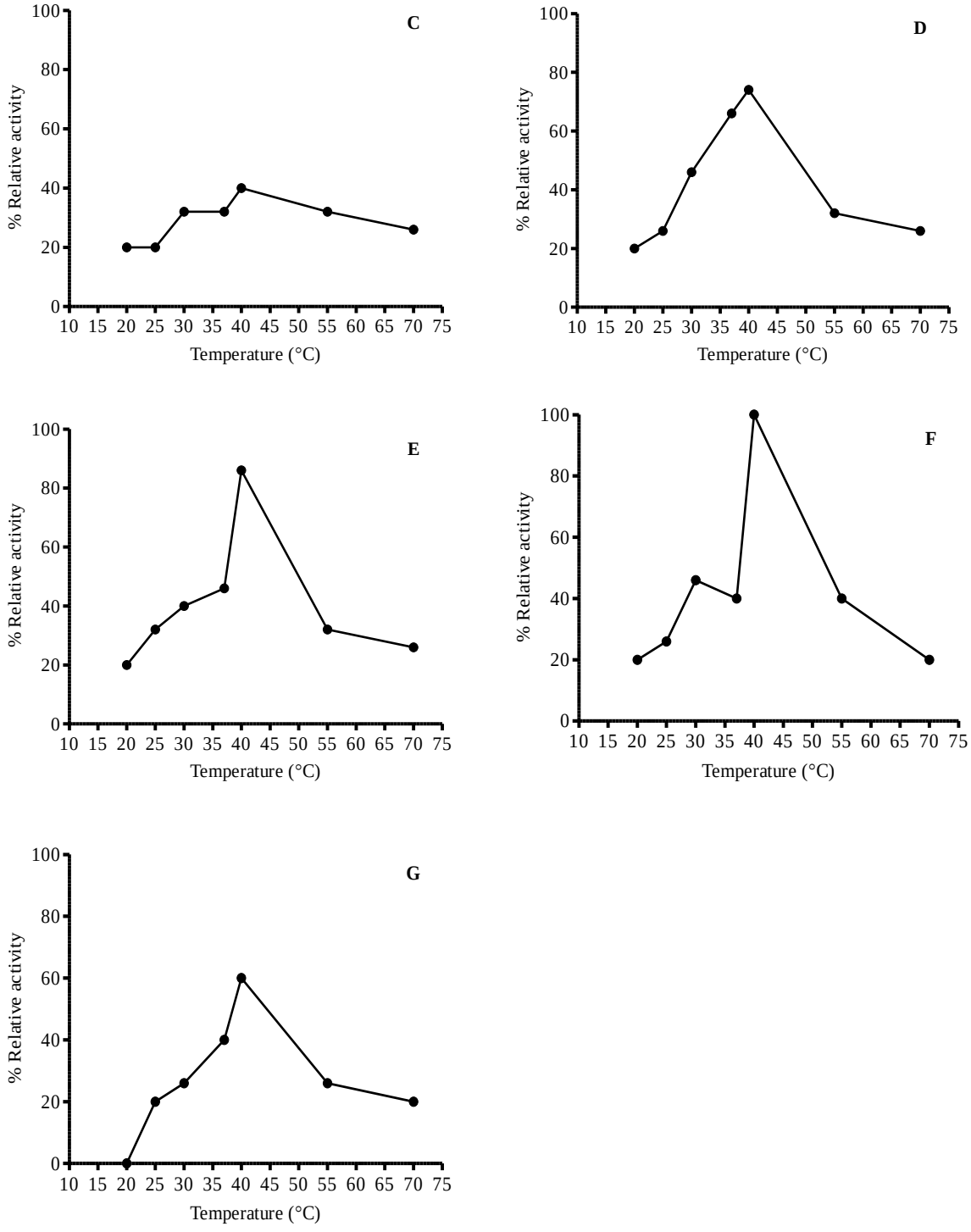

Figure F1: Graphical presentation of temperature stability study of *Tb*HK at (A) T0, (B) T15, (C) T30, (D) T45, (E) T60, (F) T90 and (G) T120.

F.2. Temperature stability studies for *h*GCK

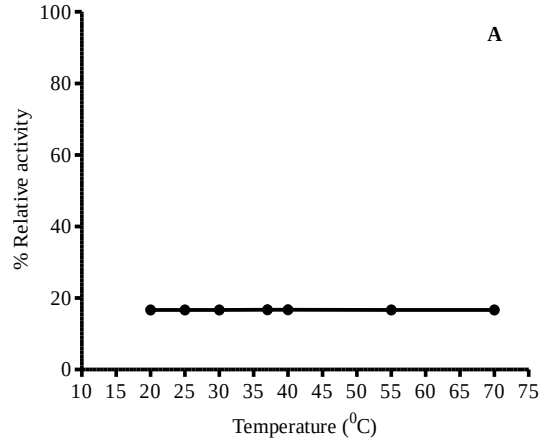
A
% Relative activity
Temperature (0C)

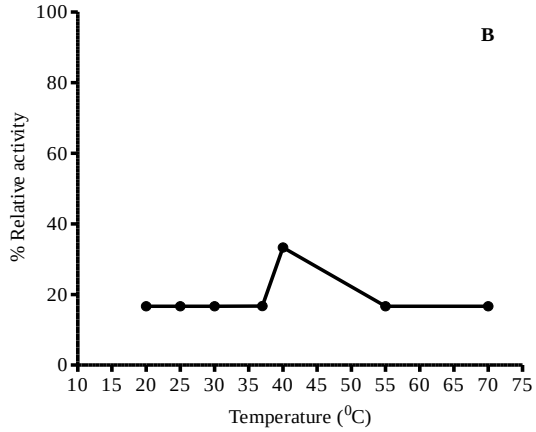
B
% Relative activity
Temperature (0C)

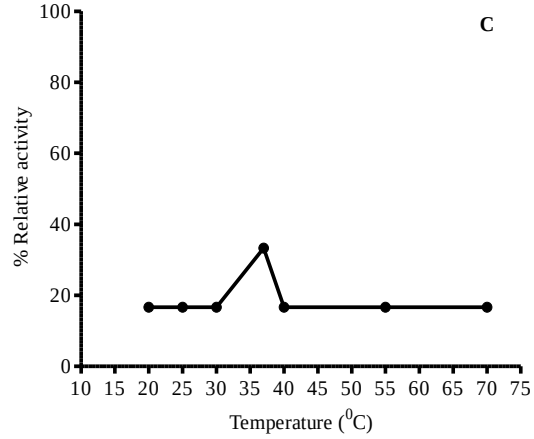
C
% Relative activity
Temperature (0C)

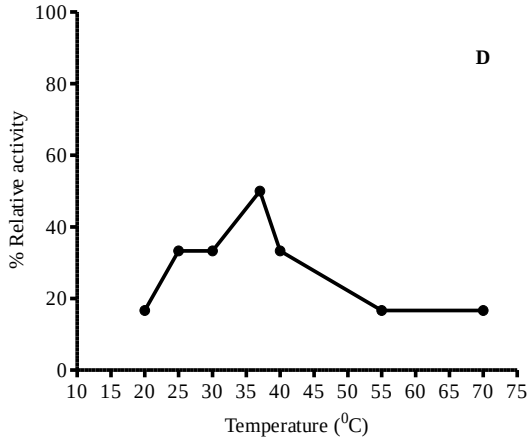
D
% Relative activity
Temperature (0C)

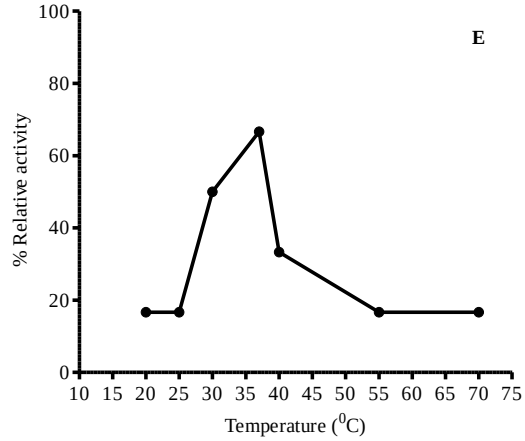
E
% Relative activity
Temperature (0C)

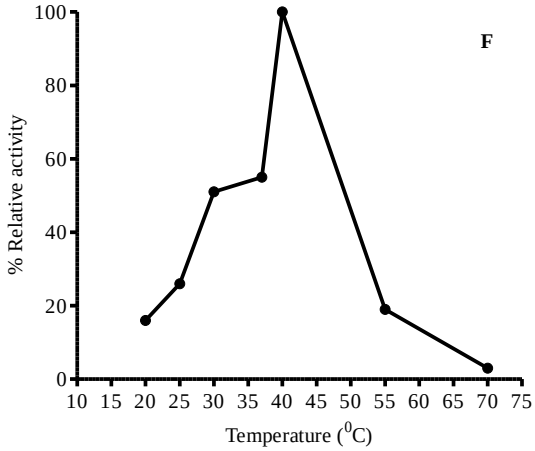
F
% Relative activity
Temperature (0C)

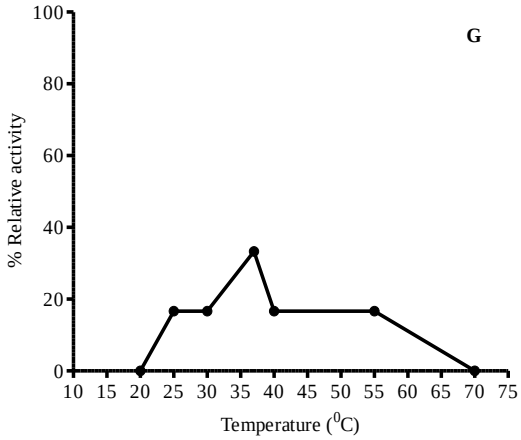

Figure F2: Graphical presentations of temperature stability study of *h*GHK at (A) T0, (B) T15, (C) T30, (D) T45, (E) T60, (F) T90, (G) T120.

F.3. pH stability studies for *Tb*HK

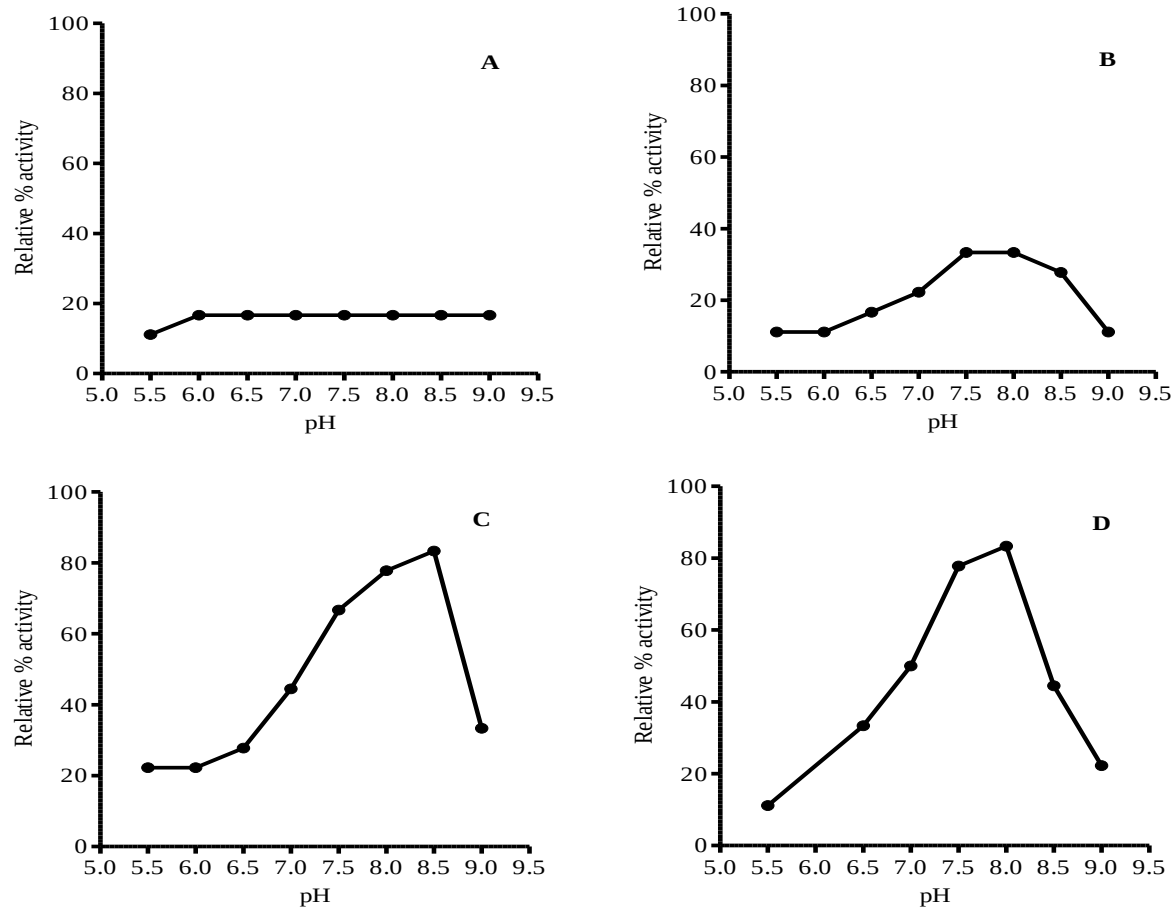

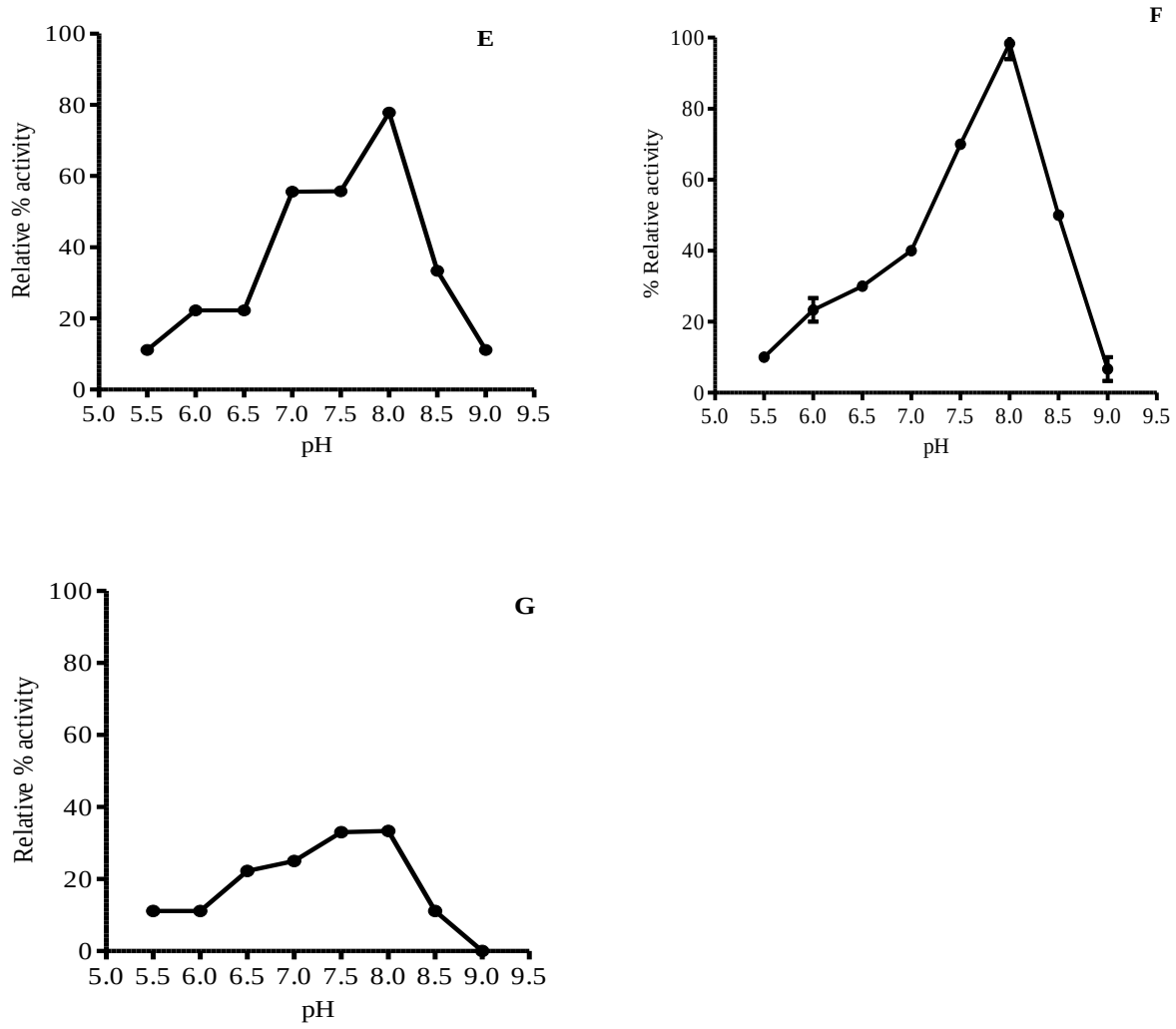

Figure F3: Graphical presentation of temperature stability study of *Tb*HK at (A) T0, (B) T15, (C) T30, (D) T45, (E) T60, (F) T90 and (G) T120.

F.4. pH stability studies for *h*GCK

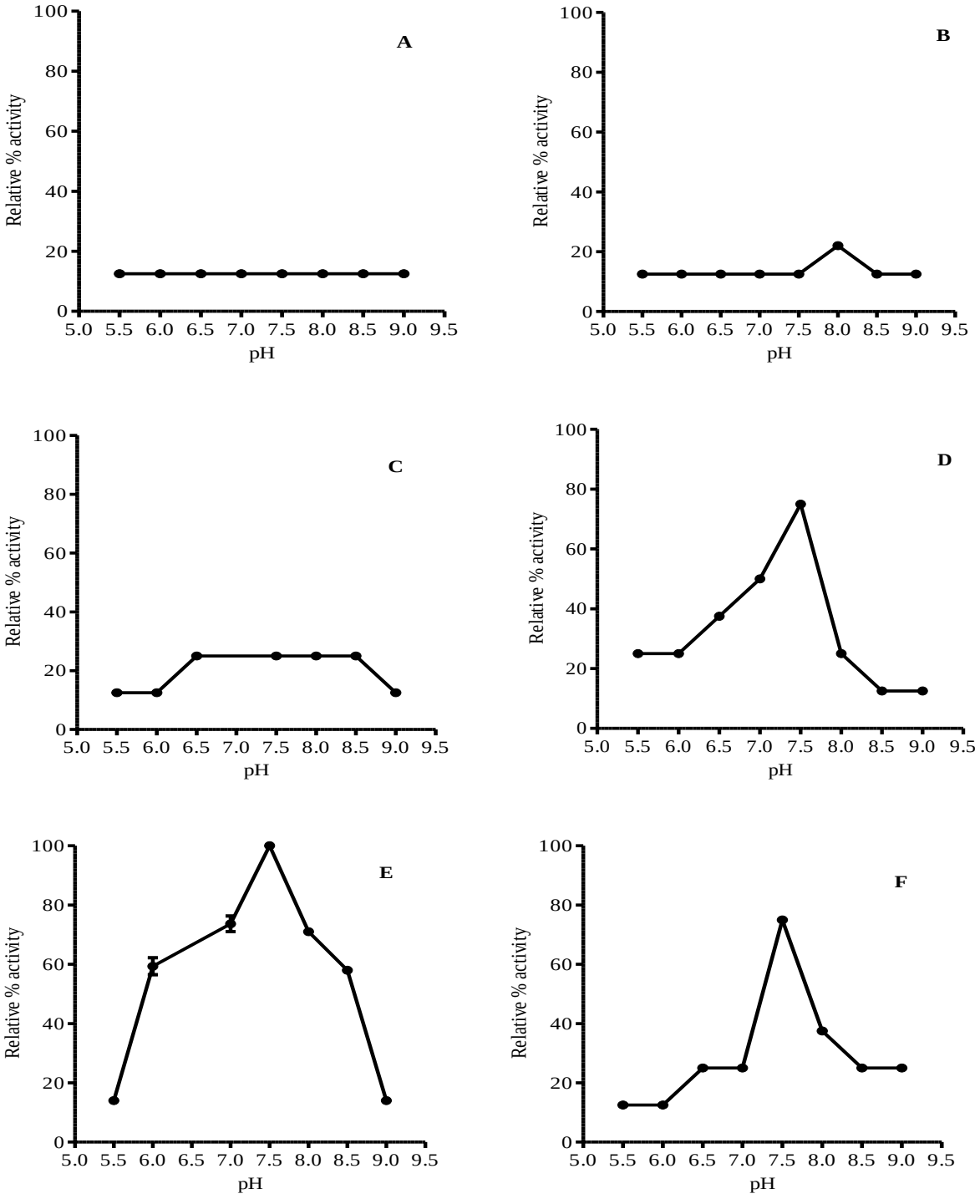
A
B
C
D
E
F
Relative % activity
pH
100
80
60
40
20
0
5.0 5.5 6.0 6.5 7.0 7.5 8.0 8.5 9.0 9.5

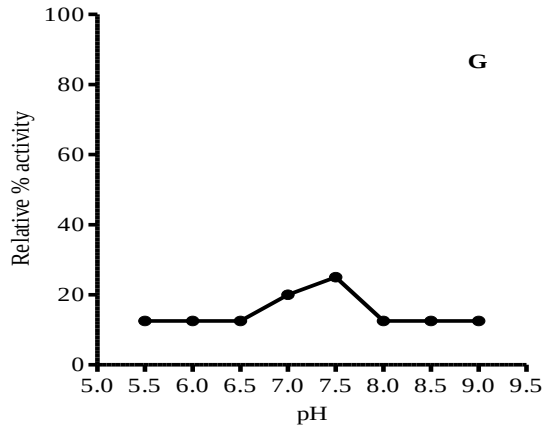

Figure F4: Graphical presentation of temperature stability study of *h*GHK at (A) T0, (B) T15, (C) T30, (D) T45, (E) T60, (F) T90 and (G) T120.

G. Zymogram

G.1. Reagents

G.1.1. 50 mM Tris.HCl pH 8.0 (mr 121.1) / 250 ml

1.5138 g Tris base- weighed and dissolved in 200 ml distilled water; pH adjusted appropriately by HCl and topped up to 250 ml.

G.1.2. 25 mM $MgCl_2$ (mr 203.3) in 50 mM Tris.HCl buffer, pH 8.0./ 0.25L

1.271g $MgCl_2$ weigh and dissolve in 0.2L 50 mM Tris.HCl, pH 8.0 buffer, top up to 0.25L.

G.1.3. 100 mg glucose/ 50 ml:

Weigh 100 mg into 50 ml of 50 mM Tris.HCl, 25 mM Mg Cl_2.

G.1.4. 25mg ATP (50 ml)

Dissolve 25 mg ATP in 50 mM Tris.HCl containing 25 mM MgCl.

G.1.5. Phenazine methosulfate (PMS) - 5 $mg.ml^{-1}$

Add 10 mg PMS into 2 ml of distilled water.

G.1.6. 5 3-(4, 5-dimethylthiazol-2-yl)-2, 5-diphenyltetrazolium bromide (MTT) - 5 $mg.ml^{-1}$

Add 10 mg into 2 ml of distilled water.

G.1.7. NADP - 5 $mg.ml^{-1}$

Add 10 mg into 2 ml of distilled water.